THE POPULATION STRUCTURE OF THE SMALL MAGELLANIC CLOUD

Norman J. Stewart

Presented for the Degree of Doctor of Philosophy

at the University of Edinburgh

October 1979

This thesis was composed by me and consists entirely of my own work.

October 1979.

"I have got my result; but I do not know yet how to get it."

K.F. Gauss

ACKNOWLEDGMENTS

Special thanks go to my supervisors, Dr M.T. Brück and Dr R.D. Cannon, for proposing the project and for their help in its execution. I would also like to thank Mike Hawkins for his great help with my electronographic observations and Paul Murdin for introducing me to the AAT.

Thanks are due to the staff of the Royal Observatory Edinburgh, in particular to Dave Fiddes for keeping the iris photometer going and Brian Hadley and his department for excellent photographic services.

I am indebted to Professor S.C.B. Gascoigne, Ken Elliott and Dave Malin for obtaining AAT plates for me and to Lucy Peake for her considerable assistance with the data reductions. I would also like to thank Joyce Shand for her skilled typing and other contributions to the preparation of this thesis and Marjory Fretwell for preparing the illustrations.

I also say thank you to my wife Ruth for her help and encouragement during the last three years.

Finally I would like to express my gratitude to the University of Edinburgh Senatus Post Graduate Studies Committee for the award of a Post Graduate Studentship.

ABSTRACT

Photographic photometry using prime-focus AAT plates has been carried out in the western regions of the Small Magellanic Cloud. To calibrate the photographic emulsions a new electronographic standard sequence was established. However this sequence disagreed in scale with the existing electronographic sequence in K3 due to Walker and the conflict was resolved by photoelectric photometry using the twin photometer on the AAT, which showed that Walker's sequence was correct. A combination of the new photoelectric photometry, Walker's K3 photometry and some photoelectric photometry by Gascoigne was then used to calibrate the photography.

The colour-magnitude diagrams which resulted showed the existence of three separate populations, all well defined in age. A group of age $\leq 10^8$ years was found near the optical centre which decayed very rapidly in surface density away from this centre. A second group of age 8×10^8 years was found to be more widespread and to be the dominant stellar population at a distance of 1 Kpc from the centre of the SMC. This latter population includes the cluster NGC152. The third group, which included the cluster K3, was found to dominate further out, at 2 Kpc from the optical centre, and to be of age 4×10^9 years.

Thus the picture envisaged is of concentric stellar groups whose radius varies directly with age. A model to account for this structure is outlined, involving slow contraction of the HI in the SMC disc, which is stabilised by rotation, and at certain well defined instants widespread star formation is initiated, after which the HI

unprocessed into stars continues its contraction. As mechanism for the initiation of star formation the perigalactic passage of the Magellanic Clouds in their orbit about the Galaxy is invoked and it is shown that the last two perigalactica coincide in time with the formation of the two oldest stellar groups discovered in the photometry.

TABLE OF CONTENTS

CHAPTER I

INTRODUCTION

1.1 Stellar Evolution and Cluster Photometry

Star clusters have proved invaluable in the development of ideas concerning stellar and galactic evolution in at least two ways;

(i) as an observational test of theories of stellar evolution, and

(ii) as a probe of the age and physical properties of the Galaxy and of external galaxies.

The value of clusters lies in the fact that their stars are subject to fewer free parameters than stars of the general field. It is widely accepted that, to a good approximation, star clusters form from material which is chemically homogeneous and that all stars are of the same age. Also cluster diameters are much smaller than their distances from the Sun, so all cluster stars may be assumed to lie at the same distance. The observed variation from one cluster star to another must thus be due solely to intrinsic properties such as mass. Clusters have been classified into two broad groups for many years, these being

(i) open clusters and stellar associations

(ii) globular clusters.

The open clusters are generally confined to the plane of the Galaxy, have few member stars and show very low symmetry. Photometry of these clusters shows a variety of star types but generally they

are dominated by hot early-type main sequence stars, with few evolved stars, e.g. h and χ Persei, Pleiades, see Fig. 1.1a. Some clusters, however, are observed to have a dominant red-giant branch, e.g. M67, NGC188, NGC2420, see Fig. 1.1b. The globular clusters, by contrast, form a nearly homogeneous set. All are rich in members, containing up to 10^5 stars, show spherical symmetry and a high degree of central concentration. The globular clusters show no preference for the galactic plane, but are distributed in a spherical halo centred on the galactic nucleus. Globular clusters are also similar in photometric properties, all being dominated by a long red-giant branch, with a main-sequence terminating at faint levels, and a horizontal branch of variable form, many containing RR Lyrae variables. Fig. 1.2 shows a typical globular cluster, M3.

The study of star clusters took on a recognisably modern form in the first decades of the 20th century, with the discovery by Hertzsprung and Russell of the correlation between the luminosity and spectral type of a star, as observed in the "main-sequence" of the Hertzsprung-Russell diagram. The early work was performed on nearby stars, the distances and hence luminosities of which were known from parallax studies. It was soon realised, however, that a star cluster, no matter how distant, should be amenable to similar study.

Shapley (1920) discovered that the H-R diagram of the globular clusters M3, M11 and M13 was quite different from that of the local stars, in the sense that the nearby stars of highest luminosity

a.

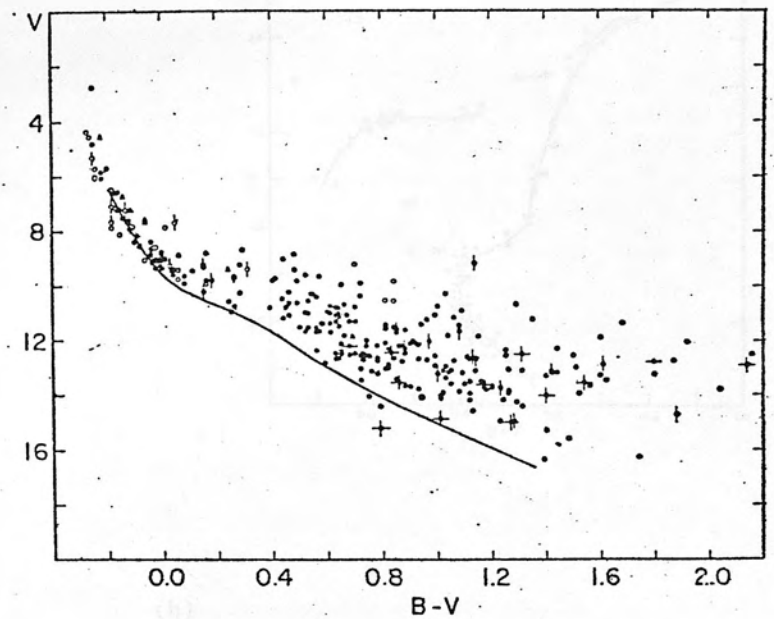

b.

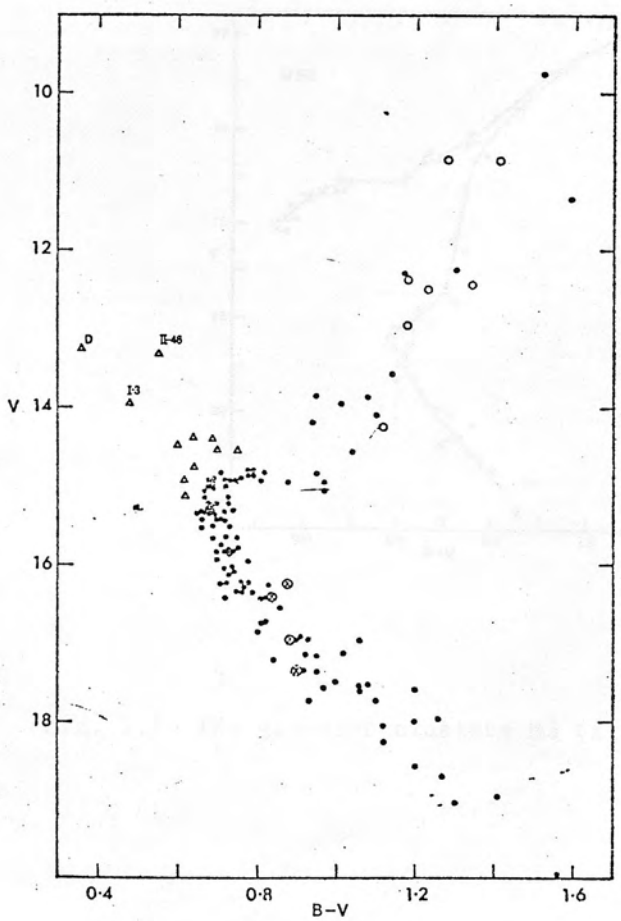

Fig. 1.1a Young cluster NGC6067

Fig. 1.1b Old open cluster NGC188

(a)

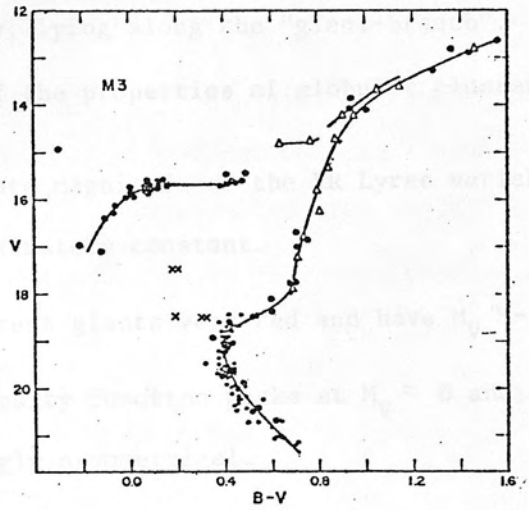

(b)

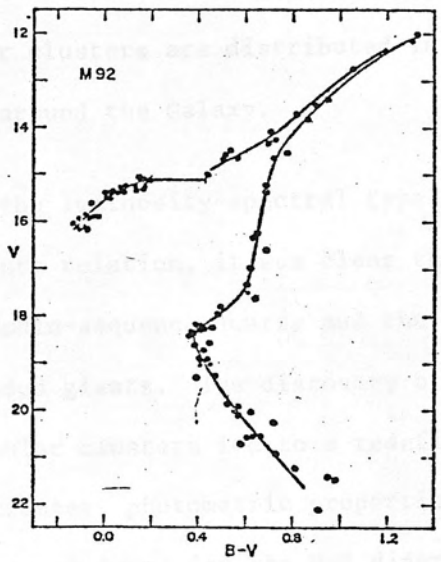

Fig. 1.2 The globular clusters M3 (a) and M92 (b).

tended to be of earliest spectral type, whereas the globular clusters behaved oppositely, lying along the "giant-branch". Shapley (1930) summarised some of the properties of globular clusters as follows:

(i) Absolute magnitude of the RR Lyrae variables approximately constant.

(ii) Brightest giants very red and have $M_V \sim -3$.

(iii) Luminosity function peaks at $M_V \approx 0$ and is strongly asymmetrical.

(iv) Fainter giants tend to be bluer.

(v) Apparent diameters and RR Lyrae observations may be used to derive distances.

(vi) Globular clusters are distributed in a spherical system around the Galaxy.

Interpreting the luminosity-spectral type relation as a luminosity-temperature relation, it was clear that two types of star were involved, the main-sequence dwarfs and the cool and luminous, and therefore extended giants. The discovery of the unusual H-R diagram of the globular clusters led to a redefinition of the terms globular and open cluster, photometric properties replacing geometrical. A range of forms for the H-R diagram was discovered among the open clusters, some showing the main-sequence extending to high luminosities while others, like M34 and the Pleiades (Hertzsprung, 1929) lay intermediate between this situation and that of the globular clusters, with a shorter main-sequence terminating at lower luminosities and diverging away from the standard

type just below the top, becoming nearly vertical, these clusters also containing some giants. Trumpler (1925) used these characteristics to define a classification scheme for open clusters. The observed correlation of the two parameters, luminosity at main-sequence turn-off and giant branch density led him to propose evolution as the reason for the differences between the clusters, some clusters being older than others. He also suggested that the highly populated sequences in the H-R diagram were loci of stars of varying mass, the mass determining the rate of evolution of a star through the H-R diagram. Another suggestion from this period was that of main-sequence fitting as a distance indicator. However, the use of this photometric distance indicator and the geometrical method of Shapley led to discordant results, the photometric consistently giving larger distances. The effect was explained by Trumpler in terms of a disc-shaped distribution of interstellar dust pervading the entire Galaxy and scattering the light from distant stars.

During the 1920's and 30's the simple picture of dwarf and giant stars was gradually augmented, first by the discovery of 'white dwarfs', very faint, hot stars lying well below the main-sequence and explained by Chandrasekhar as being degenerate helium stars with no energy sources left apart from thermal energy. Subgiants were later identified as a class by Stromberg (1933, 1936) i.e., stars lying between the main-sequence and the giant branch in a vertical line. Kuiper (1939) from a study of large proper motion stars, postulated the existence of a subsidiary main-sequence lying approximately 2 magnitudes below the standard and running parallel to it. The stars in this sequence, called sub-dwarfs by him, he found to have unusual

spectral properties, in particular, some of them showed no calcium H + K absorption lines. Greenstein's (1939) photometry of M4 confirmed the great difference between globular and open clusters in their stellar content, and the marked uniformity of the globulars amongst themselves. Coupled with the already established differences in galactic distribution, appearance and richness, this distribution was incorporated by Baade (1944) into his scheme of "stellar populations". He postulated that certain types of stars, star groups and interstellar matter were more likely to occur together. To his Population I he assigned the late-type galaxies (spirals and irregulars) which he suggested contain open star clusters, young OB associations, a strong blue main-sequence like that observed locally, few red giants and a large population of interstellar dust and gas. The Population I component was found to be strongly concentrated towards the plane of the Galaxy, with a thickness of approximately 400 p.c. and to have very small velocities in the direction of the galactic pole. The chemical composition of Population I objects in the Galaxy is found to be remarkably uniform, all having heavy-element compositions within a factor of 2 of the solar value.

To Population II, Baade assigned the early-type galaxies (ellipticals), the nuclei of spirals and the high velocity nearby stars, with globular clusters, no blue main-sequence, strong red giant branch, sub-dwarfs, RR Lyrae variables, and little interstellar matter. Population II objects in the Galaxy are found to occupy a large, spherical region with a strong central concentration. The kinematics of these objects is also striking as they tend to move in orbits of very high eccentricity round the galactic centre, in

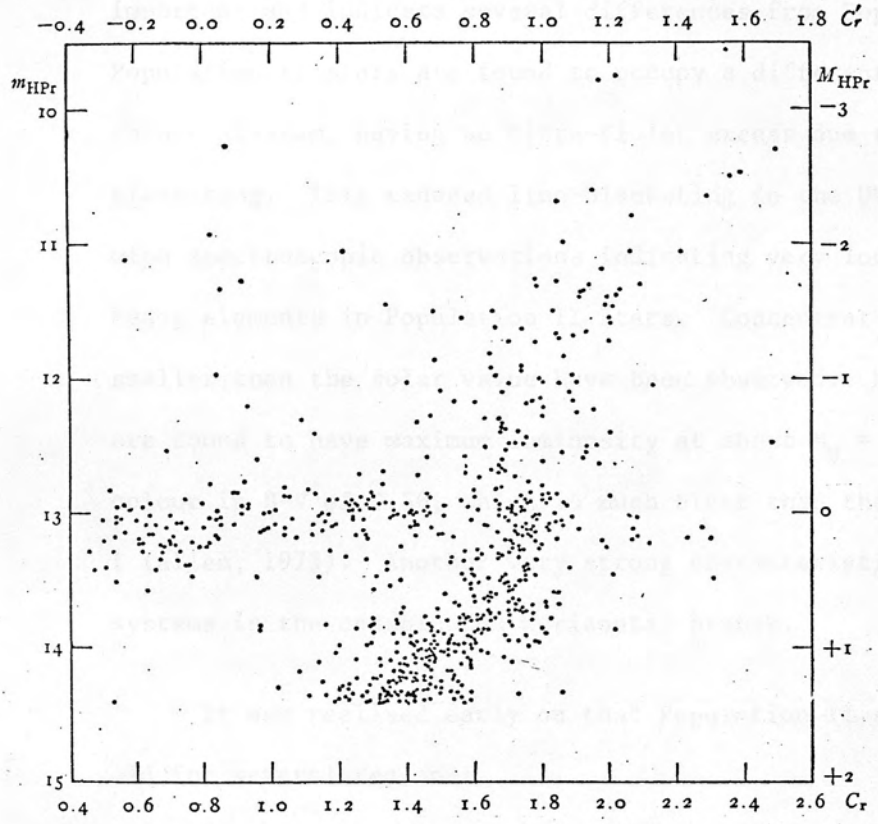

Fig. 1.3 Globular cluster M4.

contrast to the nearly circular orbits of Population I. As a result of their great height at maximum above the galactic plane, Population II stars observed nearby have very high velocities perpendicular to the galactic plane.

Photometric observations of Population II systems are extremely important and indicate several differences from Population I. Population II stars are found to occupy a different locus in the two-colour diagram, having an Ultra-Violet excess due to reduced line blanketing. This reduced line-blanketing in the UV is consistent with spectroscopic observations indicating very low concentrations of heavy elements in Population II stars. Concentrations up to 200 times smaller than the solar value have been observed. Population II stars are found to have maximum luminosity at about $M_V = -3$ and a mean colour in B-V of 0.56, which is much bluer than the 0.85 of Population I (Allen, 1973). Another very strong characteristic of Population II systems is the conspicuous horizontal branch.

It was realised early on that Population II stars must be very old for several reasons:

(1) The main-sequence of globular clusters ends at very faint levels and hence stars of low mass have had time in which to consume their central hydrogen and leave the main-sequence, since if each star can consume only a given fraction of its fuel and does so at a rate proportional to its luminosity, the main-sequence life-time must be given by

$$t_{ms} \propto \frac{M}{L} \approx M^{-3}$$

(2) If the formation of heavy elements occurs in stellar interiors then earlier generations of stars will have lower abundances, the material having had less processing and enrichment, thus Population II stars with very small abundances of heavy elements, must be the oldest objects remaining in the galaxy.

The allocation of sub-dwarfs to Population II, along with globular clusters, led Baade to suggest that the main-sequence of globular clusters was composed of sub-dwarfs and therefore lay fainter than supposed, implying that distances based on main-sequence fitting would be too large if referred to a Population I cluster such as the Hyades.

A great amount of work carried out in the following years was referred explicitly to Baade's Population criteria. Popper (1947) showed the spectra of globular cluster stars in M3 and M13 to be weak in CN absorption lines, providing support for the identification of globular cluster stars with local high velocity stars. The weakness of lines due to heavy elements in Population II stars was explained by Schwarzschild, Spitzer and Wildt (1951) as being due to a composition difference between Populations I and II, resulting from a primordial composition difference in the interstellar material from which the stars formed. Population II stars were seen as forming from the gas of the pre-galactic nebula, which was taken to be almost pure hydrogen.

The advent of accurate photoelectric photometry and the Mount Palomar 200" telescope, along with continued support for Baade's model

led to an increased effort in the study of globular clusters. Arp, Baum and Sandage (1952, 1953) studied M3 and M92 to very faint levels ($V \leq 19.5$) revealing the junction between the subgiant branch and the main-sequence, thereby establishing exactly how the Population II H-R diagram differs from Population I. Baum (1952, 1954), Sandage (1953), Johnson and Sandage (1956), followed up this work on faint photometry and Arp (1955) made a comparative study of seven globular clusters; M2, M3, M5, M10, M15 and M92. These developments were extremely important and established several points on the nature of globular clusters. It transpired that although globular clusters are qualitatively similar with respect to the important loci in the colour-magnitude diagram, viz. continuous locus leading from main-sequence to subgiant branch, red giant branch, asymptotic giant branch leading to a horizontal branch with RR Lyrae variables gap, they differ markedly in details.

The properties common to all globular clusters were found to be:

1. Colour range of the RR Lyrae gap.
2. Luminosity of RR Lyrae variables.
3. Heavily populated main-sequence with relatively few subgiants and thinly populated red giant branch.
4. Low abundance of heavy elements compared to the Sun, varying from a factor of 3 to 300 in mass fraction less than the solar value.
5. Luminosity function strongly peaked at $M_V = 0$ with an asymmetrical distribution on either side, increasing to fainter magnitudes, the peak being due to the horizontal branch.

Certain properties were found to vary from one cluster to another:

(1) Some clusters (e.g. M3) have a high density of stars on the red side of the horizontal branch with respect to the variable gap, while others (e.g. M92) have only blue stars (see Fig. 1.2b).

(2) The shape of the red giant branch is variable, most notably the slope.

(3) The colour of the sub-giant branch varies.

(4) Heavy element abundance as derived from spectra of bright stars varies between clusters.

(5) The absolute magnitude of the main-sequence at any given colour is variable, i.e. the globular cluster main-sequence is not unique, when the luminosity of the RR Lyraes is assumed constant.

Some of these characteristics were found to be correlated so that relatively metal rich clusters tend to have many red horizontal branch stars and a gently sloping red giant branch. Thus globular clusters were thought to belong to a one parameter family, with metal abundance as the variable property.

Sandage and Schwarzschild (1952) extrapolated from observed globular cluster C-M diagrams to derive semi-empirical evolutionary tracks for Population II stars. The results showed the general features of post-main-sequence evolution up to the giant branch.

Johnson and Sandage (1955) made a detailed study of several open clusters whose characteristics were successfully explained by the evolution of hydrogen burning main-sequence stars to the giant branch

on reaching a point where they have consumed a certain fraction of their hydrogen fuel, known as the Schonberg-Chandrasekhar limiting mass. Calculations of rates of burning (Hoyle and Haselgrove, 1959) allowed the determination of the age of any given cluster from the known luminosity, and hence mass, at the main-sequence turn-off which was found to be a monotonically decreasing function of age. However, the characteristics of globular clusters made it appear that a single parameter, viz. age, was insufficient to characterise a cluster C-M diagram. It was found that the turn-off luminosity of M67 was as faint as that of the globular clusters, which did not agree with the notion that the globular clusters are extremely old, the oldest stellar objects in the Galaxy. Also the shape of the sub-giant branch of M67 differed from that of the globulars, containing a region of negative slope, which the globular clusters do not possess. With the discovery that globular clusters are metal poor, it soon became generally believed that metal abundance was the required "second parameter". Sandage and Walker (1955) found that the stars of globular clusters fell on a different locus in the (B-V, U-B) plane than did Population I stars, the giants exhibiting an "Ultra-Violet excess", apparently being over luminous in the U range. In line with the evidence on metal abundance the authors attributed the effect to the fact that a low heavy element concentration could be expected to lead to a reduced line-blanketing in the stellar atmosphere, i.e. the redistribution of scattered light away from frequencies near to these of metal lines. The great density of metal lines in the UV leads to greater reduction in intensity in this range when a high metal content exists. This observed variation in the metal content led to model

calculations assuming a variety of metal abundances and it was found that the similarity in turn-off luminosity of old open clusters and globulars could be reconciled with a great age difference when metallicity was taken into account. It was in fact found that even though the time taken to reach turn-off for a given stellar model is independent of composition, the properties of stars near turn-off depend sensitively on abundance of carbon, nitrogen and oxygen, the more metal-rich stars being fainter and cooler. Thus for a given turn-off luminosity in more metal-rich clusters, stars at the turn-off will be more massive and hence the cluster will be younger (Simoda and Iben, 1968).

Determinations of metal abundance of globular cluster stars had been qualitative, based on apparent spectral type (Kinman, 1959) until the curve-of-growth analysis was applied by Helfer et al. (1959).

The stellar population concept of Baade had received considerable attention during this time, and the simple dichotomy between Population I and Population II was found to be too restrictive. Also it was found that the nucleus of M31 contained strong-lined stars and the nucleus of the Galaxy contained M giants, suggesting that galactic nuclei were not in fact pure Population II. Oort (1957), at the Rome Conference on the Stellar Population topic, presented a richer framework with five categories:

Extreme Population I; containing young OB associations, spiral arms, Cepheids, supergiants and a high gas and dust content.

Older Population I; A-type stars, strong-line stars, old open clusters.

Disc population; galactic nuclei, planetary nebulae normal weak-line stars.

Intermediate Population II; high velocity stars with $z < 30$ Km s^{-1}, long period variables.

Halo population; globular clusters, sub-dwarfs, RR Lyrae variables.

As well as luminosity, effective temperature, metal content, cluster richness etc. as criteria of population types, kinematics was given considerable weight in Oort's classification. The model of star and galaxy formation that resulted was one of an initial pre-galactic nebula of spherical symmetry, large extent ($D \lesssim 50$ kpc) and low angular velocity. At a point some 10^{10} years ago, the globular clusters condensed out and retained their initial distribution. The remaining gas however, condensed toward the galactic centre, increased in angular momentum, breaking the spherical symmetry and leaving axial symmetry only. A galactic disc thus formed, viscous damping and cloud-cloud collisions dissipated turbulent motions and a smooth, axial rotation resulted. Stars formed at this stage remained in the disc, performing circular orbits. Since all of the gas had become concentrated toward the galactic plane, star formation was then confined to this region, continuing at a decreasing rate until today, mainly in spiral arms where shock fronts are thought to precipitate star formation. The heavy element content of the stars and interstellar medium was correlated with this picture in terms

of a rapid metal enrichment following the initial burst of star formation, principally from supernovae, which were seen as essential for the production of r-process elements (Sm, Sb etc.). The succeeding generations of star formation would, on average, have higher heavy element abundance, the proportions changing little since the early period. Hence the kinematical properties of stars and the metal content are determined by age, the very old globular clusters and halo stars having low metal abundance, spherical distribution, highly eccentric orbits and large peculiar motions, while the youngest stars are confined to the galactic disc, have low peculiar motions, circular galactic orbits and high metal abundance.

This process was put on a dynamically quantitative basis by Eggen, Lynden-Bell and Sandage (1962) who found that the contraction time for the galaxy was extremely short, less than 2×10^8 years. Hence the initial burst of star formation was very short and intense, metal enrichment very rapid. Mixing of reprocessed material seems to have been slower, leading to a range in the metal abundances of globular clusters and to metal-poor disc stars, presumably formed from un-enriched gas which collapsed with the enriched material onto the plane. Hence the correlation between age and metal content has a large amount of dispersion and is unreliable as an age indicator in any specific case.

The evolution of the helium content of the galaxy is not as clear as that of the heavy elements. In general, He lines can only be observed in very hot stars (O and B spectral types) so that no Population II stars exist for which the abundance is indicative of the initial abundance and is measurable. Horizontal branch stars

are hot enough for He abundance determination but are highly evolved stars and have probably undergone mass loss so that the present He concentration would give little information on the primordial value. The mass-luminosity relation might also be used but very few Population II stars have known masses. It was initially assumed that He was produced in stellar interiors along with heavier elements, so that the He content of pre-galactic material was almost zero. However, there were problems with this view since massive stars are very inefficient at returning He to the interstellar medium. If most of the heavy elements are produced in supernova explosions, very little He would be produced as He may be expected to have been destroyed in earlier stages of the star's evolution. Iben (1969) from considerations of evolution rates in different parts of the H-R diagram of globular clusters derived a high He content ($Y \simeq 0.3$) similar to the Population I value. Cosmological calculations of the He in the post-big-bang material lent support to this high value. Observations of emission nebulae in extra-galactic systems (Peimbert, 1975) also suggest a near - "normal" value for Y. In Magellanic Clouds (Peimbert and Torres-Peimbert, 1974) despite a much smaller heavy element content (Van den Bergh, 1975) a He content almost as high as the galactic Population I value is observed. The observations are thus consistent with a cosmic He abundance of at least $Y \sim .22$, with individual objects exhibiting values up to .4 (Peimbert, 1975). Even though He abundance varies from one galaxy to another, there is no evidence that different objects within galaxies have different He content apart from the anomalous "He-stars".

The problem of determining the dimensions and age of the Galaxy via the photometry of globular clusters had been complicated by the discovery of the identity of sub-dwarfs and Population II main-sequence stars. It thus become necessary to calibrate the main-sequence luminosity at a given colour index as a function of metal abundance, or same parameter thereof. Eggen and Sandage (1969) studied nearby sub-dwarfs of known parallax and Ultra-Violet excess and found a strong correlation between UV excess and difference in luminosity with respect to the Hyades main-sequence. Using theoretical estimates of line-blanketing effects (Eggen and Sandage, 1959, Melbourne, 1960) it was found that all of the sub-dwarfs could be translated onto the Hyades main-sequence by compensating for the effects of low metals. Hence it was established that sub-dwarfs do not form a distinct stellar species and the Population II main-sequence in the (L,Te) plane is unique. The method was extended by Wildey et al. (1962) and the shifts in V, B-V and U-B due to line-blanketing effects were calibrated as functions of U-B excess. This work led to a renewed effort in the photometric study of globular clusters (Sandage, 1964) and in particular of luminosity of RR Lyrae variables and its dependence on composition, age, mass, temperature and period. Tifft (1963a) reported a correlation between period and luminosity of SMC RR Lyraes, suggesting the observed spread in period to be due to a mass and age spread, further suggesting the luminosity of the globular cluster horizontal branch to be time dependant. Christy (1966) in a tour-de-force study explained the theoretical aspects of RR Lyrae pulsation, using the structure model of Faulkener (1966). Among his conclusions were

(1) The blue edge of the instability strip increases in temperature with increasing helium abundance.

(2) An He mass fraction of 0.3 best fits the observations.

(3) The absolute magnitude of RR Lyraes varies from $M_{BOL} = 0.57$ for very metal-poor stars to $M_{BOL} = 0.96$ for slightly metal-poor stars.

(4) Masses of RR Lyrae stars are approximately 0.5 M_o.

The model of RR Lyrae variables used was that of a post-giant branch star with shell H-burning and core He-burning and an He ionization zone in the outer regions acting as working material. Studies of periods, amplitudes and light curves of RR Lyrae variables led to the Bailey-type classification scheme, with type a and b variables having long periods ($\sim$0.6 days), large amplitude and asymmetrical light curves, while type c variables pulsate in the first harmonic.

On plotting the number of RR Lyraes in a globular cluster as a function of period it is found that the clusters fall into two distinct classes, the Oosterhoff classes. Class I clusters are observed to have a mean period for a b-type variable of $\sim$d.55, while class II clusters have (Pab) $\sim$ d.65. Oosterhoff class is found to be well correlated with metallicity (Arp, 1955), class I being of higher metallicity (e.g. M3) and class II having very low metallicity (e.g. ω Cen, M15).

The available photometric data for globular and old open clusters were collected and assessed (Sandage and Eggen (1969); Sandage (1969); Sandage (1970)) and the implications for galactic evolution explored.

Fig. 1.4 shows the schematic colour-magnitude diagrams of a sample of open clusters with the age scale for given turn-off luminosity attached. It can be seen that a large age-range is observed in the galactic open clusters, from 10^7 to 5×10^9 years. Patenaude (1978) has recently recalculated open cluster isochrones and determined ages for a sample of old open clusters, including NGC2477 and NGC2420, the colour-magnitude diagram of the latter being shown in Fig. 1.5.

The globular clusters studied were M3, M13, M15 and M92. The distances to these clusters were estimated by main-sequence fitting, leaving the luminosity of the RR Lyraes free. It was found that the metal-rich cluster M3 had brighter variables than the metal-poor M92 and M15, contrary to the theoretical result of Christy. Sandage explained this as being due to poor photometry, and merely observed that the mean absolute magnitude of the RR Lyraes was $+0^m.6$, agreeing with Christy. Other conclusions from this work were:

1. The average age of the globular clusters is approximately 11.5×10^9 years (interpreting observations using the calculations of Iben and Rood, 1970).
2. The age spread of globular clusters is less than 10^9 years.
3. Magnitude difference between horizontal branch and main-sequence turn-off is equal for M3, M15 and M92 to $3^m.4$.
4. Average helium abundance is approximately 0.3.

M13 was exempt from many of these results since it was found to behave anomalously. In particular, its relatively high metallicity

$$\left[\frac{Fe}{H}\right] = \log\left(\frac{Fe}{H}\right) - \log\left(\frac{Fe}{H}_{solar}\right) = -1.4$$

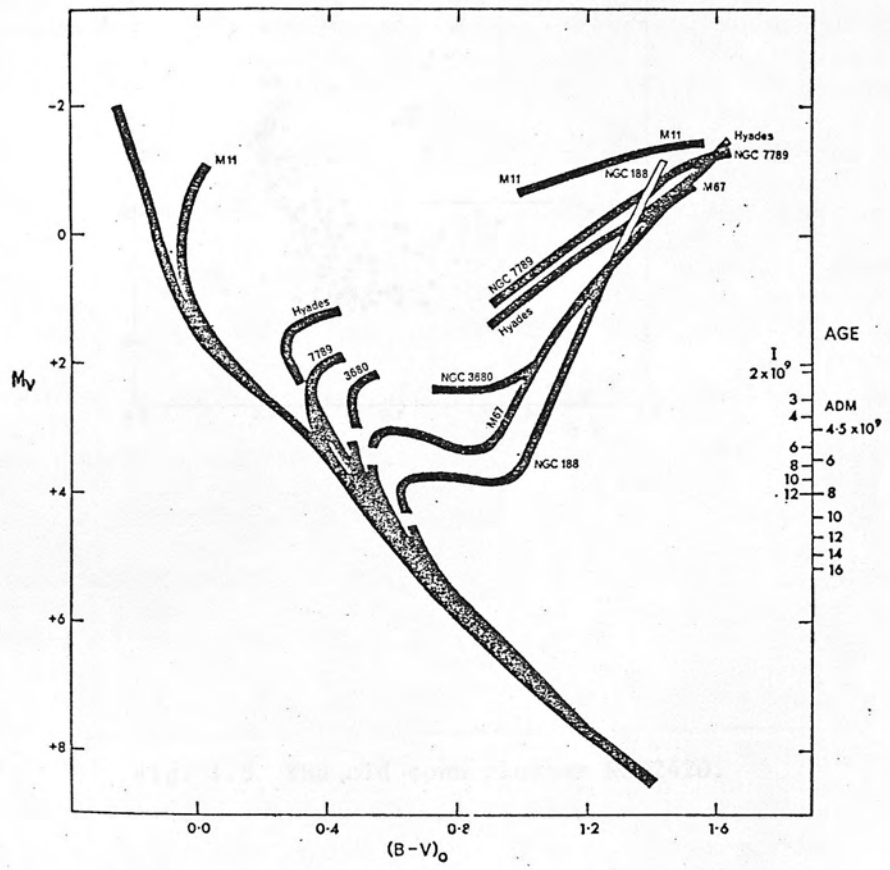

Fig. 1.4 A sample of open clusters of various ages.

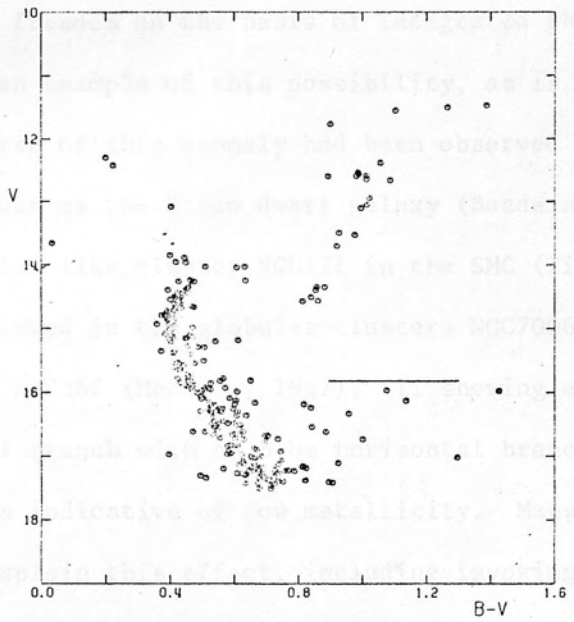

Fig. 1.5 The old open cluster NGC2420.

seemed incompatible with the highly populated blue horizontal branch. Van den Bergh (1967) had earlier suggested the existence of a further degree of freedom on the basis of integrated photometry. M13 (Sandage, 1970) is an example of this possibility, as is NGC288 (Cannon, 1974). The converse of this anomaly had been observed in extragalactic systems such as the Draco dwarf galaxy (Baade and Swope, 1961) and the globular-like cluster NGC121 in the SMC (Tifft, 1963b), and was later observed in the globular clusters NGC7006 (Sandage and Wildey, 1967) and NGC362 (Menzies, 1967), all showing a densely populated red horizontal branch with no blue horizontal branch but exhibiting other parameters indicative of low metallicity. Many attempts have been made to explain this effect, including invoking helium abundance variations (Sandage and Wildey 1967; Hartwick, 1968), CNO variations (Hartwick and McClure (1972), Hartwick and Van den Bergh (1973)) but no clear explanation has emerged so that at present a detailed understanding of horizontal branch morphology is lacking. At present it would appear that progress is most likely to come from the accumulation of detailed observational results to constrain the abundant models.

A crucial step is the study of globular clusters in extragalactic systems, which may be expected to have had an entirely different evolutionary history in terms of dynamics, formation rate and chemical enrichment and which may exhibit a greater range of age than clusters in the Galaxy. It is thus apparent that the Magellanic Clouds play an important role in this respect, allowing detailed study of star clusters to well below the horizontal branch, so that it is essential to our understanding of stellar structure and evolution, as well as to our knowledge of the Clouds themselves, and of galaxies

in general, to determine how clusters in the Clouds differ from those in the Galaxy and how they are similar.

1.2 Interpretation of Cluster Colour-Magnitude Diagrams

A summary is presented in the following paragraphs of the useful information obtainable from a study of star clusters. Methods of obtaining information are manifold but can basically be summarised as:

(a) Distances, both within the Galaxy and to external systems

(b) Ages

(c) Chemical composition of component stars

(d) Mass distribution function, of interest in star formation theories

(e) Interstellar reddening, giving information on the interstellar medium.

(a) Cluster distances can be calculated in several ways depending on the distance to the cluster. A hierarchy of distance indicators has been constructed, based on geometrical measures for nearby clusters, the known distance to which is then used to calibrate the photometric distance indicators.

(α) Moving cluster method. Assuming a nearby cluster ($d \leq 200$ pc) to be a rigid body, a relative motion of the whole cluster and the Sun will cause a proper motion for each star, all the proper motion vectors pointing toward a convergent point or away from a divergent point,

depending on whether the Sun is moving away from or toward the cluster, respectively. Combining the proper motion data, the observed angular diameter of the cluster and the mean radial velocity allows the geometry to be solved and the cluster distance found.

(β) Variable stars. The period-luminosity relations for certain classes of variable, such as Cepheids, RR Lyraes, etc., has proved extremely valuable in the determination of distances. In order to make use of the method, the relation must be calibrated. In the case of Cepheids, the calibration was performed by observing stars in the Magellanic Clouds, assuming all cloud members to be equidistant. However, a zero point must be obtained and this must be done by finding the distance to a similar variable by a more direct method such as (α).

(γ) Main-sequence fitting is another widely used procedure, at present confined to clusters in the Galaxy. The principle behind the method is the fact that the luminosity-temperature relation for main-sequence stars of a similar composition is unique, so that if the main-sequences of two clusters differ in apparent magnitude at any given temperature, one can ascribe the difference to distance effects alone, and use the inverse square law of light to calculate the distance ratio, according to

$$\Delta m = 5 \log \frac{R_1}{R_2}$$

One of the clusters must be of known distance, found by a geometrical

method. For Population I objects, the Hyades is generally taken as reference, the distance being known by the moving-cluster method. For Population II clusters the procedure must be modified to take account of line-blanketing effects. Such effects are found from knowledge of the UV excess $\delta(U-B)$ (Wildey et al., 1962) and the observed colours and magnitudes corrected (Sandage, 1970). The corrected main-sequence may then be fitted to the Hyades.

(δ) Cluster diameter can be used to determine an approximate cluster distance using the method of Trumpler (1925) who found a good correlation between richness and central concentration of open clusters and their diameters. He then used this correlation to derive diameters for clusters, and thus distances. Arp (1956) more recently used a similar technique.

(b) Age determination is possible by inspection of the colour-magnitude diagram. A cluster of zero age will possess only a main-sequence, extending to very luminous blue stars. As the cluster ages, the bluest and brightest stars evolve most rapidly, leaving the main-sequence to become giants and supergiants. Thus the blue end of the main-sequence tends monotonically to become redder and fainter with time. Calibration of the main-sequence turn-off luminosity as a fraction of age is achieved using stellar evolution calculations. An interpolation formula used by Sandage (1970) derived from calculations by Iben and Rood (1970) for Population II models, is given by

$$\log T = \frac{\log \frac{L_{To}}{L_{\odot}} + (0.92 + .11 \log Z)Y + .219 \log Z - .79}{.10 \log Z - 0.59}$$

and is valid in the ranges $0 \leq Y \leq .3$

$$10^{-5} \leq Z \leq 10^{-3}.$$

(c) The evolution of the colour-magnitude diagram depends not only on age, but also on the composition of the member stars, so the form of the diagram can give information on helium and heavy element abundances. As mentioned earlier, many parameters of composition have been used.

(α) ΔV, the visual magnitude difference between the horizontal branch and the giant branch in globular clusters measured at $(B-V)_o = 1.4$. ΔV decreases with increasing metallicity, from $3^m.3$ for the metal-poor cluster M92 (Sandage, 1970) to $2^m.0$ for the metal-enhanced 47 Tuc (Hartwick and Hesser, 1974).

(β) The unreddened colour of the subgiants also has been found to depend on composition, being bluer for lower Z. This effect, however, is complicated by the fact that the subgiant colour index increases as mass decreases, and hence as the age of the cluster increases (Iben, 1967), so that an unambiguous composition determination is not possible.

(γ) The length and slope of the Hertzsprung gap, lying between the main-sequence and the subgiant branch, in young clusters has been found (Schlesinger, 1969) to be well correlated with heavy element abundance. Metal-rich clusters are found to have a larger gap and negative slope.

(δ) The morphology of the horizontal branch of globular clusters has been employed extensively in composition determinations. However,

as discussed above, a unique relation between horizontal branch morphology and chemical composition is no longer believed to exist.

(ε) Since the pulsation of RR Lyrae variables depends on the existence of a partial helium-ionization zone at a suitable mass-fraction below the surface, the surface temperature above which pulsation is no longer possible (the blue edge of the RR Lyrae gap) may be expected to depend on the helium abundance in the outer atmosphere through the opacity, as well as on luminosity and mass. An expression derived by Christy (1966) and used by Sandage (1969) to obtain helium abundance is given by

$$Y = 1.6(B-V)_{BE} - 0.34\frac{M}{M_\odot} - .16\, M_V + .901$$

where $(B-V)_{BE}$ is the intrinsic deblanketed colour of the blue edge of the variables gap.

(ζ) Ultra-Violet excess has been used to determine heavy element abundances, using the calibration of Wallerstein and Helfer (1966). The UV excess is found by plotting the (U-B, B-V) diagram for a cluster along with the standard Population I relation and finding the difference in U-B between the two at a chosen value of B-V.

(η) Iben (1968, 1969) successfully applied a method for the determination of helium abundance based on the lifetimes of stars along the giant branch and the horizontal branch. By counting the relative numbers of stars on the two branches, an estimate of the helium abundance may be obtained.

(θ) Intermediate-band photometry has proved valuable in abundance determinations, the most widely used being the DDO system (McClure and Van den Bergh, 1968).

(d) Because the light from stars is dimmed and reddened by galactic dust, the extent of this must be determined before the observed properties of the star can be converted into the intrinsic properties. Photometry of clusters also gives information on the interstellar medium itself. Simple dust-particle scattering models are used to deduce relationships between absorption in the V spectral band and reddening in B-V and U-B etc., so that only one free variable remains. On fitting to observations it is found that the relations

$$A_V = 3\ E(B-V) \qquad \text{(i)}$$

$$E(B-V) = .72\ E(U-B) \qquad \text{(ii)}$$

are valid for early-type stars, while the relation

$$E(B-V) = 1.0\ E(U-B) \qquad \text{(iii)}$$

is used for late-type red giants.

The observationally determined parameter of scattering is usually the reddening in B-V, which can be found for a cluster from the plot of B-V versus U-B. The relation (ii) above is used to translate the cluster locus onto the standard Population I locus (Johnson and Morgan, 1953) and the required shift gives the reddening.

In the case of Population II stars, the situation is complicated by the UV excess, which removes the cluster locus from the standard even in the absence of reddening. In these cases, several methods

have been used, including:

(i) The position of the bluest horizontal branch stars in the two-colour diagram may be used. These stars do not have observable UV excess, due to the fact that metal lines do not contribute to the spectra of early-type stars of either Population I or Population II since all metals are highly ionized, hence fitting to the standard sequence gives a reasonable assessment of the redeening (Sandage, 1964, Cannon and Stobie, 1973).

(ii) Sandage (1969) used the known high temperature cut-off for the sub-dwarfs of the galactic halo ($B-V \approx .36$) to determine the reddening of globular clusters, assuming the cluster to have undergone the same reddening.

CHAPTER II

THE MAGELLANIC CLOUDS

2.1 The Structure of the Small Magellanic Cloud

The Magellanic Clouds have both been classified (de Vaucouleurs et al., 1964) as of type SB(s)m, i.e. they are barred spiral galaxies with spiral arms emanating from the Bar and exhibiting the characteristic asymmetry of which they are archetypes, viz. a dominant asymmetric spiral arm with some less prominent arms and spiral 'arcs' remote from the Bar.

The physical sub-systems of the SMC have been defined by de Vaucouleurs and Freeman (1973), and by Westerlund (1972), in the former case with regard to morphology and in the latter, with regard to stellar content.

The SMC is believed to be a highly flattened system seen at an inclination of 45° and rotating about an axis orthogonal to the plane. From a study of surface photometry, star counts, direct photography, cluster distribution and radial velocities, de Vaucouleurs and Freeman have isolated the following four sub-systems of the SMC:

A. The Bar, a densely populated region subtending a solid angle $2^{\circ}.5 \times 1^{\circ}$ is the most prominent optical feature, with position angle 45° and is a typical galactic bar. It is tapered as seen on the sky, being narrower at the northern end.

B. In this category are included the spiral arms. The dominant

spiral arm, of length approximately 2^{o} (2 kpc), is to the north-east, adjacent to the narrow end of the Bar.

C. A loop of diameter 7^{o}, foreshortened to an ellipse, is observed to lie to the south-west of the Bar. This feature may be continued round the Bar or may be localised to the south-west, as the large inclination makes it difficult to observe the opposite end.

D. The Wing, an elongated region of length 6^{o}, extending to the east toward the LMC forms a unique object. There is some evidence of related structure in the Bar. Two "knots" of stellar condensation are seen in the Wing at distances of 3^{o} and 5^{o} from the Bar.

The relative positions of the sub-systems are indicative of the lack of symmetry of Magellanic-type galaxies, the spiral arm lying outside the plane of the loop and the centroid varying greatly with the class of object used to determine it.

Westerlund (1972) also discusses four sub-systems of the SMC, the stellar content of which are as follows:

1. The Bar shows evidence of an extreme Population I component as well as older Population I. OB associations, young clusters and HII regions form the extreme Population I objects, while the older examples are Cepheids and Ib supergiants. The existence of a young stellar component and also of large amounts of neutral hydrogen (Hindman, 1967) suggest that the Bar is a region of present-day star formation. Ardeberg and Maurice (1977) and Azzopardi and Vigneau (1977) have studied the structure of the SMC through the distribution of supergiants.

Osmer (1973a), Osmer (1973b) and Przybylski (1976) have also studied these objects individually in abundance determinations, which indicate that young SMC objects are systematically lower in heavy elements than similar objects in the Galaxy. The same conclusion has been reached through studies of many types of object, including HII regions (Peimbert et al.,(1976), Dufour and Harlow (1977), Pagel et al., (1978)) and planetary nebulae (Dufour and Killen, 1977). Brück and Marsöglu (1978) have presented the colour-magnitude diagram of the NE extension of the Bar which exhibits a young blue main-sequence indicating recent star formation. Sanduleak (1969) has studied the distribution of bright stars in the Bar and correlated this with that of HI.

2. The Wing of the SMC appears to consist almost exclusively of extreme Population I, including a large neutral hydrogen envelope, observed at 21 cm (Hindman et al., 1963). Westerlund (1964) performed star counts on the bright stars near NGC602 and in a field in the Wing further from the Bar. On this basis the observed red component was found to be a foreground galactic contribution, only blue stars being SMC members. Brück (1978) finds the Wing to be composed of a young stellar population.

Morgan and Nandy (1978) obtained extreme UV observations of the SMC Wing and were able to reproduce the observed spectral indices with their assumed luminosity function and reddening law.

Many OB associations are found in the Wing along with HII regions, Ia supergiants and blue globular clusters (e.g. L72, Westerlund, 1964).

3. The central system of the SMC, a flattened region of diameter 7^{o}

centred to the south-east of the Bar, is thought to be the analogue of the galactic disc and contains representatives of both old Population I and Population II according to Arp (1958a), who asserts red giants as being characteristic of Population II while open clusters and planetary nebulae are characteristic of old Population I. Carbon stars are found in large numbers in the central system, in many cases in association with clusters (Lloyd Evans, 1978a, Lloyd Evans, 1978b). Blanco et al. (1978) find the relative number of carbon to M-type stars much larger in the SMC than in the LMC which is in turn much higher than in the galactic centre. No conclusive explanation is offered for this effect, although it is suggested that it may be due to lower heavy element abundance. Feast and Lloyd Evans (1973) suggest that carbon stars may be an indicator of age, and in particular that intermediate-age populations may possess C stars in large numbers. This is corroborated by observations of C stars in known intermediate-age clusters in the Galaxy, such as NGC2477.

4. The SMC is believed to be surrounded by a halo similar to that of the Galaxy. The most clear-cut candidate for a halo species is the RR Lyrae variables discovered in large numbers by Graham (1975). The cluster NGC121 appears also to contain three RR Lyraes (Thackeray, 1958) and was believed by Tifft (1963a) to be a classical globular cluster, as found in the galactic halo. If this identification is correct, NGC121 is the only known true globular cluster in the SMC. It is also the most distant of the red clusters from the optical centre of the Galaxy.

Brück (1978) finds the halo by star counts to be approximately

circular on the sky and of diameter 10^{o}. Graham (1973) discusses the old population in the Magellanic Clouds.

2.2 Magellanic Cloud Clusters

An understanding of the properties and parameters of star clusters has proved valuable in studies of the Magellanic Clouds system. Baade originally suggested that the LMC consisted of almost pure Population I and the SMC of almost pure Population II. However, the C-M diagram of the SMC field was studied by Schilt, Epstein and Hill (1955) who found many of the stellar components of the Galaxy present, bright blue main-sequence, red giant branch and supergiants. Gascoigne and Kron (1952) found a sharp dividing line between integrated colours of globular-like blue and red clusters (Fig. 2.1). The SMC was found to contain mainly red clusters and the LMC approximately equal numbers of red and blue. Kron (1956) classified 69 clusters in the Clouds according to integrated colour, diameter and central concentration. Further catalogues were compiled by Lindsay (1958), Shapley and Lindsay (1963), Westerlund and Glaspey (1971), Hodge and Wright (1974) and Brück (1975).

Arp (1958b,c; 1959a,b) carried out a systematic photometric study of Cloud clusters. In the SMC Arp observed NGC419 and NGC361, which showed characteristics of old clusters, well developed red giant branch, no Hertzsprung gap, with an estimated age of $1\text{-}5 \times 10^{9}$ years, but with both exhibiting a young field component. NGC458 proved to be a "blue globular cluster" with a large number of yellow giants and a well-defined Hertzsprung gap, embedded in a field similar to that near NGC419 and NGC361. The dissimilarity between the CMD of

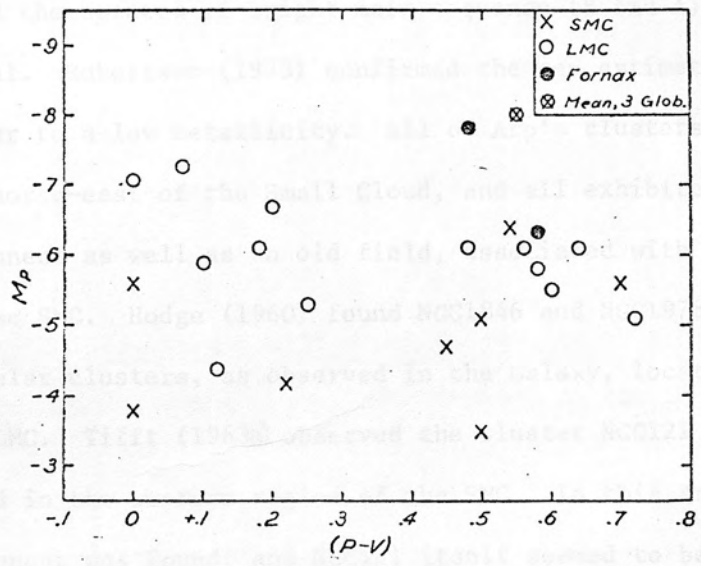

Fig. 2.1 Integrated CMD for various clusters.

NGC458 and that of clusters in the Galaxy of similar age led Arp to propose that it might have low metallicity. Schlesinger's (1969) theoretical cluster-fitting study supported this conclusion, principally on the grounds of the very blue giant sequence, and an age of 2×10^7 years was estimated. NGC330 exhibited similar features, young blue main-sequence, but a narrower Hertzsprung gap and more giants. Arp suggested NGC330 to be metal-poor also, but Feast (1964) found the spectra of bright main-sequence (B and A) stars to be normal. Robertson (1973) confirmed the age estimate and gave slight favour to a low metallicity. All of Arp's clusters lay to the east and north-east of the Small Cloud, and all exhibited a young field component as well as an old field, associated with the central system of the SMC. Hodge (1960) found NGC1846 and NGC1978 to be normal globular clusters, as observed in the Galaxy, located in the halo of the LMC. Tifft (1963a) observed the cluster NGC121 and surrounding field in the western region of the SMC. In this area no young field component was found, and NGC121 itself seemed to be a typical globular cluster, with strong red giant branch. The giant branch of the field showed a large scatter in luminosity which Tifft attributed to a range of metallicity in the various components. However the RR Lyraes showed no such dispersion, which led him to conclude that the RR Lyrae luminosity is approximately independent of metallicity. Arp (1962) and Arp and Cuffey (1962) studied the slightly metal-poor intermediate-age open clusters NGC2158, 752 and 7789 in the Galaxy, in order to compare them with Magellanic Cloud clusters. Gascoigne (1966) chose these as prototypes for his intermediate-age group in a study of thirteen populous Cloud clusters, which he classified as follows:

1. True globular clusters. Included in this category were NGC1466, 1841, 2257 in the LMC and NGC121 in the SMC. The criterion of these objects was whether or not they would be included in Hogg's (1963) catalogue of globular clusters.

2. Intermediate age. To this class were assigned Lindsay 1, Kron 3, NGC339, 361 and 419 all in the SMC.

3. LMC type. Three LMC clusters were assigned together, NGC2209, 2231 and Hodge 11. These clusters had more faint blue stars and fewer giants than the intermediate-age group, and it was tentatively suggested that they were very old clusters, the faint blue stars being horizontal branch stars.

4. NGC1873 was classified on its own, being similar to the intermediate-age SMC group but belonging to the LMC.

A further category of cluster in the LMC is that of young globular cluster, to which group have been assigned NGC1818, 1866 and 2100 (Gascoigne, 1971).

Schematic results for several clusters in the Wing of the SMC were presented by Westerlund (1964) who found a young blue main-sequence component. He also found that the cluster L113 resembled a classical globular. Walker (1970, 1971, 1972a, 1972b, 1974, 1979a, 1979b) performed electronographic photometry on the clusters K3, NGC2209, 2257, 419, 1866, H11 and NGC2231, respectively, confirming the observations of Gascoigne but with different interpretations in some cases. He suggested K3 to be similar to the metal-rich galactic globular cluster 47 Tuc, with a strong red giant branch extending very

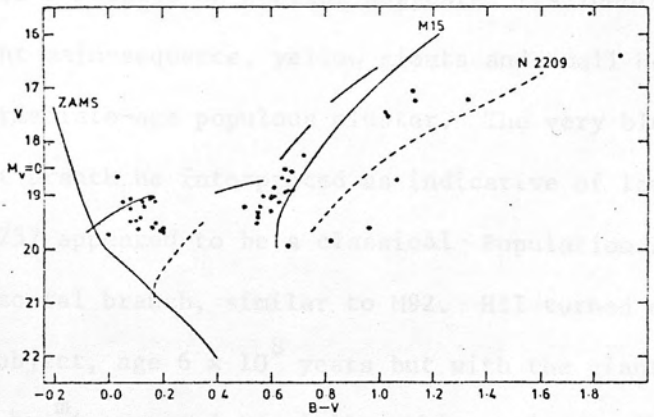

Fig. 2.2 CMD for the LMC cluster H11.

far into the red and a short red horizontal branch. However this identification was thought not to be certain as the cluster could also be classed along with M13 if the HB stars were in fact asymptotic giant branch stars. Walker's results cast doubt on the identification of NGC419. He concluded that the cluster could be either Hyades-like or an old globular cluster. The integrated spectrum was found to be similar to that of a metal-poor globular cluster, unlike that of K3. Walker's results on NGC2209 suggested its identification, with a bright main-sequence, yellow giants and small Hertzsprung gap, as an intermediate-age populous cluster. The very blue extension of the giant branch he interpreted as indicative of low metallicity. NGC2257 appeared to be a classical Population II system with a blue horizontal branch, similar to M92. H11 turned out to be an intermediate-age object, age 6×10^8 years but with the giants displaced to the blue by $^m.4$ compared to similar objects in the Galaxy. NGC1866 was found to be even younger at an age of 6×10^7 years. NGC2231 was similar to NGC2209 with an age of 10^9 years.

Freeman and Gascoigne (1977) present photographic photometry of H11, their interpretation of which is that H11 is either of intermediate-age or is an old globular cluster, the ambiguity arising from the identification of the group of faint blue stars ($V \geq 19$, $B-V \approx .1$, see Fig. 2.2).

Penny (1976) remeasured NGC1466 electronographically and confirmed the identification as a normal globular cluster. Two colour plots indicated a large UV excess, implying that the cluster is very metal-poor. Gascoigne et al. (1976), using plates from the AAT, have confirmed

the identification of NGC2209 as an intermediate-age ($\sim 8 \times 10^8$ years) cluster. They derived a metal-abundance from the observed colour of the giants, which was very low. This abundance was challenged by Gustaffson et al. (1977) who pointed out that the giants in NGC2209 were blue because of age rather than because of metallicity, this leading to a metallicity only slightly less than that of the Sun. Harris and Deupree (1976), in a theoretical cluster-fitting study, found the observations of young clusters in the Clouds to be well explained by a metal abundance smaller than the value in the Galaxy, $Z \sim .01$ as compared with $Z_o \sim .03$. Fig. 2.3 shows the photographic colour magnitude diagrams of K3 and NGC2257 derived by Gascoigne (1978) and suggests the appearance of faint blue stars in K3 while NGC2257 is clearly a classical globular cluster.

Fig. 2.4 shows the integrated colours of a sample of clusters (from Freeman and Gascoigne, 1977). An interesting group exists at $B-V \approx .7$, where the range of U-B is large. Janes and Carney (1977) have observed the SMC cluster NGC330 and agree with Arp's conclusion that it is young, with a bright blue main-sequence. Chun (1978) has derived masses for several Magellanic Cloud clusters and derived mass-light ratios. The masses calculated are typical of globular clusters in the Galaxy ($10^4 \leq M/M_o \leq 10^5$), and mass-light ratios of the red clusters observed agreed with those of galactic objects. Also the mass-light ratios of blue objects were found to be consistent with the known colour-magnitude diagrams. Grindlay (1978) has suggested K3 as the optical counterpart to the X-ray source 4U 0026-73, although the X-ray error box includes several other SMC clusters.

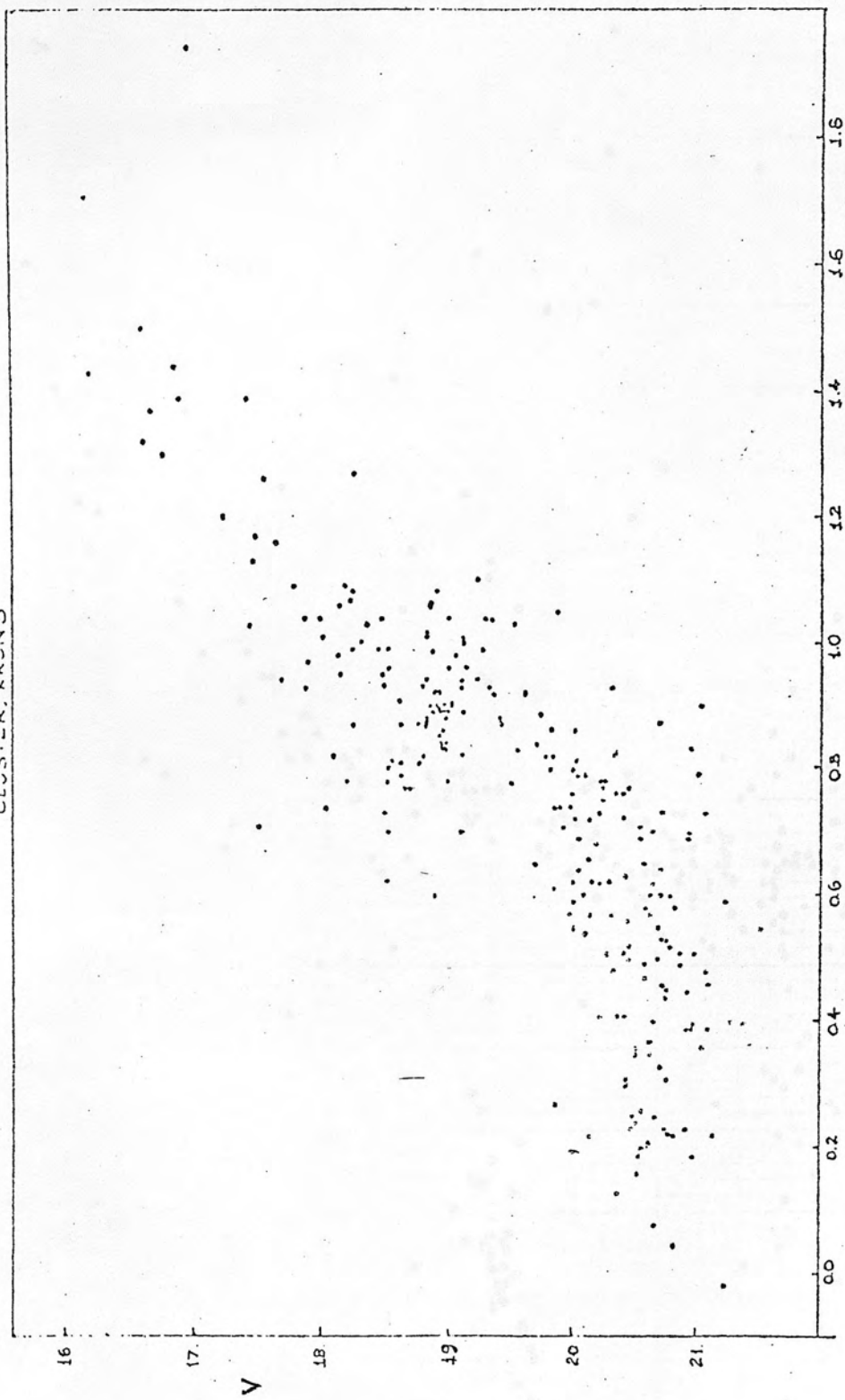

Fig. 2.3a SMC cluster K3.

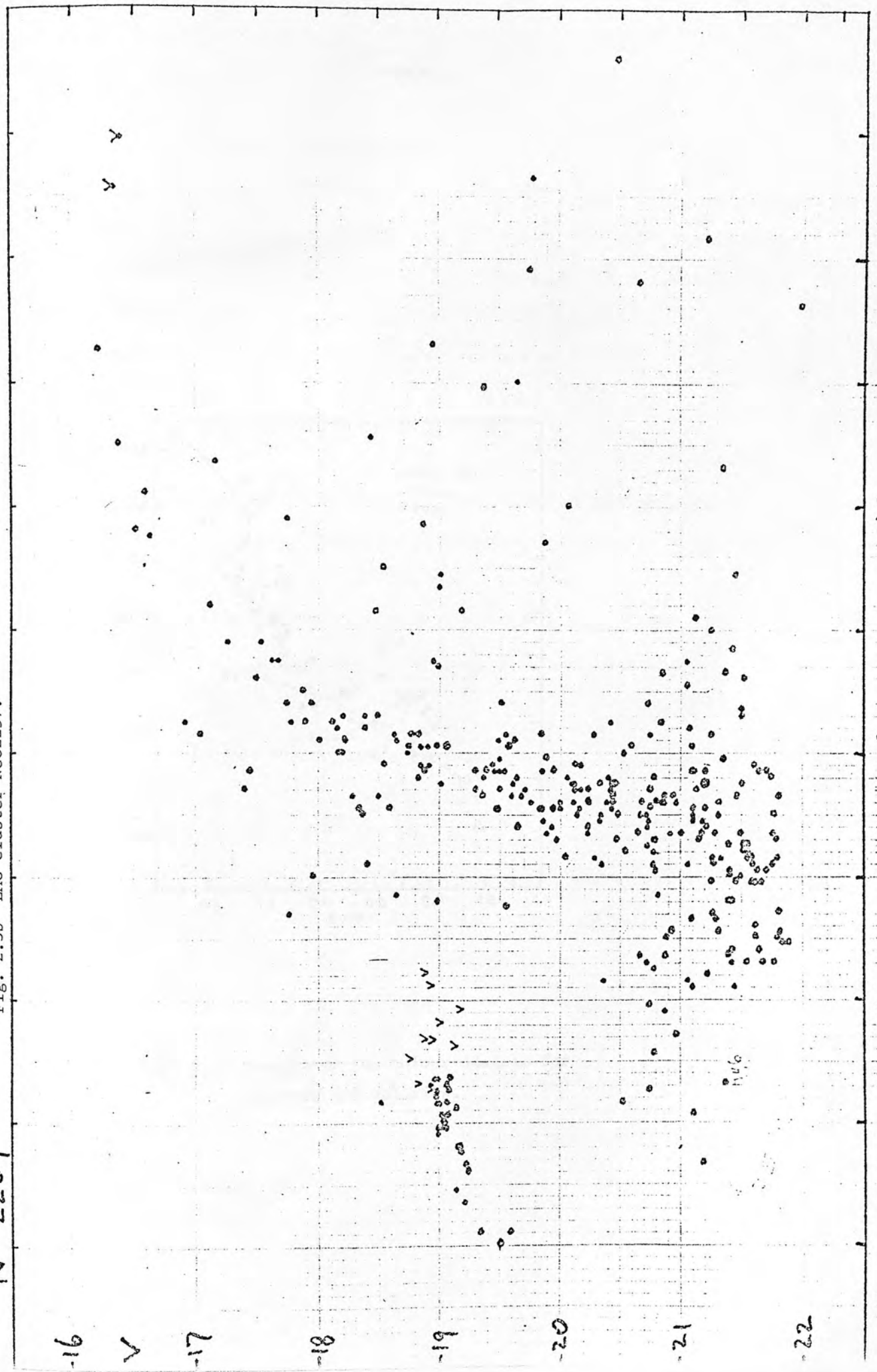

Fig. 2.3b LMC cluster NGC2257.

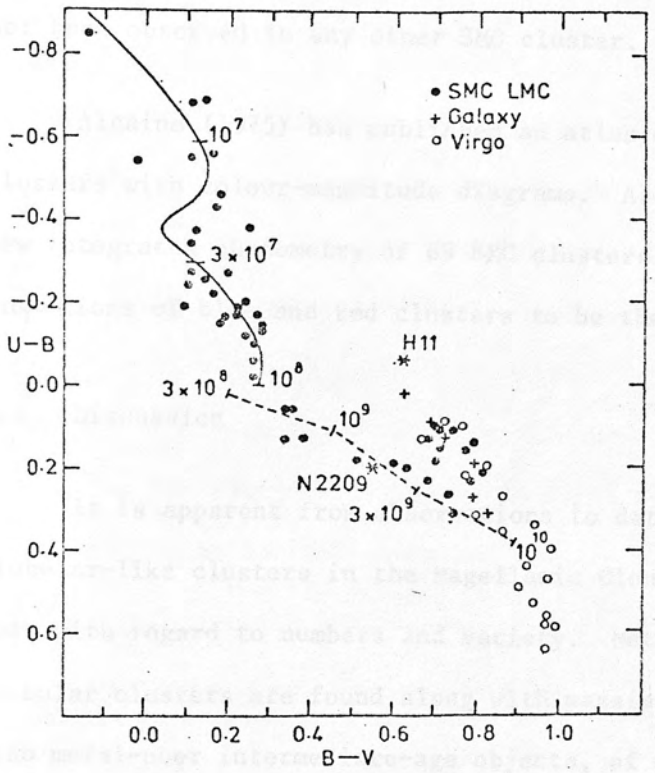

Fig. 2.4 Integrated two colour diagram for clusters and galaxies.

An extensive study of 20 SMC clusters was carried out by Kontizas (1976) using plates from the UK 48" Schmidt Telescope, who found an old component of the SMC, the age of which was judged to be between 1 and 5 billion years, to be widely distributed over that Galaxy. A group of apparently old clusters was studied, some of which showed evidence of horizontal branch structure, e.g. L11, L13, L15. L13 was suspected of having a blue horizontal branch, which has not been observed in any other SMC cluster.

Alcaino (1975) has published an atlas of Magellanic Cloud clusters with colour-magnitude diagrams. Alcaino (1978) presents new integrated photometry of 69 SMC clusters and finds the relative proportions of blue and red clusters to be the same as that in the LMC.

2.3 Discussion

It is apparent from observations to date that the system of globular-like clusters in the Magellanic Clouds is extremely rich, both with regard to numbers and variety. Metal-poor classical globular clusters are found along with massive young clusters and also metal-poor intermediate-age objects, of which the Galaxy possesses none. The mean level of heavy element enrichment in clusters, emission nebulae and bright stars also appears to be lower than in the Galaxy, and many clusters are observed to lie in fields of a similar population type, so that mixing appears to be less efficient in the Clouds.

Thus it seems that the history of star and cluster formation and of chemical and dynamical evolution has been very different in the Magellanic Clouds from that in the Galaxy. In the Galaxy, star formation

and metal enrichment were very intense and recent clusters formed have been of the low mass, open, metal-rich type. In contrast to this situation, the Magellanic Clouds seem to have experienced a relatively uniform rate of star formation and massive globular-like clusters have formed continuously right up to the present. Thus whatever conditions are required for the formation of massive clusters exist at present in the Clouds.

The globular-like clusters in the Clouds, of which there are many, thus form an extremely important source of information on the formation and evolutionary history of the Clouds. Thus it is necessary to obtain photometry which will allow the determination of age, chemical composition and position (including distance) for as many Cloud clusters as possible. Because clusters are numerous in the Clouds, a large number must be observed to form a representative sample and the photometry must be as faint as possible, at least to the level of the horizontal branch and preferably to the main-sequence.

CHAPTER III

INSTRUMENTATION

3.1 Photographic Plates

The primary detector used in this investigation is the photographic plate, all others being employed solely to calibrate the response of the photographic emulsion. Prime focus plates taken on the Anglo-Australian telescope were used. Table 3.1 lists the general specifications for such plates (AAT Users Guide) and table 3.2 gives details of the actual plates used. The final column in table 3.2 gives an estimate of the limiting magnitude of each plate, as estimated by eye using a small lens. This figure is slightly brighter than the measurement limit for a microdensitometer but is a useful guide.

The reasons for using photographic plates as detectors were principally economy and efficiency. The information storage capacity of the AAT plates is such that approximately 50,000 images may be recorded to a limiting magnitude of B $\approx$ 22 in 40 m. In a similar time using a photoelectric photometer only 20 or so images may be measured as discussed in section 5. Thus photographic emulsions are much more efficient at using telescope time. However they require a great deal of time and effort away from the telescope. This effort, which involves the acquisition of standard images in the field of interest, measurement of programme and standard stars using a photometer and reduction and transformation of these measures to useful results will be discussed in the following sections.

TABLE 3.1

AAT Prime Focus Plates

Focal Ratio	f/3.3
Plate Size	10 in x 10 in
Plate Scale (with triplet corrector)	$15.''3\ mm^{-1}$
Unvignetted field	60'
Field with images < ".5	60'

TABLE 3.2

Plate	Emulsion	Filter	Exposure	m_{LIM}
1496	2aO	GG385D	20m	21.2(B)
1497	2aD	GG495C	20m	21.1(V)
1501	2aD	GG495	40m	21.5(V)
1520	2aO	GG385	40m	21.4(B)
1521	2aD	GG495	40m	21.6(V)
1535	2aO	GG385D	40m	21.9(B)
1536	2aD	GG495C	30m	21.5(V)
1571	2aO	GG385	50m	22.5(B)
1581	2aO	GG385	50m	22.3(B)

3.2 Becker Iris Photometer

To obtain measures of magnitude of individual stellar images on the plates, the Becker Iris Photometer of the Royal Observatory Edinburgh was used. Fig. 3.1 shows a diagram of such a photometer (Becker & Biber, 1956) which operates by passing a beam of light through the stellar image and an iris of variable diameter. The flux in the transmitted beam is compared with that in a reference beam, which is obtained by splitting the original. The flux in the image beam is clearly reduced by insertion of the image so the iris is opened to compensate by a sensor mechanism so that reference and image beams remain equal. The recorded measurement and the measure of stellar magnitude is thus the iris diameter required to maintain the flux through the iris and image equal to that through a fixed aperture.

The advantages of this arrangement are that the ratio of the standard and incident beams remains unchanged even if fluctuations in the lamp source occur. Also the variable diaphragm diameter allows a range of image magnitudes to be measured without areas of background fog appearing in the iris, which degrades the response of the photometer with fixed diaphragm diameter. This allows an iris photometer to measure over a range of approximately 10 magnitudes (Argue, 1960).

When iris readings have been obtained a graph is plotted of magnitude against iris reading for standard stars. It is a basic property of stellar images that this graph is injective, i.e. that for each stellar magnitude there exists a unique iris reading and vice versa. Thus a best fit relation may be drawn through the standard points and used to convert iris readings for programme stars to magnitudes. Such

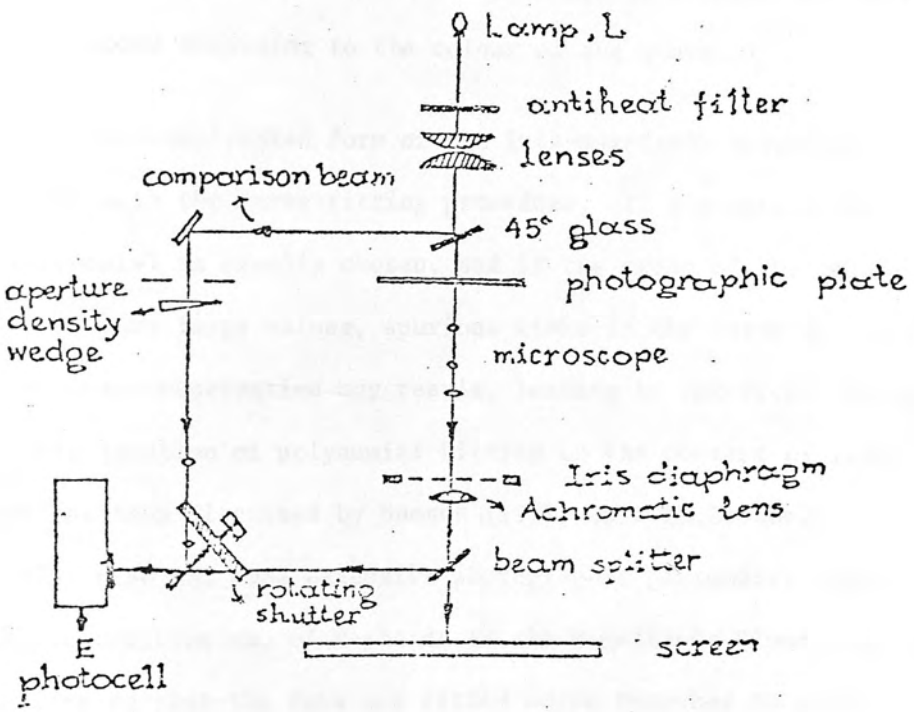

Fig. 3.1 The Becker iris photometer.

a best-fit line may only be used for interpolation as it is in general a complicated curve whose behaviour outside the calibrated range is quite unknown. Magnitude residuals for the standard stars, defined by $\Delta M = M_{PE} - M_{PG}$ are used to test for systematic errors in the fitted magnitudes, such as differences in the spectral response of the emulsion and the standard photometric system. A plot of ΔM versus B-V, for instance, indicates whether a "colour equation" is necessary, if so a fitted line is drawn and used to correct the photographic magnitudes according to the colour of the stars.

Due to the complicated form of the iris-magnitude relation, care must be taken with the curve-fitting procedure. If a computer fit is made, a polynomial is usually chosen, and if the order of the polynomial is allowed to take large values, spurious kinks in the curve due to a single inaccurate observation may result, leading to incorrect fitted values. This question of polynomial fitting in the context of iris photometry has been discussed by Samson (1971) in a Ph.D. thesis. Butler (1976) also has done extensive photographic photometry, with photoelectric calibration, of Cepheids in the Magellanic Clouds. It is thus necessary to plot the data and fitted curve together to check that the computer fit is sensible. Fig. 3.2 shows a typical calibration curve. Although high order polynomials ($n \leq 8$) have been used (Argue, 1960) in photometry of bright stars, for faint stars the increased dispersion in the calibration curve associated with increased photoelectric and photographic errors makes low-order polynomials equally accurate, without the danger of spurious kinks. Particular care must be taken near the plate limit where the sensitivity of the iris to changes in magnitudes drops considerably, i.e. the calibration

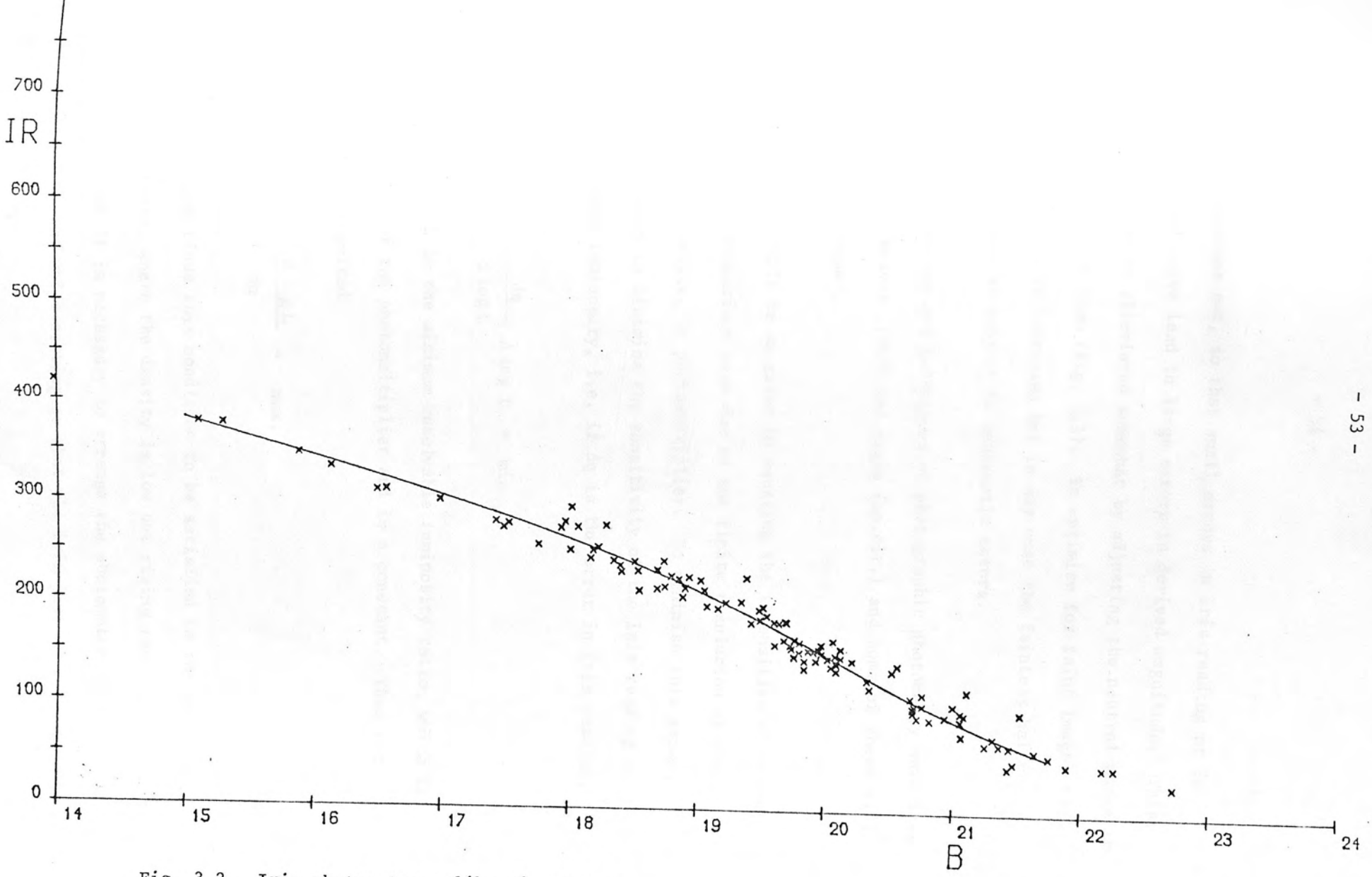

Fig. 3.2 Iris photometer calibration curve.

curve flattens out, so that small errors in iris reading or in the fitted curve lead to large errors in derived magnitude. This problem can be alleviated somewhat by adjusting the neutral wedge in the comparison beam (Fig. 3.1). To optimise for faint images the wedge density is increased but in any case the faintest half-magnitude may be subject to systematic errors.

The errors and techniques of photographic photometry have been treated by Weaver (1962) and Argue (op.cit.) and some of these will now be discussed.

(a) There will be an error in equating the intensities of transmitted and comparison beam due to the finite resolution of the comparison device, a photomultiplier. To minimise this error, it is necessary to minimise the sensitivity of the iris reading to transmitted luminosity, i.e. if Δq is the error in iris reading,

$$\Delta q = \frac{dq}{d \log L} \Delta \log L = \min$$

where $\Delta \log L$ is the minimum resolvable luminosity ratio, which is a property of the photomultiplier and is a constant. Thus the condition required

$$\frac{d \log L}{dq} = \max.$$

Argue finds this condition to be satisfied in the outer regions of the image, where the density is low but rising rapidly towards the centre thus it is necessary to arrange the photometer zero point as defined by the wedge setting so that the iris just circles the image

for the faintest stars, in which case for the bright stars the iris perimeter will be just inside the edge of the image, but not too close to the centre.

(b) Centring errors result from incorrect positioning of the image in the iris. The procedure for centring is to define the centre as that position which gives maximum iris reading, thus if the image is scanned in two dimensions, the maximum reading is taken as the "true" reading. Repeated measurement of the same image shows centring error to be unimportant as long as a consistent procedure, such as the above, is adopted. This procedure may also be used for distorted images, due to trailing, flexure, etc. although with slightly less justification.

(c) Due to the finite size of the photographic grains, statistical fluctuations occur in the density which leads to random errors in the measured iris reading, i.e. a random variation from plate to plate. Argue finds that this can lead to large errors in the results so it is necessary to optimise one's statistics by increasing the number of grains measured so it is found that the optimum setting agrees with that found in (a), i.e. iris just cutting into image edge.

(d) Background variations can affect results of iris photometry appreciably as stellar images projected on backgrounds of high surface brightness will give a higher iris reading than an identical image on a low brightness area. If background variations are small, no explicit account need be taken if standard stars are situated at random in the measured region as background variations will be calibrated out and a mean background will remain. However, if large background variations

are present due to rapidly varying unresolved star distribution or nebulosity it is possible to correct systematically. Ahmed et al. (1965) calibrated the background effect photoelectrically. Assuming photoelectric observations are corrected for background, one can find the difference between photoelectric and fitted photographic magnitudes and find the dependence on iris readings obtained for the background near the image alone. Having thus calibrated the background effect, photographic values can be corrected in proportion to the nearby fog reading.

Weaver (1962) discusses an uncalibrated approximate procedure using the same principle. One measures the iris diameter for a star with fog, D, for the fog alone, d_F, and for the 'average' fog on the plate $\bar{d}_F$, and then corrects the iris diameter according to

$$d^2 = D^2 - (d_F^2 - \bar{d}_F^2)$$

where d is the diameter that would be obtained with average fog.

A third procedure involves resetting the iris zero point each time the background changes to maintain the background iris reading constant. This will affect a partial compensation in that one is measuring the difference between background and star plus background and essentially corresponds to the method of Weaver for small values of $d_F - \bar{d}_F$, i.e. for small variations in fog.

None of these methods can be considered completely satisfactory and for accurate photometry it is essential to obtain standards throughout the measured region and, if necessary, to obtain a set of standard

for each of several smaller regions and draw a calibration curve for each. In the Small Magellanic Cloud, large variations occur in the density of faint stars in the Bar of the Galaxy so that it is necessary to establish a standard sequence in each cluster measured or to choose clusters lying in areas of low background star density. The latter course was chosen in the present investigation.

This problem also puts constraints on the regions of any given cluster that may be measured as the centre is generally saturated and the regions near the centre will have a high background density. One is thus forced to compromise between the desire for a large sample of cluster members and choosing stars that are measurable. It is possible to eliminate field stars in certain situations through proper motions, radial velocities, multi-colour photometry, or statistical subtraction. However, in the case of faint photometry of clusters in the SMC, radial velocities are unobtainable due to the faintness of the stars, proper motions will not discriminate field stars in the SMC nor even halo Galaxy stars, all showing zero proper motions. One is thus forced to choose clusters for measurement which are in relatively uncrowded regions of the SMC, i.e. well away from the Bar. Thus halo clusters are particularly well suited for faint photographic photometry. The situation can also be improved by increasing the plate scale, allowing a closer approach to the cluster centre. For photometry of faint sources it is thus essential to use a large aperture telescope, the 4-m AAT proving admirable.

Another method of coping with contamination by field stars in B V photometry is to sample the objects at varying distances from the

cluster centre. One can thus determine which regions of the C-M diagram are occupied by field stars and interpret the results accordingly. A quantitative estimate of the field star contamination can be obtained by star counts at varying distances from the cluster centre. Assuming a constant surface density of field stars and a suitable model for the cluster density as a function of radial distance allows the field star density to be calculated. One can then determine the number of field stars to be expected in the photometrically measured areas and subtract these from the observed C-M diagram.

(e) Misidentification, variable stars etc. can lead to measurements which are very different on different plates, and can be discovered and removed by measuring several plates in each colour and systematically comparing each plate with the others and with the mean of them all. This procedure is also necessary to average out plate errors, such as the fluctuation error discussed above, and also averages out measurement errors, although this could be achieved by simply remeasuring a single plate.

Output and Data Reduction.

The output from the Becker iris photometer of the ROE is written to a Texas Instruments Silent 700 terminal where two copies are made. The primary copy is simple line printer output while the second is on cassette magnetic tape for reading into a computer. Due to the fact that no accessible computer was equipped with a cassette reader, the secondary output was read onto paper tape via a teletype and read into a computer in this form.

The computer used for all data processing was the ERCC 4-75 twin machine in multi-access mode, known as EMAS (Edinburgh Multi-Access System). All input was checked and edited after reading into the computer, partly because the photometer readout produces much spurious output and partly because of corruption in the data transfer to computer, the primary line-printer output being used for corrections. A suite of programmes was written to convert iris readings into magnitudes, which process will now be described.

The first programme, DATAED, edits the raw data and sorts the images into three categories, standard stars, programme stars and those to be ignored, by means of a single character read in at the time of measurement, viz. 0, 1, 2 respectively. The list of standards and the list of programme stars are output to two files and used as input to the next programme, POLYFIT, which fits a polynomial of order up to 4 to the iris reading/magnitude data and transforms the programme star data into magnitudes. One output from this programme is a table of values for the best fit calibration curve along with the standard star data. This is input to a programme, CALGRA, which plots both sets of data on a graph. This graph, Fig. 3.2, is used to check for bad data points and to ensure the acceptability of the fit.

Having obtained a set of magnitudes for all the stars of interest on a single plate it is required to combine the data together to form averaged magnitudes in each filter and colours. This is performed by DATOUT2 which finds average values for B and V, colours $\overline{B}-\overline{V}$ and evaluates rms errors for each plate by comparing $\overline{B}$ with the value for each plate individually, according to a procedure due to Penston and Cannon (1970).

This programme also outputs the $\overline{V}$, $\overline{B}-\overline{V}$ data in a form suitable for graph plotting by CMDPLOT, which plots a colour-magnitude diagram.

At each stage of this process the data are checked to ensure that no errors are created in the computations and that all results are reasonable.

3.3 The St Andrews Photometer

In order to set up a calibrating sequence for bright stars and to provide a zero point for electronographic photometry, the St Andrews photometer was used on the 1-m telescope at the South African Astronomical Observatory. A description of this instrument may be found in Kelly (1977) so in the present context only a few salient points will be noted. The photometer is semi-automated in that it may be programmed by inserting keys in appropriate slots and the user can define a sequence of measurements composed of integrations on either star or sky and in each of up to five filters. Having finished a series of observations through different filters the sequence stops to allow the observer to switch from star to sky or vice versa, the sequence being restarted when the telescope is repositioned.

The system is a photon-counting one and results are displayed in the form of counts which may be read in real time. A hard copy is produced on a teletype and on punched tape. Results were reduced at the observatory in Capetown using the software written by A.J. Penny, which corrects raw data for atmospheric absorption and colour equation in the system.

Limitations of the telescope/photometer combination are of two kinds, photon statistics and image location. Due to inaccuracies in the R.A. drive of the telescope a large aperture must be used, 11 and 14 arc seconds being typical. For any given sky brightness there exists a stellar magnitude for which the flux from the star is so much smaller than that from the sky that integration times are prohibitively long. This limitation is clearly much more stringent where large apertures are used. Location of images is achieved by inserting a prism into the main beam, bypassing the photometer and viewing through an image intensifier. Hence there exists also an absolute limit to the faintness of objects which can be detected, and hence observed.

The former of these limits depends strongly on sky brightness and demands that observations be made at a dark site and at the dark phase of the Moon. The second limit depends sensitively on seeing, a decrease of 50% in image point spread leading to objects at least one magnitude fainter becoming visible. Thus optimum conditions for good, faint, photoelectric photometry are clear skies, dark sky, no Moon and small seeing disc.

3.4 Electronography

The aim of this project is to obtain photometry of faint stars on deep AAT plates so it is necessary to obtain a faint sequence of standard stars in the field of these plates in order to calibrate the response of the photographic emulsion. As explained in the previous section, photoelectric photometry on a small telescope is only possible for bright stars. To obtain a faint sequence, the McMullan electrono-

graphic camera was used, also on the 1 m telescope at SAAO.

Electronography seeks to convert the incident light from a star field into an electron beam which is then allowed to impinge on a nuclear emulsion, which forms a developable track. The advantage of electronographic detectors is that, in principle, their response is linear, i.e. the output, which is the photographic density of the developed image, is a linear function of the incident light level. Thus stellar magnitudes may be determined by measuring the density in an image over a raster and to integrate, or to fit a model profile and thus to find the density volume for the image. This quantity is proportional to the total flux of the image since

$$F = \int_R I \, dA \propto \int_R D \, dA \qquad 3.1$$

where R is a suitable chosen raster area, thus by definition of the magnitude:

$$m = \text{const} - 2.5 \log F = \text{const} - 2.5 \log \int_R D \, dA \qquad 3.2$$

and magnitude can be determined for all images on a plate to within a zero point. This zero point can be fixed by measuring a sample of stars photoelectrically. Thus all images on a plate may be measured, and in particular faint images can be measured just as easily as bright ones which is the crucial reason for employing electronography. The linearity of the electronographic process is discussed in Walker and Kron (1967), Walker (1974), Penny (1975) and Hawkins (1977).

The instrument used in the present investigation is the RGO electronographic camera, described by McMullan et al. (1972) and McMullan and Powell (1976). A schematic diagram is shown in Fig. 3.3. This design represents an improvement over earlier systems in having a larger field of view, viz. 4 cm diameter. A mica window is required to protect the photocathode from nuclear emulsion reaction products, and the pressure gradient which this window can withstand determines the maximum diameter and hence the maximum field of view. The RGO camera has a small pressure gradient across the window by maintaining a low pressure in the film chamber with a gate valve to allow insertion and extraction of the film, thus allowing a larger window to be used.

Measurement of electronographic films was performed using the COSMOS automatic measuring machine at the Royal Observatory Edinburgh, and data reduction effected through a suite of programmes written by M.R.S. Hawkins.

COSMOS is a high speed automatic microphotometer providing a step size of 8 or 16 μm and an illuminating spot size of 8 μm in principle but 25 μm in practice. A discussion of this instrument may be found in Pratt (1977), but for the present purpose the following points are important. For increased measuring speed, the illumination is provided by a cathode ray tube whose spot is scanned over a phosphor by electric fields. The width of a scan, called the lane width, contains 128 pixels and the CRT moves down a lane at a uniform velocity, the spot being constrained to lie in an orthogonal scan by appropriate fields.

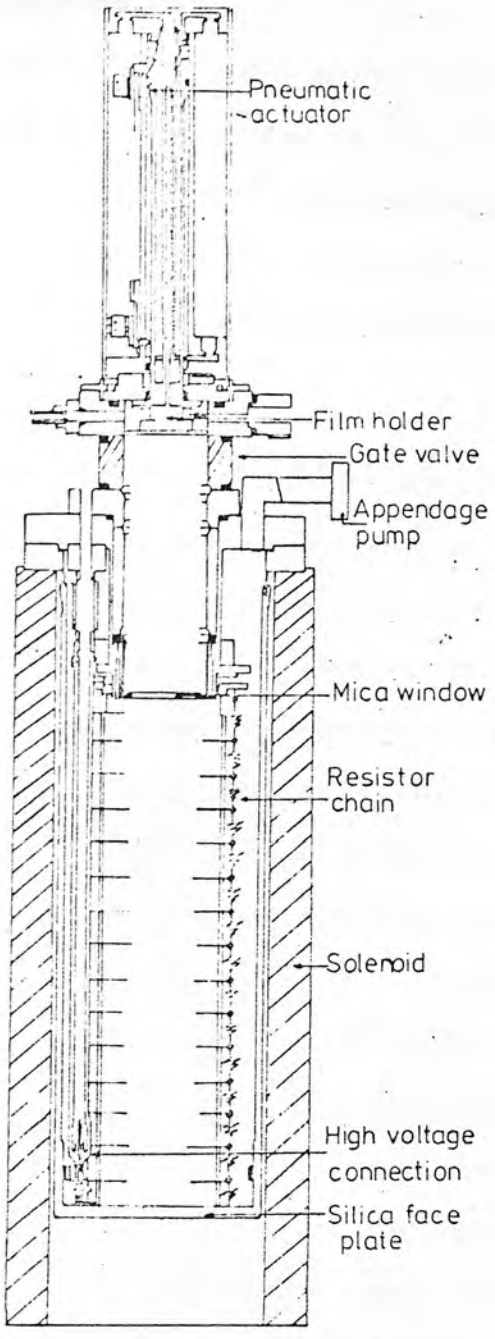

Fig. 3.3 RGO electronographic camera.

Detection and signal output are effected by a photomultiplier tube. A small computer directs the operation and data is written to magnetic tape which may be accessed by user software. The analogue output signal is digitised into 128 transmission levels and the dynamic range is a factor of 10^3 in transmission or a range of 3 in photographic density. This is a serious constraint for electronography as will be discussed later.

For measurement the films are placed between glass sheets and measured in the normal way, as for a photographic plate. Each film is measured in transmission at 8 μm steps in the COSMOS mapping mode, and the data are written to magnetic tape for off-line reduction. Use of COSMOS has two principal advantages over other measuring machines, such as PDS. Firstly the speed of COSMOS is such that measurement of an entire film can be performed in approximately 10 minutes, which is short enough that any secular instabilities in the machine may be ignored, contrary to the situation with conventional measuring machines, which can exhibit considerable drift during a measuring run. The second advantage of COSMOS is also related to speed and involves the problem of correcting for inhomogeneities in the photocathode sensitivity which appear as a background variation on the developed film. To correct for this effect one exposes a film to uniform illumination, either in the laboratory or at the telescope, maps the resulting density pattern onto the star plate and corrects the measurement of density at any point on the star plate according to the density at the corresponding point on the sky plate. To aid the mapping between plates, fiducial marks are provided on the photocathode.

The speed of COSMOS allows the entire sky plate to be measured so that corrections can be found off line to any point in the field, allowing greater flexibility in the choice of stars to be measured.

The first step in reduction of data is the production of a map of the area of interest in the form of a two dimensional array giving the density at each pixel as a single digit. A list of images can then be drawn up taking into account such factors as image quality, background variations, machine saturation etc. Another advantage of using COSMOS is that faint images can be found much more easily from the digital map than by visual inspection of the film.

Having selected a set of images of interest a block of data is extracted from the magnetic tape store corresponding to the area around each image, and also the data for the corresponding area on the sky plate is extracted. To obtain magnitudes these data are now input to a further programme which integrates up the density in the image and also fits a standard profile to the data and outputs the corresponding magnitudes. The profile fitted is a two dimensional Gaussian and the parameters fitted for are central coordinates, height and standard deviation, width in each of the X and Y directions. Cathode sensitivity corrections are effected by simply integrating the density over an array concentric with the image on the sky plate and subtracting the magnitude for sky from that for star, i.e.

$$m_c = m_u - 2.5 \log \sum_i D_{i\,SKY} \qquad 3.3$$

where m_c and m_u are the corrected and uncorrected magnitudes, and

$D_{i\ SKY}$ the density on the sky plate at point i.

Having obtained electronographic magnitudes, what remains is to find the transformation from these to a standard photometric system which is achieved by measuring images with known magnitudes and fitting electronographic to standard magnitudes by least squares variation of such parameters as zero point. This aspect of the technique will be discussed in Chapter 4, which deals with the general problem of setting up a standard photometric sequence.

3.5 AAT Twin Channel Photoelectric Photometer

5a General

This instrument, designed and built at Mount Stromlo Observatory and described in the AAT Observers Guide is basically a conventional photoelectric photometer which has been designed to make efficient use of the excellent setting and tracking facilities of the AAT and to be run by the AAT's Instrument Central System.

The photometer essentially consists of two single-channel photometers working in parallel and simultaneously. Thus in normal operation one channel is used to observe the object of interest and the other is used to observe a nearby patch of sky. After an integration the channels are interchanged and the integration repeated in order to transform away possible differences in the response of the two photomultipliers.

5b Geometry of the Photometer

Fig. 3.4 shows an illustration of the layout of the twin photometer (Fig. 4.6 in Guide). The entire instrument rotates about an

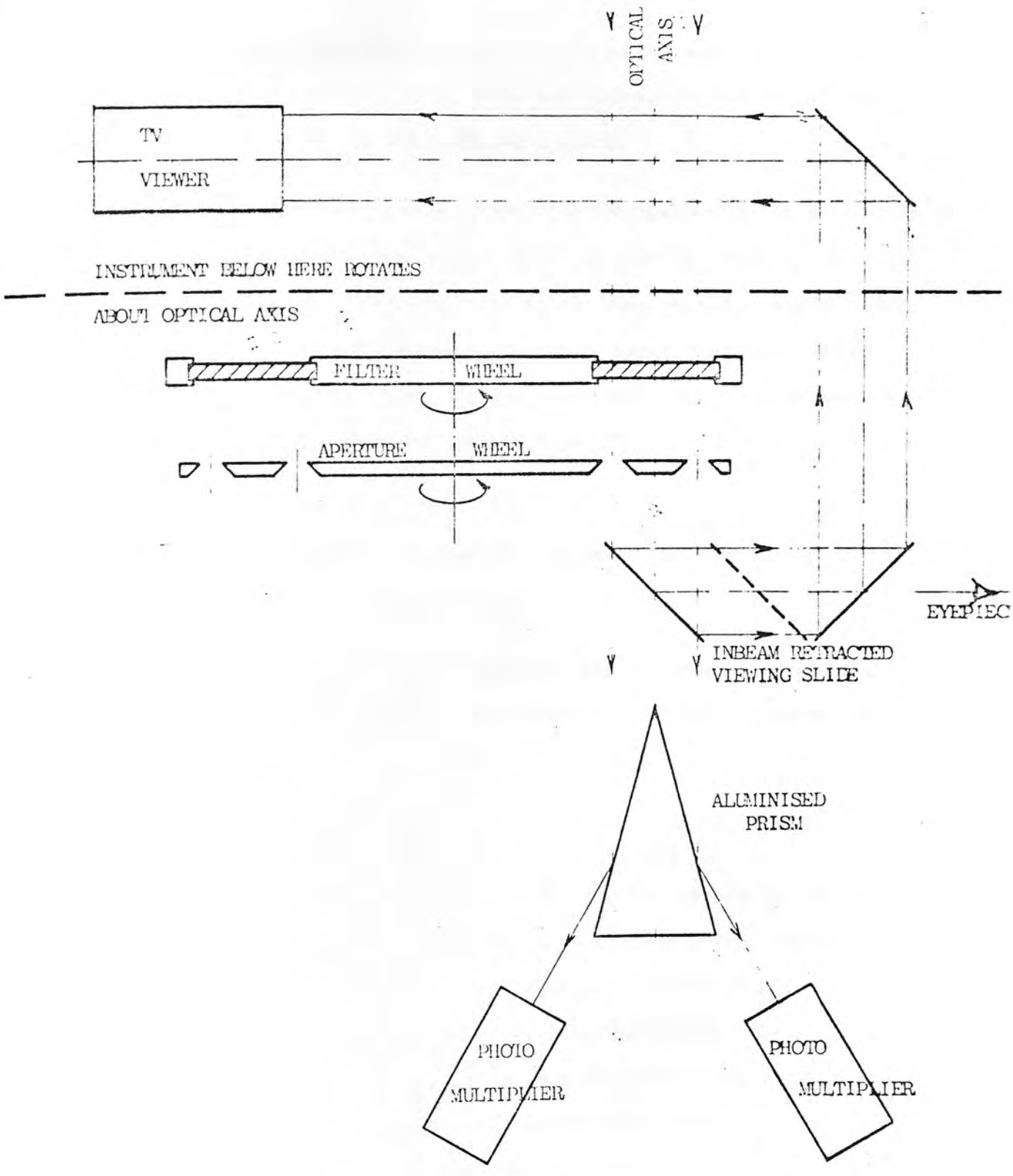

TWIN PHOTOMETER

MECHANICAL LAYOUT

Fig. 3.4 Schematic diagram of AAT twin photometer.

axis coincident with the optical axis of the telescope in accordance with the scheme in Fig. 3.5. There are sixteen allowed orientations, separated by $22^{o}\frac{1}{2}$, with NS numbered 1 and 9.

The light that finally reaches the photomultiplier is determined by the orientation of the filter wheel and aperture wheel and by that of the photometer as a whole. The filter wheel contains matched pairs of filters, diametrically opposite filters being identical, either standard or user supplied. The aperture wheel also contains matched pairs in opposite locations with a range of apertures as given in table 3.3.

Photomultipliers supplied are ITT FW-130 and FW-118 with S20 and S1 photocathodes respectively.

A sliding mirror may be placed in the main beam and viewed by eye at the Cassegrain focus or by remote TV acquisition system in the control room.

5c Preparing an Observing Run

The photometer design is such as to allow the user to specify some very simple properties of the photons he ultimately counts, viz. area of sky integrated over, wavelength and place of origin. Thus when the observer arrives at the telescope he must be able to specify the filter and aperture he requires and the orientation on the sky of his sky-object axis, as defined by one of the positions in Fig. 3.5. In choosing an appropriate sky hole one is constrained by the allowed orientations which are discrete, and by the unique separation for any given aperture, as shown in table 3.3. It is thus necessary to plan

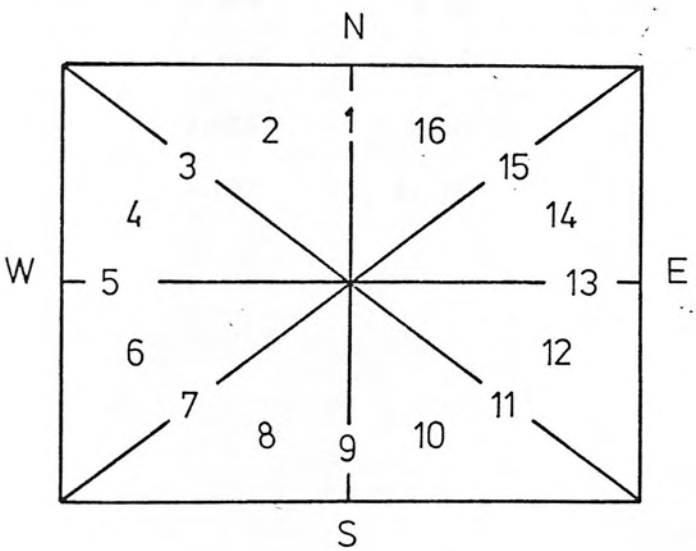

Fig. 3.5 Arrangement of rotator positions.

TABLE 3.3

Ap.	Ap. sizes		Sepn.	Projected Angular Dims. @ f/15 arc sec	
1	.672 mm	.672 mm	4.80 mm	2.4	17.1
2	.973	.972	4.82	3.5	17.2
3	1.398	1.393	4.88	5.0	17.4
4	1.953	1.951	4.86	6.9	17.3
5	2.802	2.809	5.32	10.0	18.9
6	3.948	3.943	8.44	14.0	22.9
7	5.609	5.614	8.40	20.0	29.9
8	7.821	7.807	11.76	27.8	41.9

an observing run carefully and to approach the telescope having a set of accurate coordinates, aperture numbers and orientations satisfactory for any seeing conditions.

To this end a procedure was developed using the TV Zeiss blink comparator at the Royal Observatory Edinburgh. A virtual diagram of the aperture wheel was drawn and reduced photographically to the form of a positive transparency, i.e. a set of dark rings on a transparent film. The diagram may be called virtual in that only apertures of uniform diameter are used in any single representation, so one has 16 identical circles at appropriate distances from the centre, corresponding to 16 allowed sky holes about an image, whereas on the actual aperture wheel there are only two apertures of any given diameter, also the centre of the diagram corresponds to the image so the radius is equal to the diameter of the aperture wheel. Having chosen an aperture diameter the corresponding representation of the aperture wheel is reduced to the appropriate size, and viewed simultaneously with a photographic plate of the area of interest through different channels of the TV Zeiss. One can then place the centre of the diagram on the star to be measured and choose a clear sky hole from those available. This method is very quick and efficient, especially where large numbers of images are involved. Obviously a different overlay is required for each aperture size and in general one must find a different sky position for each aperture, also one must prepare several apertures in order to have one appropriate to the seeing conditions.

All the data required to specify an observing programme are

punched onto cards and read into the instrument control computer and from this point on all observing is performed by the user issuing instructions via a VDU. In addition, the information on cards may be edited, to take into account changing circumstances, via the VDU. To initiate a measurement cycle the control programme requests an image, the observer responds with an image name and asks the night assistant to set the telescope. This last step will eventually be automated by linking the telescope control computer and the instrument control computer. At the time of use, however, the instrument control programme simply displayed the coordinates of the image, transformed to a suitable system to take account of refraction, precession, etc. which were then dictated to the night assistant.

Having set on the image, the centring is checked via the Cassegrain TV acquisition system, and the cycle is resumed by the observer. While photons are being counted the programme displays all the parameters describing the state of the photometer at that time, so the observer knows exactly what he is measuring. In addition, an approximate magnitude is calculated quickly and displayed after each integration so the observer can keep track of the objects he measures and their magnitudes. When the image has been observed through each of the filters specified, the sky is observed by one of two mechanisms. The simpler option is to translate the telescope so that the sky hole appears in the channel previously occupied by the image while the other channel moves onto the image. Thus one is employing two sky positions, symmetrically disposed on either side of the image. If one cannot find two suitable patches of clear sky but only one, the second option may be employed, viz. to rotate the photometer through

180^{o}, thus interchanging image and sky in the two channels. This second is very slow compared to the first and is prohibitively inefficient unless integration times are of the order of 15 minutes, i.e. for faint stars, but generally it is only required for faint stars in any case.

As well as being twice as efficient as a conventional single channel photometer, the AAT twin photometer has several very important advantages over earlier designs. As discussed in the section on the St Andrews photometer, the limits to measurement of faint sources are set by three factors, (1) detection, (2) photon statistics, and (3) availability of sky positions. The AAT twin photometer helps enormously in extending the limits imposed by these constraints by having TV acquisition, very accurate tracking and a rotating photometer and aperture wheel.

The AAT TV acquisition system allows integration of the signal coming from a patch of sky surrounding the image for up to 20s, allowing very faint sources to be detected. In the present work sources with B = 21 were found easily with an integration time of 5s.

Improving photon statistics can be achieved by decreasing the contribution to the photon count by the surrounding sky, i.e. by using a small aperture. The aperture which may be used is constrained, however, by the image point spread function, or seeing disc, and by the accuracy of the telescope's tracking. The tracking of the AAT is accurate to a fraction of an arc second so one can employ a much smaller aperture for given seeing than for many less advanced telescopes. Another improvement to the photon statistics is obviously

effected by the large (3.9 m) aperture of the telescope, with 1 photon per second being detected through the standard B filter from a star with B = 24. Table 3.4 shows the integration times required to accumulate sufficient counts to give statistical accuracy of approximately 5% or $^{m}.05$ i.e.

$$\frac{\sqrt{N_{SKY}}}{N_{STAR}} = .05 \Rightarrow N \approx 10^4$$

The use of a drilled aperture wheel makes location of a sky position arbitrarily accurate since they are chosen from deep photographic plates, whereas with conventional photometers, sky positions are either chosen by observing through the main telescope beam with the naked eye or using an offset head. The former of these is unsatisfactory because of the limit to resolution of faint objects while the second is very inefficient because of the time involved. With the twin photometer one can switch star and sky in 30 seconds with the sky known to be free of faint objects.

Output from the photometer takes several forms. The primary hard copy is on line printer, recording identifications, integration times, photon counts etc. As mentioned earlier, a running output also appears on the observer's VDU. There is also a telescope control computer output on line printer, recording the state of the telescope at each integration which is useful for checking later that one had the correct object in the aperture. Finally, a magnetic tape record identical to the line printer output from the instrument control programme may be obtained for off-line reduction.

TABLE 3.4

B	t(secs)
18	20
19	127
20	690
21	4000

CHAPTER IV

A FAINT PHOTOMETRIC SEQUENCE

In this chapter the results of several approaches to establishing a standard photometric sequence for calibrating photographic plates are discussed. Firstly original results are presented and accuracy discussed, then these are combined with existing data to produce what is believed to be the best available deep sequence in this area of the sky. Data used, apart from original work, are due to Professor S.C.B. Gascoigne (private communication) and M.F. Walker (1970).

Results of original work are presented in sections (1) to (3) which discuss data from the St Andrews photometer, electronography and the AAT respectively.

4.1 Bright Star Photometry

The basic photometric sequence of brighter stars was set up using the 1 m reflector at Sutherland, and the St Andrews photometer on 11th - 19th October 1977. This period was in the first quarter of the lunar month so the Moon was present for the early part of the night. Bright stars ($7 \leq V \leq 13$) were measured during the first part of the night and faint stars ($13 \leq V \leq 17$) observed during the dark, late part. The measurements were transformed into the UBVRI standard system via the secondary standards of Cousins in the SMC, of Arp in the SMC (Arp, 1958a) and of Cannon in 47 Tuc (Cannon, 1974). On most nights, an aperture of 11 arc seconds was used and this required an integration time of 60s for the faint stars, while 10s was adequate

for bright objects. Brighter images were observed through each of five filters, UBVR and I, while fainter stars were observed in UBV and R. Table 4.1 shows the results of this photometric programme, with Fig. 4.1 showing a finding chart for these bright stars. The coordinates of all of these objects can be found in Appendix I. The final column in Table 4.1 gives the number of observations of each star in B and V while the numbers in parenthesis indicate the internal dispersion (standard deviation) in hundredths of a magnitude for those objects with more than one measure.

4.2 Electronography

Since the stars to be measured on the AAT plates are faint, it is necessary to establish a photometric sequence which is considerably fainter than can be provided by a 1 m telescope. The McMullan electronographic camera was therefore used to extend the 1 m sequence. Since, in principle, the electronographic process is linear, one simply needs to determine the zero point of an electronographic sequence by fitting to one photoelectric star. However, in the light of uncertainty as to whether the system to be employed was performing correctly or not, it was decided to establish a substantial photoelectric sequence to check the linearity of the electronography, for which purpose the 1 m observations were made. The electronographic observations made turned out to be non-linear, as illustrated by Fig. 4.2, which shows the electronographic magnitude obtained via the measurement and reduction process described in 3.4. These results are very similar to those obtained by Hawkins (1979) in that the slope of the relation is not unity, as one would expect, but it is still a straight line in so far as can be ascertained. Following a suggestion of M.R.S. Hawkins, it was assumed

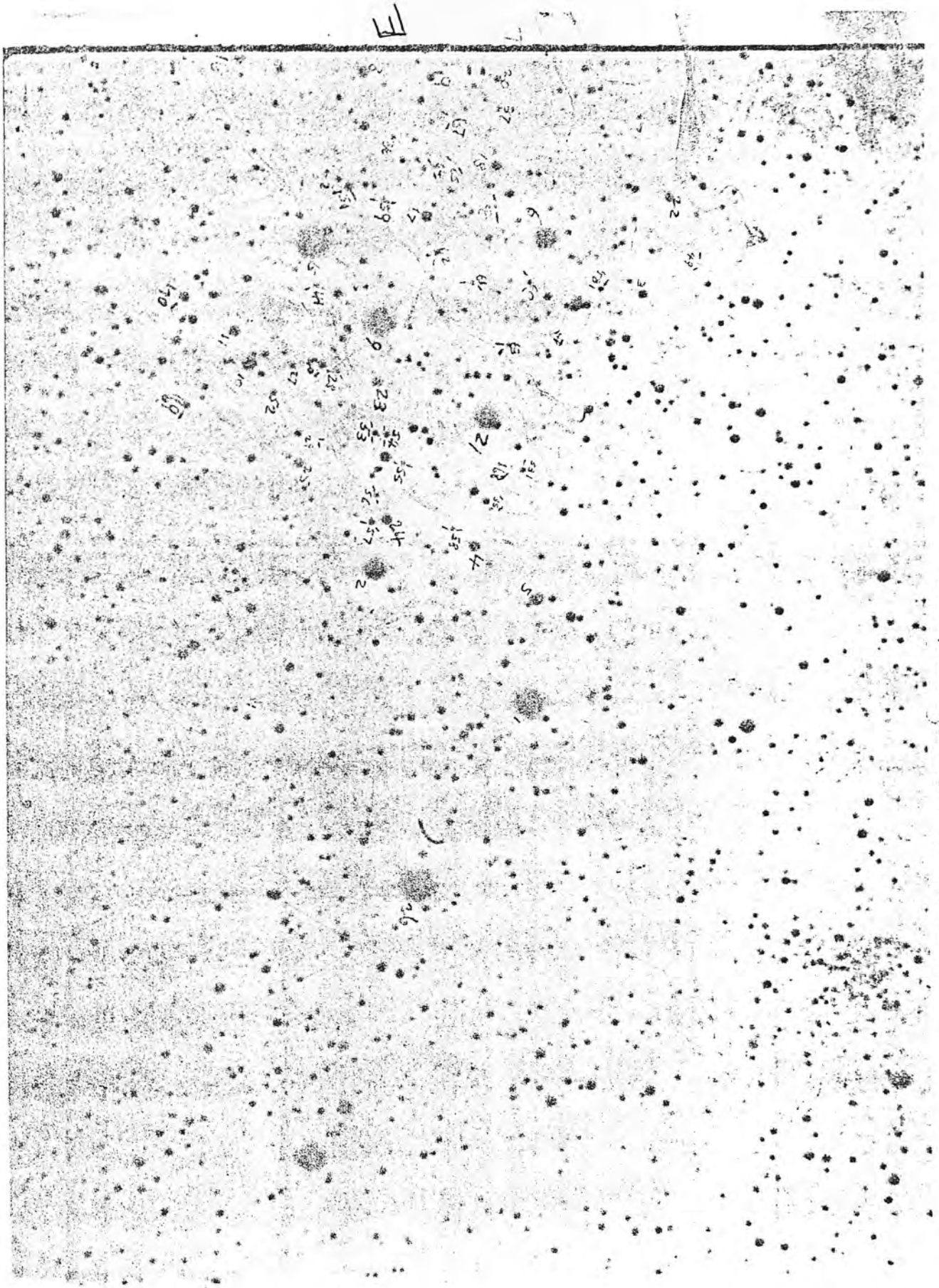

Fig. 4.1 Finding chart for photometric sequence.

TABLE 4.1

1 m Photoelectric Sequence

Star	V	B-V	U-B	V-R	V-I	n
1	11.38(1)	1.02(1)	.73(2)	.55(1)	1.09(2)	12
2	13.08(1)	1.02(2)	.82(3)	.54(1)	1.00	3
4	16.35	.63	-.06	.36		1
5	15.35	.53	-.03	.32		1
6	13.42(3)	.55(1)	.00(4)	.31(1)	.70	4
7	14.63(2)	.95(1)	.59(2)	.51(1)		2
8	15.75(5)	.74(2)	.27(8)	.41(4)		2
9	11.86(2)	.56(2)	.00(2)	.33(1)	.67(1)	16
10	15.24(4)	.89(1)	.60	.50		2
11	16.28(4)	.28(1)	.09	.15		2
13	14.89(4)	.21(1)	.18(2)	.11(2)		2
15	11.05(2)	.57(2)	-.04(1)	.35(2)	.67	9
16	16.15(1)	1.33(1)	1.01	.89		2
17	16.66(5)	1.74(2)	.98	.95		2
18	16.94	1.74	1.00	.89		1
19	17.00	1.40	.55	.84		1
21	12.54(2)	.61(2)	.04(2)	.36(2)	.69	6
23	16.84	1.66	.91	.85		1
24	16.74	.78	.24	.44		1
25	16.81	.61				
26	10.66(3)	.53(1)	.03(2)	.30(1)	.60	

that the response of the electronographic system was such that the relation between electronographic magnitude and photoelectric magnitude was a straight line but of a slope different from unity. There is no simple physical effect that would give rise to such a relation (Hawkins, 1979) but it is certainly consistent with the data. Thus one is essentially calibrating the electronographic magnitude for bright stars and transforming magnitudes for faint stars from the electronographic system to the standard system. Thus a least squares best fit straight line was found to the calibration data as in Fig. 4.2 for each electronographic plate. Two deep plates in each of B and V were measured and several short exposure plates to test the linearity assumption near the plate limit. Fig. 4.3 shows the calibration graph for a 30 minute exposure with plate limit V ~19. It can be seen that the relation, although not of slope one, is straight to quite near the plate limit.

Having corrected for response, the electronographic magnitudes were then compared with those of Walker (1970) in K3 via photographic plates. To effect this comparison, Walker's sequence was used to calibrate the response of the photographic plate and magnitudes were then found for stars in the present sequence from their iris readings. The results of this comparison are shown in Figs. 4.4a and b, where it is clear that there is reasonable agreement in B but a systematic difference in V at the faint end. Figs. 4.5a and b show the results of a comparison of electronographic magnitudes on different plates, both corrected for response. The agreement between different plates is good which implies that if the present electronography is at fault, the error is repeatable from plate to plate.

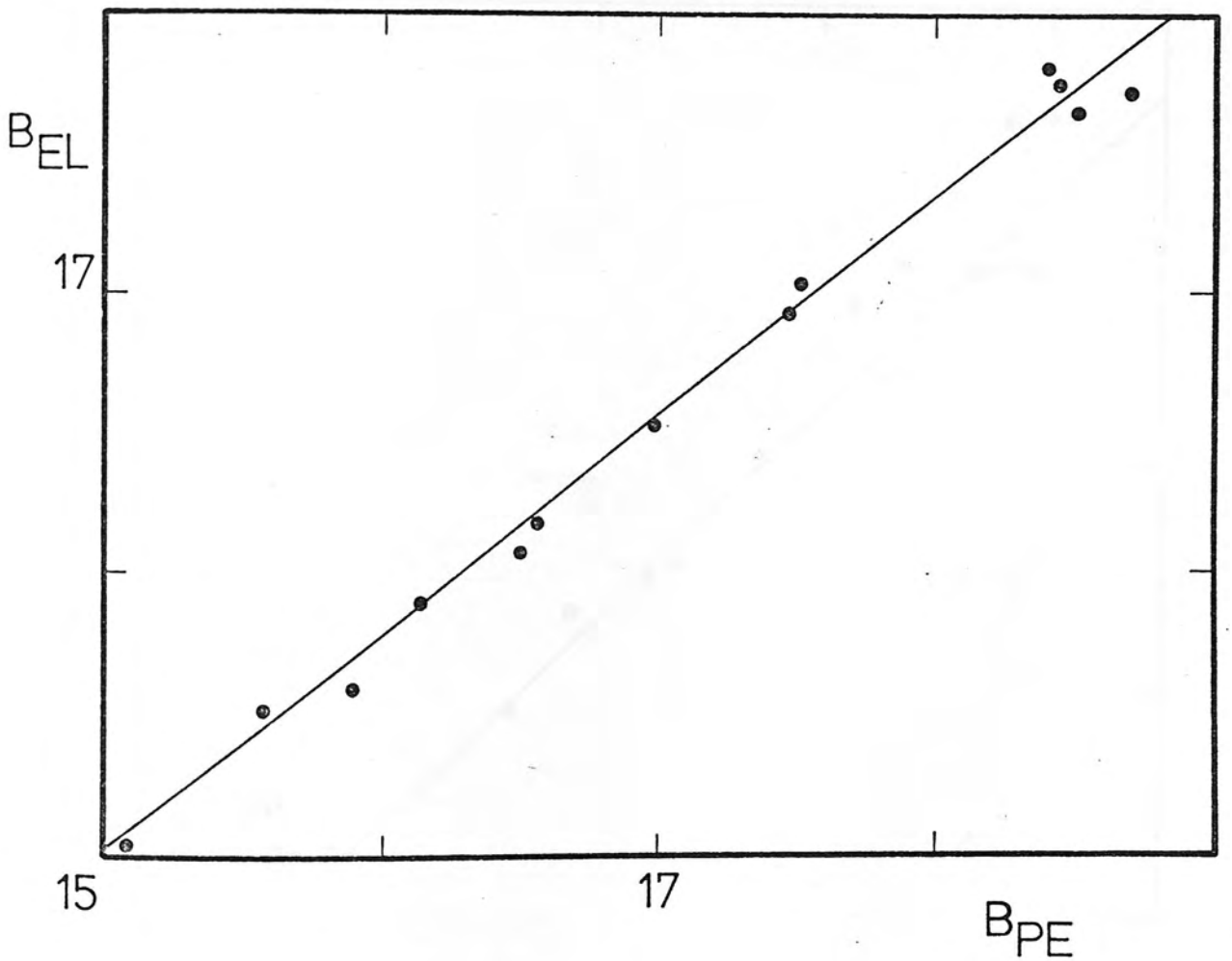

Fig. 4.2 Electronographic magnitude versus photoelectric magnitude.

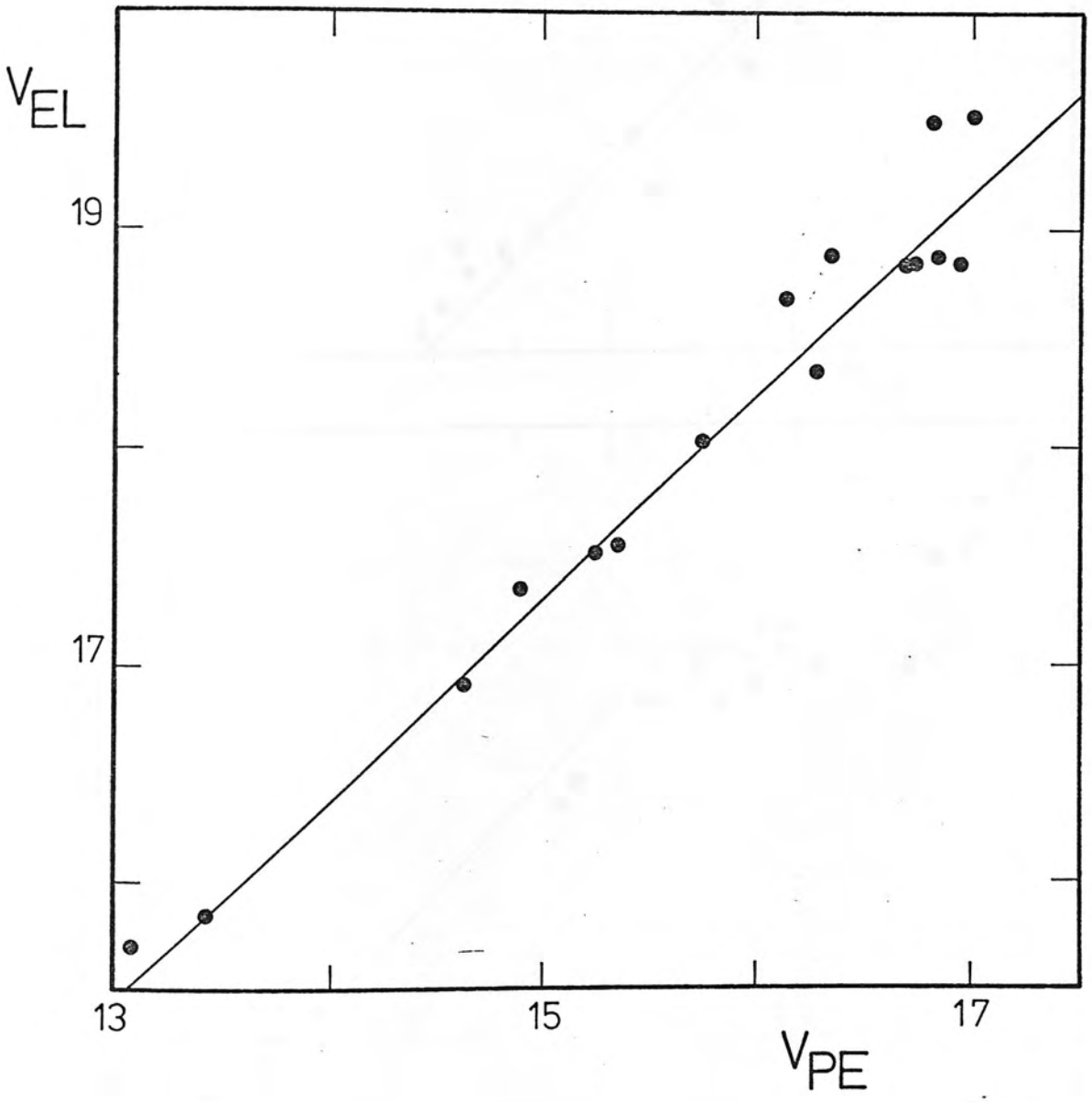

Fig. 4.3 As Fig. 4.2 for a short exposure plate.

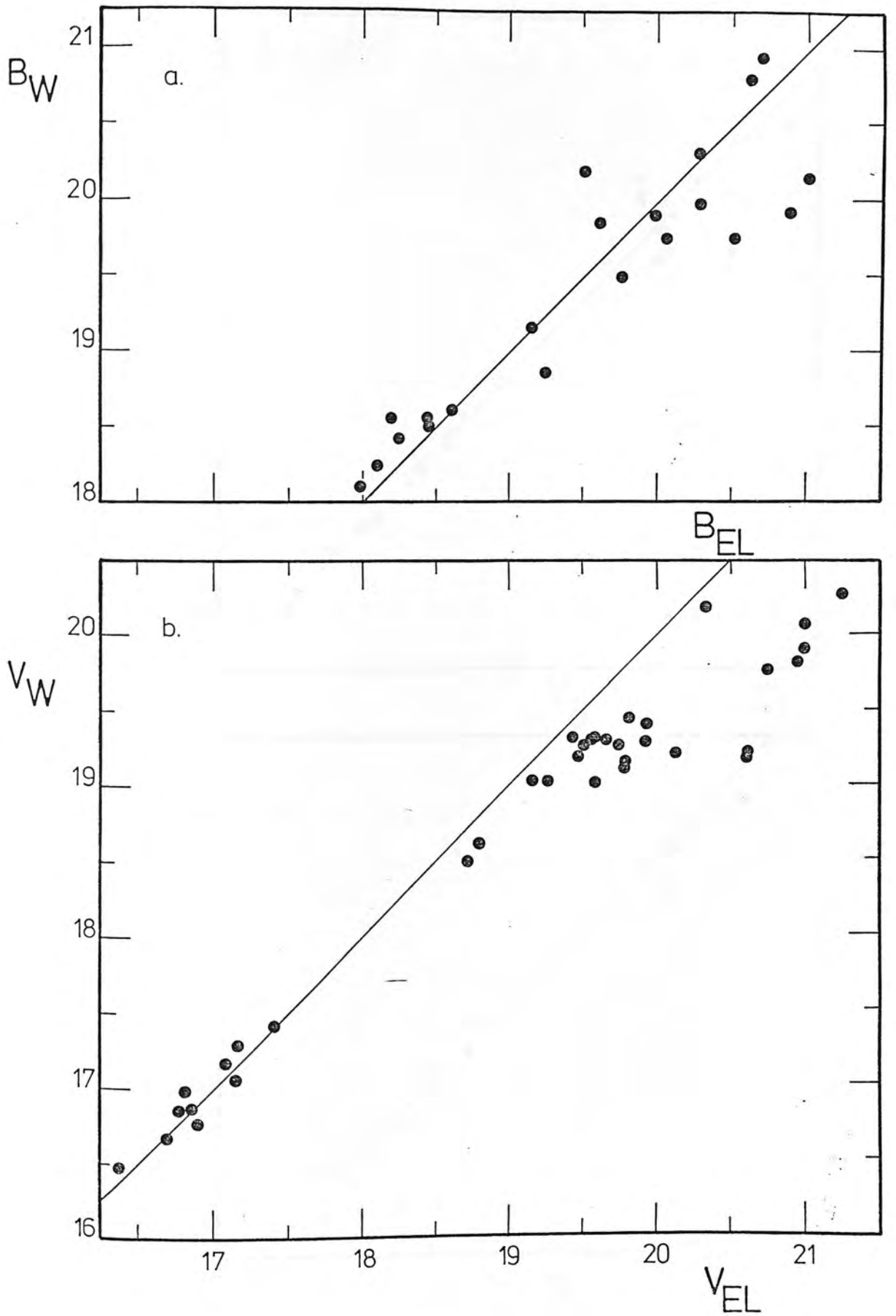

Fig. 4.4 Comparison of Walker's K3 sequence with new electronographic sequence.

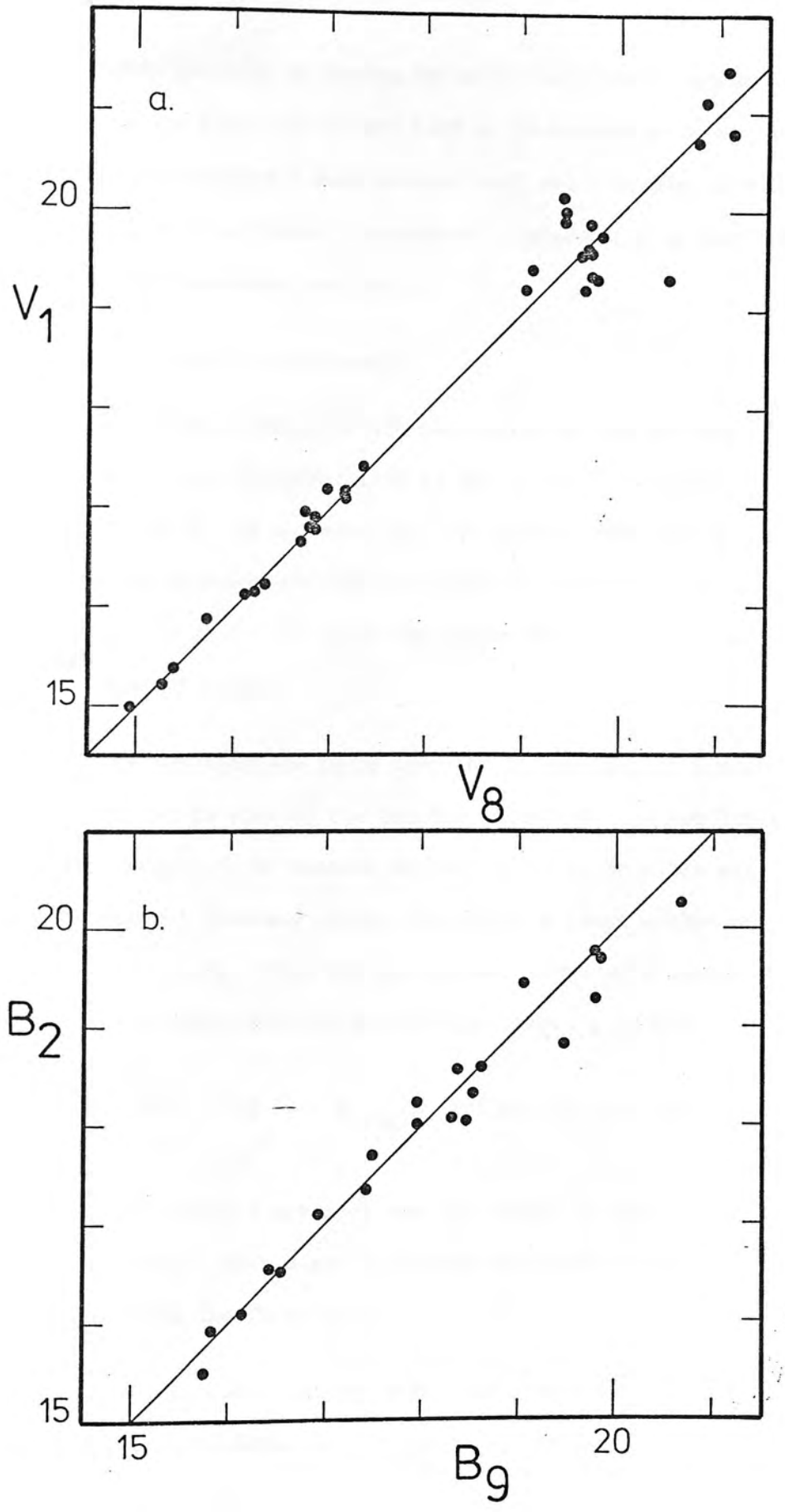

Fig. 4.5 Comparison of different electronographic plates.

Given this position of having two electronographic sequences disagreeing at the faint end it was felt to be desirable to resolve the conflict by employing a more conventional and reliable technique. To that end, the twin channel photoelectric photometer on the 3.9 m Anglo-Australian Telescope was used.

4.3 Faint Photoelectric Photometry

The twin channel photoelectric photometer at the AAT was employed on 7th - 9th September 1978 to set up a faint photometric sequence in B and V. An aperture of 7 arc seconds was used for all observations and integration times as given in Table 4.2 were used. The last column in Table 4.2 gives the approximate number of photons detected at each magnitude.

Since the sequence was to be used for calibration of photographic plates and in view of the limited amount of time available, it was felt appropriate to measure as many stars as possible with limited statistical accuracy rather than count a large number of photons on a few stars. Thus the integration times were chosen on the basis of magnitudes derived electronographically to give

$$\sigma = \frac{\sqrt{N_{SKY}}}{N_{STAR}} = {}^{m}.05 \Rightarrow N_{STAR} \approx 10^4 \text{ photons per integration,}$$

i.e. so that the standard error of the sky counts is much smaller than the star count. Only B and V filters were used, these filters being supplied with the instrument.

Since the instrument had not been used previously for B V photometry, the spectral response was not known, so it was necessary to find

TABLE 4.2

B	t (secs)	N_{APPROX}
14	10	6×10^4
15	10	2.4×10^4
16	10	9.6×10^3
17	20	7.7×10^3
18	60	9.2×10^3
19	100	6.1×10^3
20	200	4.9×10^3

the "colour equation" via the observed standard stars, which were those measured on the 1 m telescope. Fig. 4.6 shows the colour equation, i.e. the differences $(B-V)_{STD} - (B-V)_{INST}$ and $V_{STD} - V_{INST}$ plotted against $(B-V)_{INST}$. Colour equations were adopted as follows:

$$V_{STD} = V_{INST} - 0.03\ (B-V)_{INST} \qquad 4.1$$

$$(B-V)_{STD} = 1.11\ (B-V)_{INST} - 0.04 \qquad 4.2$$

Table 4.3 gives the final magnitudes corrected for colour equations and differential extinction.

This sequence was used to define the zero point of the photometric sequences of Walker (1970) and Gascoigne as described in section 3.4.

Figures 4.7a and b show the relation between electronographic magnitude and photoelectric magnitude of those stars with both measurements. It is seen that the electronographic sequence of section 4.2 agrees with the faint photoelectric sequence in B but the two diverge in V, thus it is the present electronographic sequence which is in error, not that of Walker. No explanation is immediately apparent as to why the electronographic process employed has failed. Possibilities are numerous, among them a faulty emulsion batch and incorrect reduction procedure seem the most likely, since it seems unlikely that the photocathode could be non-linear and the measuring machine, COSMOS in this case, is working within its dynamical range. No further attempt was made to trace the source of error since a deep photoelectric sequence coupled with Walker's deeper electronographic

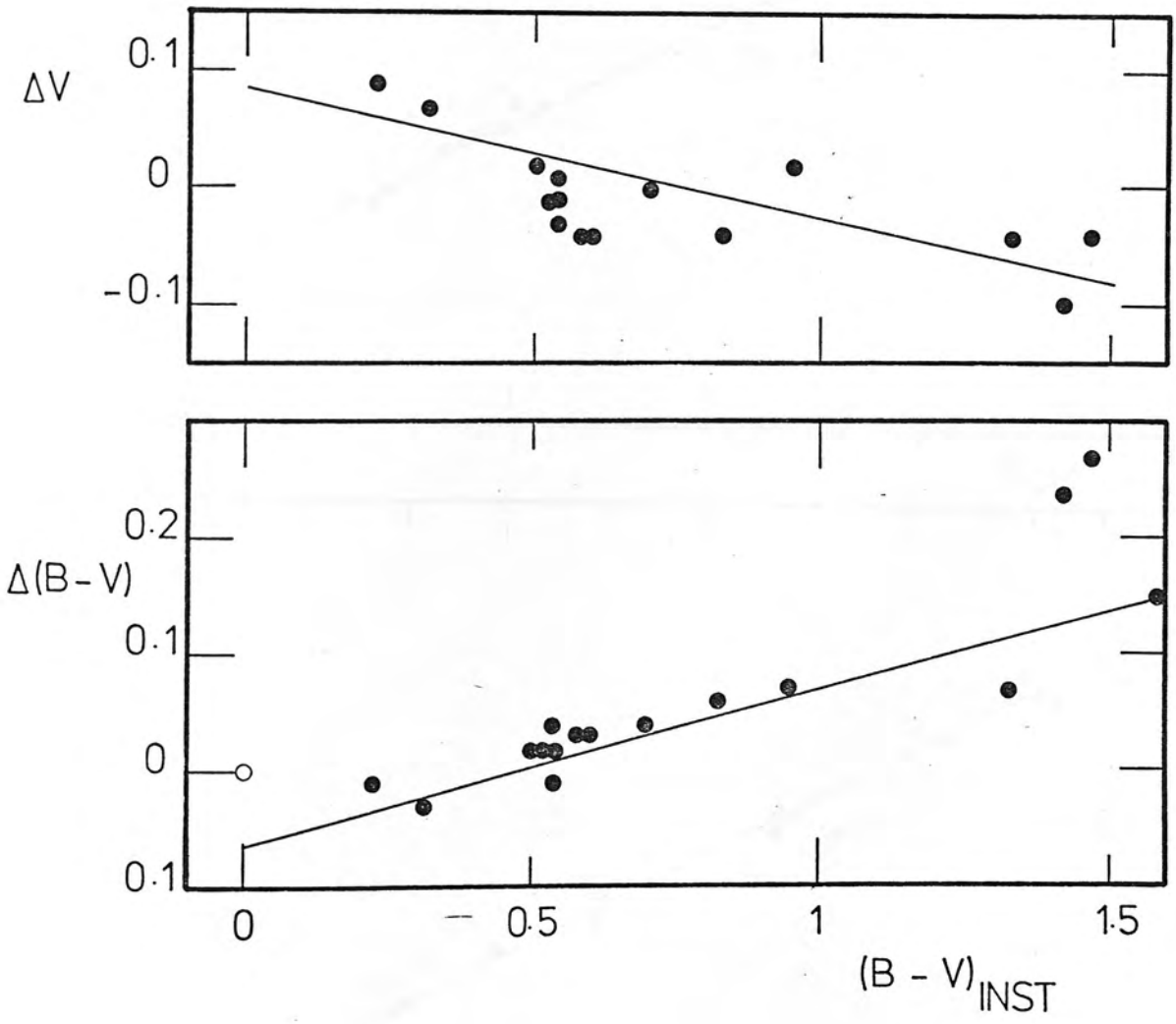

Fig. 4.6 Colour equation of AAT photoelectric sequence.

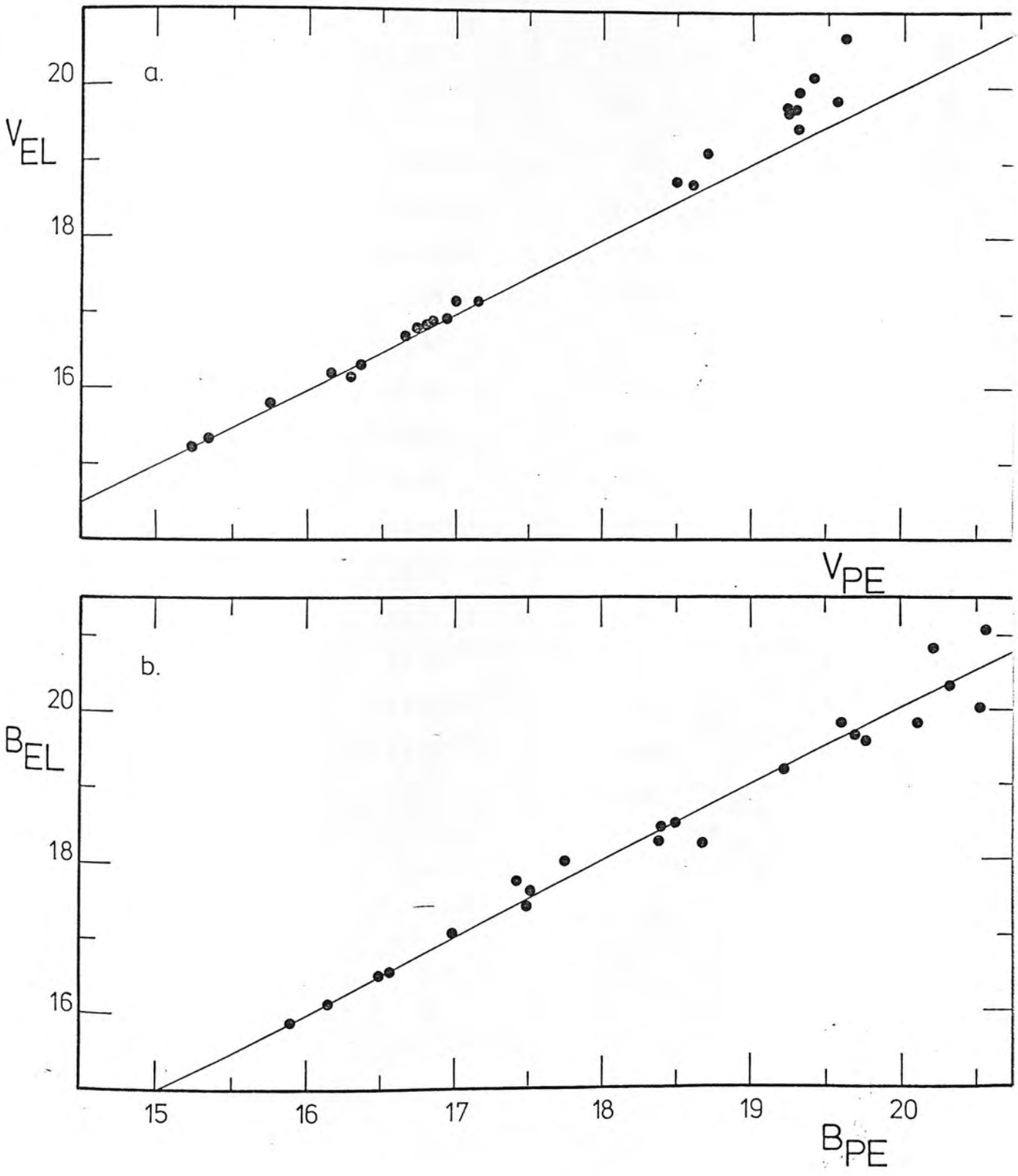

Fig. 4.7 Photoelectric magnitude compared with new electronographic magnitude.

TABLE 4.3

Star No.	V	B-V	n
33	19.28	.40	1
40	18.71	1.05	1
41	19.42	.67	1
42	19.28	.74	1
48	19.62	.94	1
51	17.15	.60	2
54	18.50	1.10	2
55	19.32	.89	1
57	18.62	.60	2
59	19.57	.76	1
61	19.31	1.21	3
62	19.24	.88	1
69	17.87	.67	2
70	17.17	1.51	2
71	15.32	.68	1

sequence made these new electronographic observations redundant.

4.4 Combination of Sequences

Figures 4.8a and b give the relation between the photoelectric AAT sequence and Walker's electronographic sequence and show satisfactory agreement at all magnitudes thus confirming the fact that Walker's electronographic process was linear. Figure 4.8 was drawn in the same way as Fig. 4.4, i.e. by measuring both sequences on a photographic plate and, using Walker's sequence as calibration, finding the magnitude for each star in the photoelectric sequence and plotting the two magnitudes together. Only stars from Walker's sequence were used which were clear of the centre of K3.

A further set of photometric data in this region of the SMC is that of Gascoigne (1978) which are also AAT twin photoelectric photometer data. Since Walker used only a small number of photoelectric standards to define the zero point of his electronographs and, in addition there is a rather large dispersion in his brighter measures, the zero point of this sequence is quite uncertain. In fact the zero points were set with reference to the resultant colour-magnitude diagram (Walker, 1970). Gascoigne's AAT measures are also uncertain in zero point so it was felt necessary to determine the zero points of these data by reference to the AAT sequence presented in the previous section, which will in future be called the Stewart-Cannon sequence. Since no stars are common to Stewart-Cannon and either of the others, comparison must be done via a photographic plate. Although unsatisfactory from several points of view, e.g. the possibility of transfer errors and the higher photometric dispersion

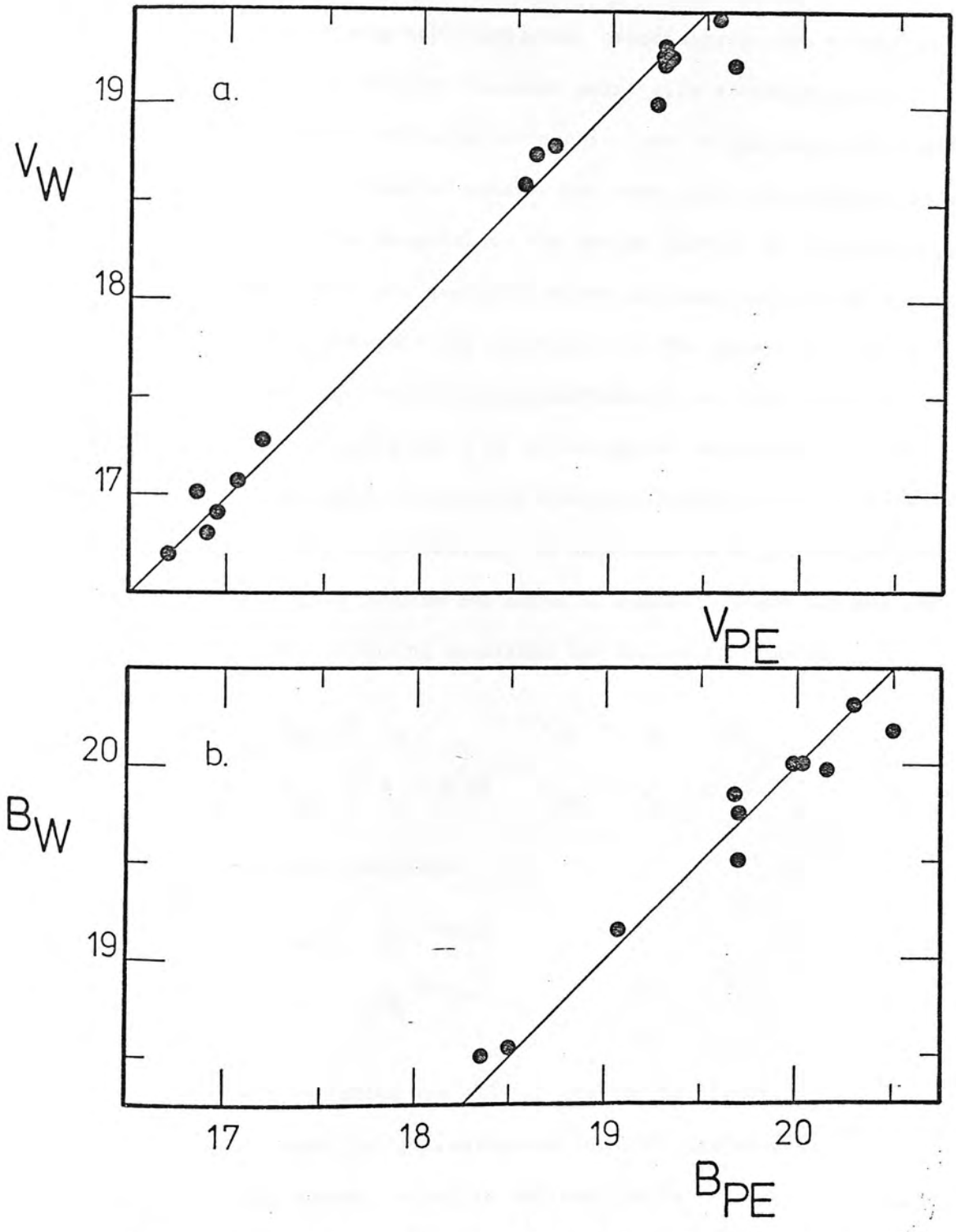

Fig. 4.8 Walker's magnitude versus AAT photoelectric sequence, via photographic transfer.

associated with a photographic plate, this approach has several advantages in the present context. Because of the large scatter in Walker's electronographic sequence, especially at the bright end, it is important to tie down the zero point with a statistically reasonable number of stars, which in this case is approximately twenty. This is difficult photoelectrically but easy via a photograph. Also, in view of the large dispersion, the spread induced by the photograph is negligible. Thus all available stars were measured in the sequences of Walker, Stewart-Cannon and Gascoigne and the region of overlap of Stewart-Cannon with the other two individually was used to fix the zero point in each of B and V by adjusting the magnitudes by a uniform amount until the mean calibration lines overlapped, i.e. by minimizing the magnitude difference between the sequences at a given iris reading. The results of this process are shown in Tables 4.4 and 4.5 and are expressed in the following equations for Walker's sequence:

$$\text{NORTH:}\quad B_{SC} = B_W \qquad V_{SC} = V_W - 0.03 \tag{4.3}$$

$$\text{SOUTH:}\quad B_{SC} = B_W - 0.07 \qquad V_{SC} = V_W - 0.06 \tag{4.4}$$

and for Gascoigne's sequence:

$$B_{SC} = B_G - 0.08 \tag{4.5}$$

$$V_{SC} = V_G - 0.10 \tag{4.6}$$

The data in Tables 4.4 and 4.5 are the magnitudes of Walker and of Gascoigne respectively transformed into the system defined by the Stewart-Cannon sequence which is believed to be reliable in both zero point and colour equation. The data of tables 4.3, 4.4 and 4.5 are used

TABLE 4.4

Star	V	B
1	20.32	21.06
2	19.65	20.70
3	21.55	22.18
4	20.95	21.32
5	17.69	18.70
6	20.06	20.82
7	21.02	21.26
8	19.02	19.84
9	19.82	20.69
10	20.40	20.72
11	21.30	21.90
12	21.60	22.27
13	19.65	20.76
14	21.18	21.76
15	20.59	21.37
16	18.98	19.76
17	20.15	20.94
18	20.72	21.48
19	22.43	22.73
20	19.08	19.80
21	19.79	20.69
22	19.17	19.84
23	20.86	21.53
24	16.45	18.85
25	20.36	21.07
26	16.77	18.22
27	19.14	19.95
28	18.99	19.97
29	19.18	20.12
30	18.83	19.64
31	18.14	19.05
32	18.59	19.69
33	18.60	19.48
34	17.81	19.02
35	16.68	18.01

TABLE 4.4 (contd)

Star	V	B
36	19.00	19.54
37	18.65	19.51
38	18.41	19.34
39	19.02	19.70
40	16.84	18.28
41	18.61	19.38
42	19.30	20.08
43	17.65	18.68
44	16.93	18.23
45	17.41	18.55
46	16.54	17.96
47	16.75	18.11
48	16.71	18.06
49	16.77	17.90
50	16.72	18.43
51	16.48	18.11
52	17.36	18.49
53	16.95	17.71
54	16.31	18.51
55	16.46	17.89
56	16.38	17.93
57	16.92	18.13
58	18.54	19.49
59	19.19	19.97
60	16.47	17.96
61	17.58	18.73
62	17.66	18.79
63	18.35	19.16
64	19.06	19.80
65	19.10	19.76
66	19.12	20.08
67	18.43	19.42
68	16.54	17.93
69	20.46	20.35

TABLE 4.4 (contd)

Star	V	B
70	20.23	21.06
71	19.13	19.91
72	18.92	19.61
73	19.06	20.05
74	20.37	21.09
75	20.94	21.65
76	17.73	18.16
77	19.87	20.67
78	17.47	18.93
79	18.83	19.74
80	20.14	21.00
81	18.88	19.73
82	20.27	21.03
83	20.21	20.76
84	21.38	21.78
85	19.66	20.52
86	20.88	21.45
87	20.97	21.44
88	19.23	20.09

TABLE 4.5

Star	V	B
4	19.42	19.93
5	18.85	19.87
6	17.58	18.90
7	17.15	18.34
8	14.48	15.29
9	18.99	20.06
10	16.58	18.06
11	16.70	18.00
12	17.87	19.07
14	16.81	18.18
16	17.92	18.88
18	17.28	18.53
20	17.72	18.74
22	19.72	21.11
29	18.04	18.67

in future for all plate calibration and are regarded as the best available photometric sequence in the area.

To summarise this chapter; a bright photoelectric sequence was established in the western region of the SMC and used to calibrate a set of electronographic plates. The magnitudes derived from these plates were found to differ systematically from those of Walker so faint photoelectric observations were made on the AAT which resolved the conflict in favour of Walker's sequence. The zero point of Walker's sequence, which is considerably fainter and more extensive was then fixed by comparison with the photoelectric sequence, as was the sequence of Gascoigne. All these sequences were then combined to use as standards for calibrating photographic plates.

CHAPTER V

COLOUR-MAGNITUDE DIAGRAMS

5.1 The Measurements

Photographic photometry was carried out on the objects listed in Table 5.1 and shown in Fig. 5.1. Finding charts for individual objects are presented in Appendix 2 along with magnitudes. The fourth column in Table 5.1 shows the number of plates in each of B and V measured and column 5 the number of images whose magnitudes were obtained.

An assessment of the errors in the photometry can be obtained by intercomparing magnitudes from different plates for the same object. This has been done for the data on NGC152 regions 3A,B, 4A,B, for which four measures in each of B and V exist. The procedure of Penston and Cannon (1970) was applied to the B magnitudes and the results are shown in Table 5.2 for σ_{1571} where σ_{1571} is the standard error of a single measurement on plate 1571 and is defined by

$$\sigma_{1571}^2 = \frac{4}{3(N-3)} \sum_{i=1}^{N} (\overline{B}_i - B_i^{1571})^2 \qquad 5.1$$

where $\overline{B}_i$ is the mean over all four plates for star i. This formula has allocated equal weight to all plates, which assumes they are of equal quality which is only approximately true. Column 3 gives the mean magnitude difference between the magnitudes from plate 1571 and the overall mean and shows a systematic difference between the two

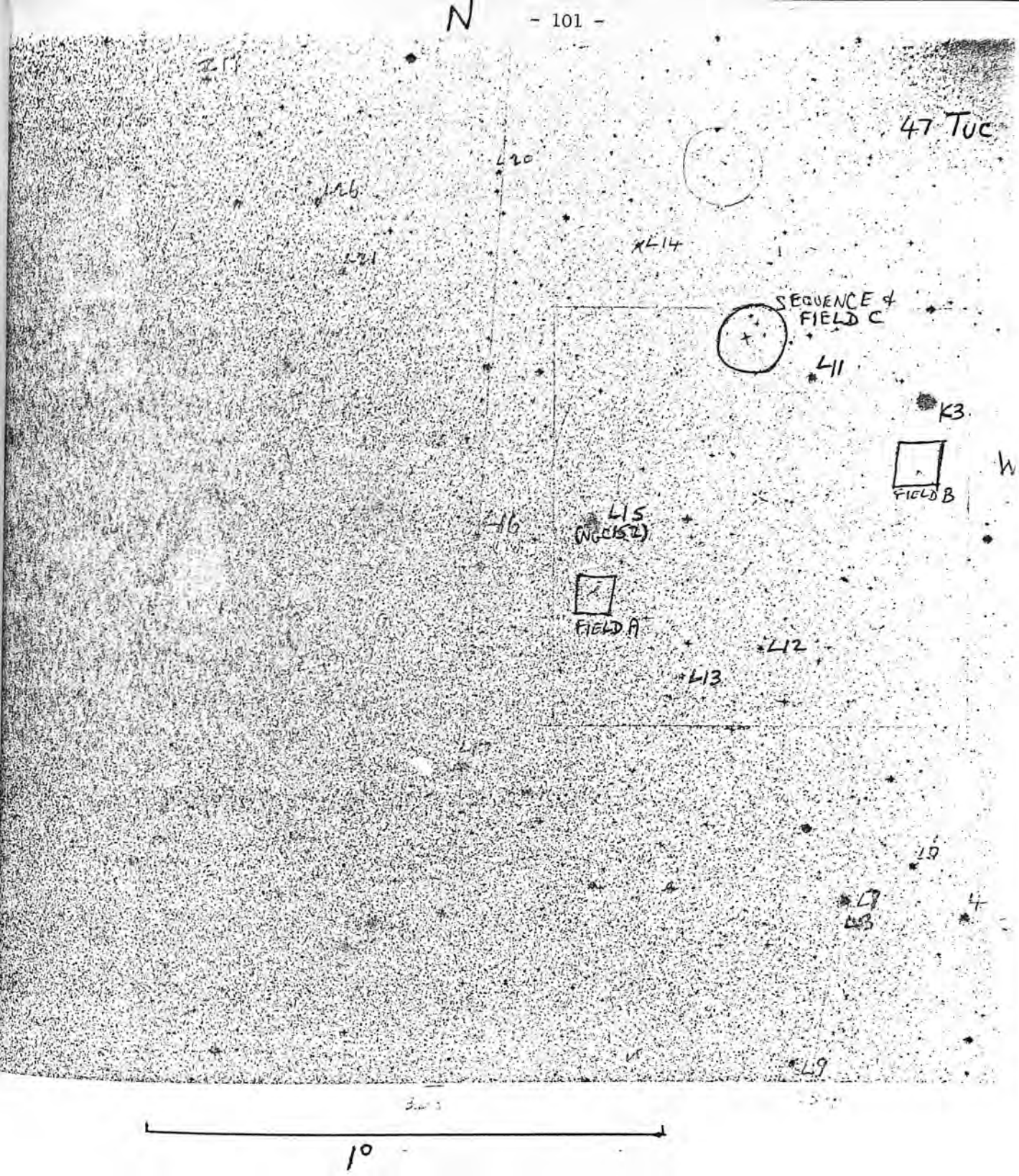

Fig. 5.1 Map of SMC showing objects measured.

TABLE 5.1

Object	R.A.(1975)	Dec.	No. of Plates	No. of Images
NGC152	$00^h31^m.9$	$-73^o16.'9$	4	770
K3	00 23.6	-72 56.1	2	649
L11	00 26.6	-72 55.8	1	119
L12	00 26.9	-73 26.9	1	52
L13	00 29.0	-73 31.7	1	92
Field A	00 32	-73 25	1	353
Field B	00 17	-73 10	2	404
Field C	00 28	-72 59	1	202

TABLE 5.2

B	σ_{1571}	$\langle \bar{B} - B_i \rangle$	σ^1_{1571}
18 - 18.5	.11	.04	.10
18.5 - 19	.09	.04	.07
19 - 19.5	.16	.08	.12
19.5 - 20	.16	.11	.10
20 - 20.5	.18	.12	.11
20.5 - 21	.15	.10	.12
21 - 21.5	.2	-.008	.2

TABLE 5.3

B	σ_{1571}
17.5 - 18	.05
18 - 18.5	.04
18.5 - 19	.05
19 - 19.5	.07
19.5 - 20	.07
20 - 20.5	.06
20.5 - 21	.06
21 - 21.5	.08
21.5 - 22	.10
22 - 22.5	.12

sets of data. When this systematic effect is removed, the dispersion is reduced to the figure in column 4. The systematic difference between different plates can most readily be attributed to photometer drift during measurement which was a problem when these data were obtained, hence the great importance of averaging over several plates. Later measurements were less affected by photometer drift as can be seen by comparing the two sets of measures available of stars in K3. Table 5.3 shows the standard error of a single measurement in B for the K3 data. All objects measured after K3 were measured on one pair of plates only.

5.2 NGC152

Four concentric annuli were drawn round the cluster and the inner two, excluding the centre, were observed completely while only a sector was observed in annuli 3 and 4. Table 5.4 gives the number of images in each region, with 3 and 4 combined, along with the same data for K3. Figs. 5.2a, b and c show the resulting C-M diagrams. It is immediately clear that all three are very similar and since the tidal radius of the cluster is approximately 1 arcmin the outer regions are largely composed of surrounding field stars, thus it appears that field and cluster are composed of similar stars. Two important groups of stars can be identified in the C-M diagrams, a group of faint blue objects at $V > 20$, $B-V \simeq .2$ and a group at $V = 19$, $B-V = .8$. The surface density of each group was determined by counting each type of star and these are given in Table 5.5, along with the surface density of objects brighter than $B = 19.5$, a small number of which appear in regions 3 and 4. The first point to be noted from Table 5.5 is the

TABLE 5.4

Object	Reg.	Inner Rad.	Area	Cluster Tidal Rad.	No. of Images
		arcmin	arcmin^2	arcmin	
NGC152	1	1.2	4	1	271
	2	1.8	4.6		224
	3,4	4.1	12		275
K3	1	.7	3	2	236
	2	1.2	10.6		412
L11	1	.8	2		
L12	1	.4	.5		
L13	1	.7	1.5		
Field A			7		
Field B		—	28.3		
Field C			9.4		

TABLE 5.5

Object		Faint Blue $arcmin^{-2}$	GB Clump	Young
NGC152	Reg. 1	23	22	
	Reg. 2	21	17	
	Regs. 3 & 4	9	9	.7
Field Reg. A		15.2	13.4	2.1

Fig. 5.2 a COLOUR-MAGNITUDE DIAGRAM FOR N152 Reg. 1

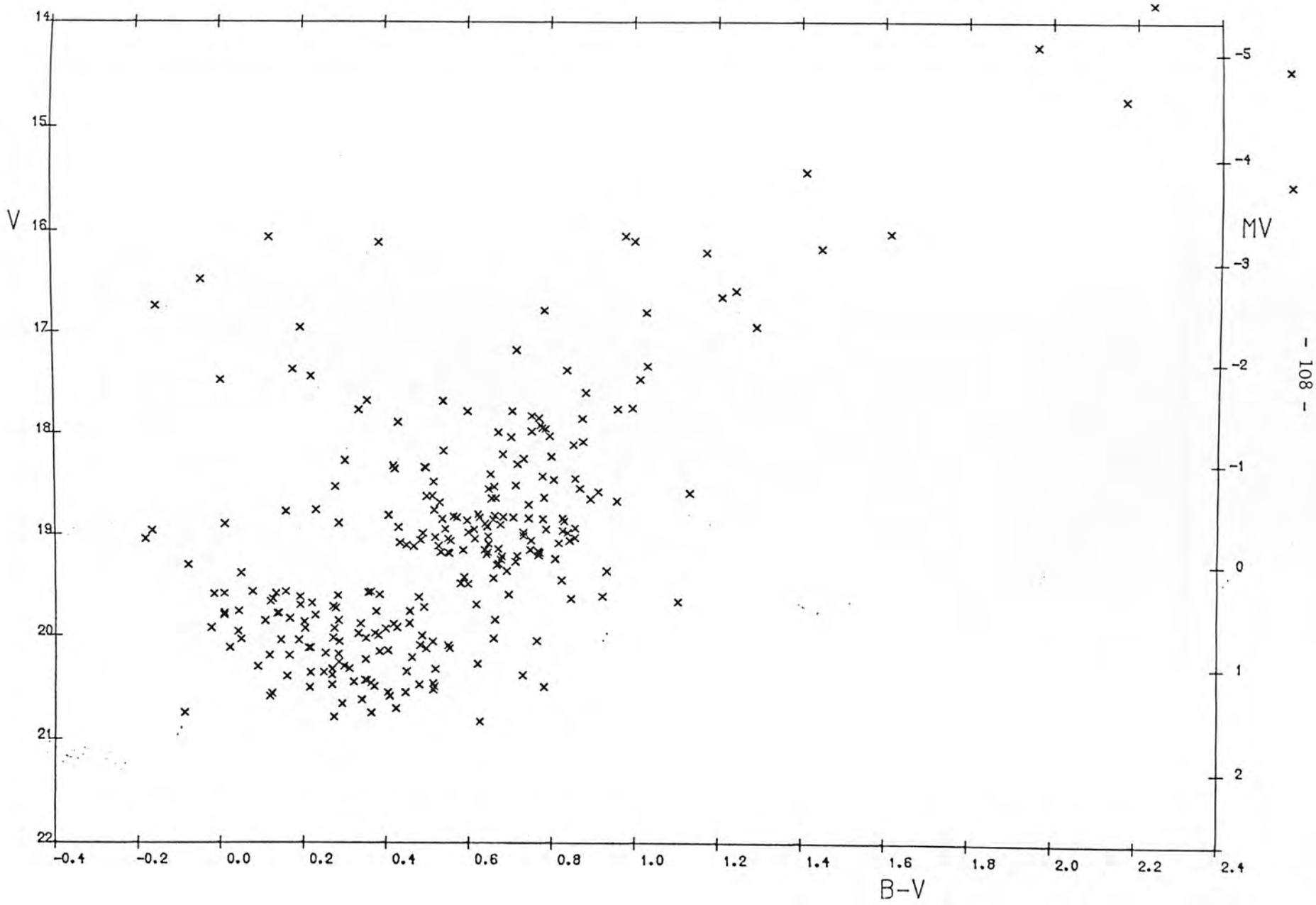

Fig. 5.2 b COLOUR-MAGNITUDE DIAGRAM FOR N152 Reg. 2

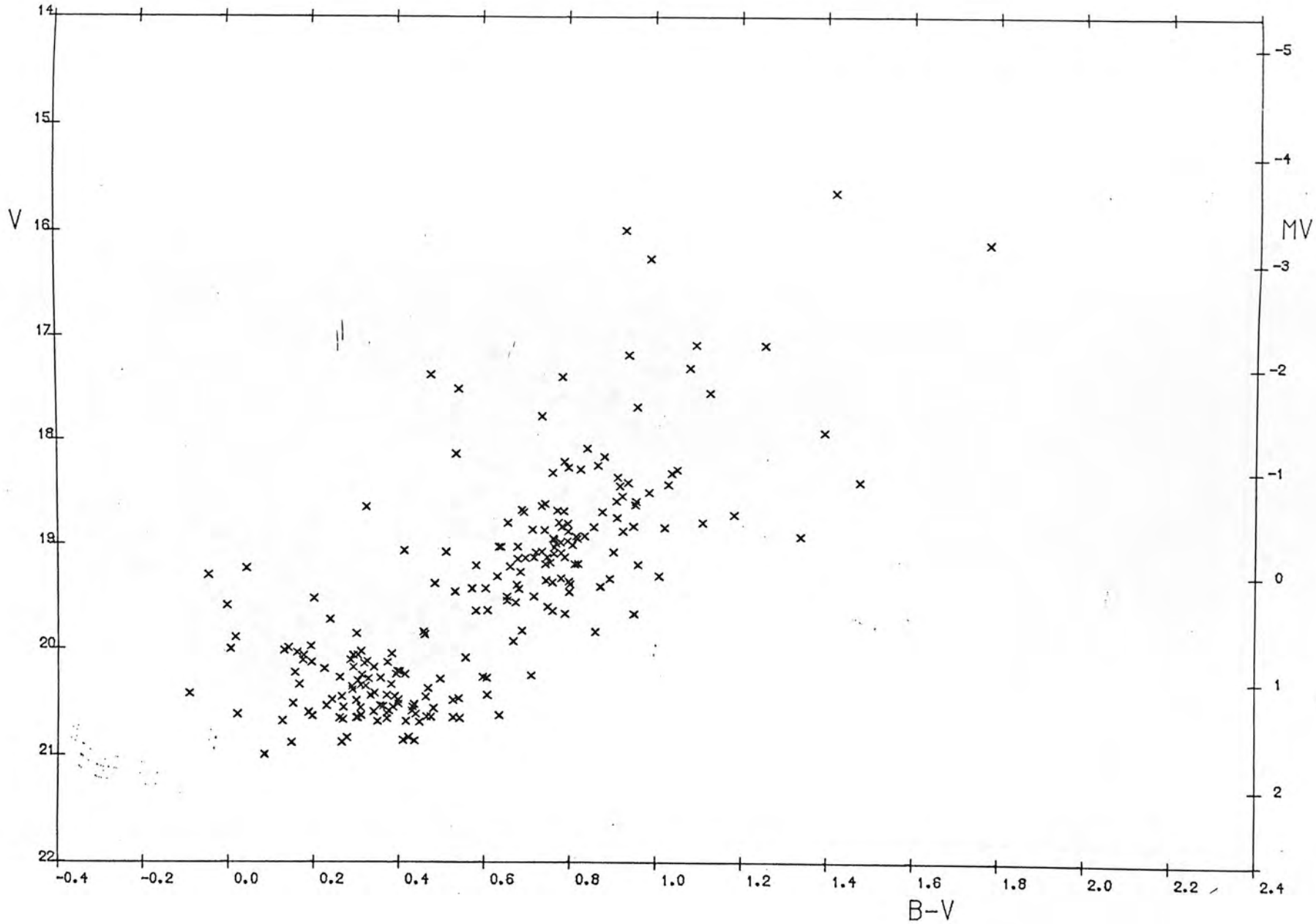

Fig. 5.2c COLOUR-MAGNITUDE DIAGRAM FOR N152 Regs. 3 and 4

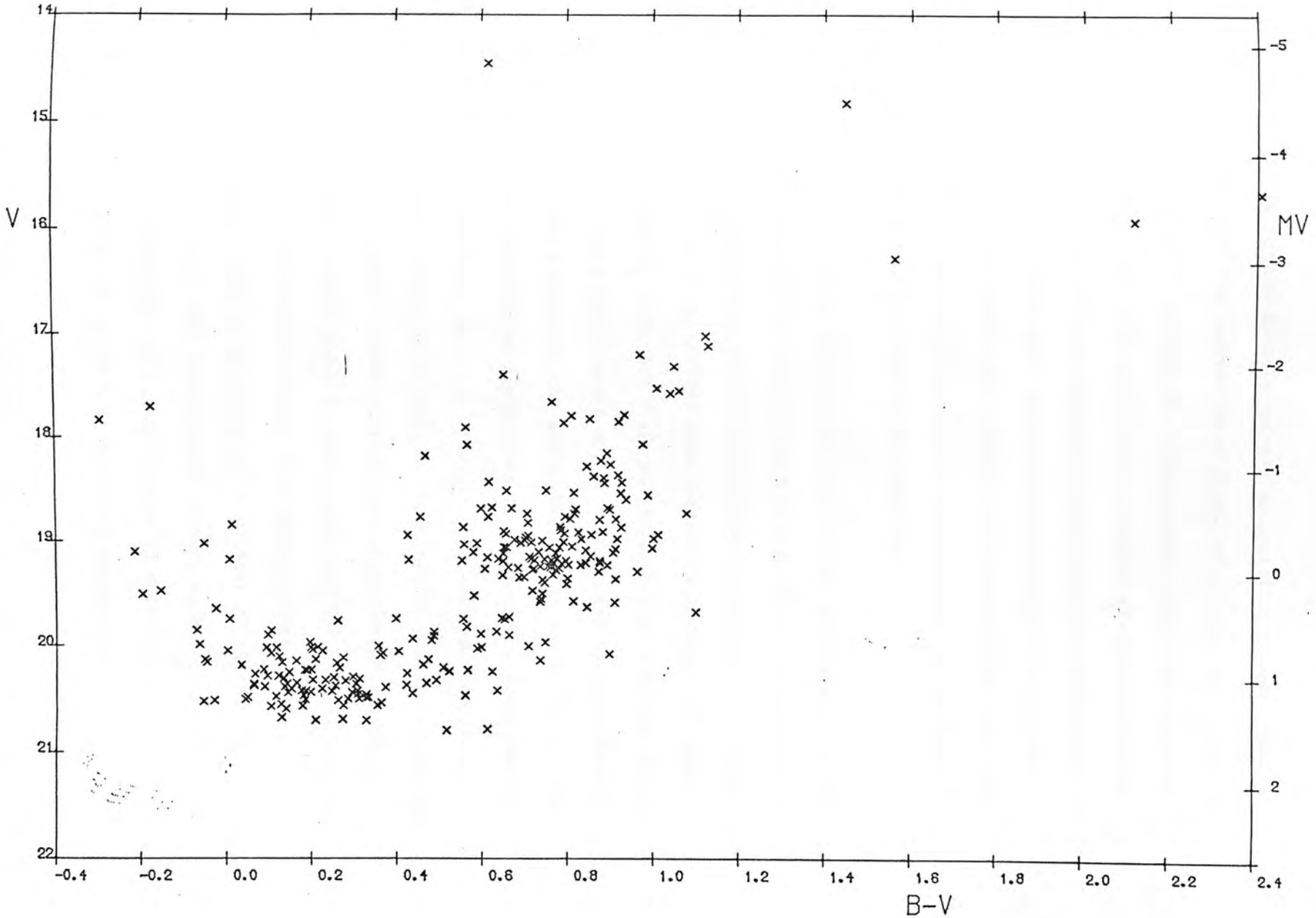

rapid fall in surface density of both main stellar groups, thus establishing that the similarity of field and cluster is not due to pollution of cluster samples by field objects, which is a serious problem when dealing with such compact clusters at great distances. Secondly, the two principal groups of stars decay in surface density at similar rates which again shows that the ratio of blue to red stars is similar in field and cluster. This result also shows that the blue and red stars belong together and are part of the same stellar population, i.e. are of the same age.

The most natural interpretation of these observations is that NGC152 is similar to the galactic open cluster NGC2477 (Hartwick et al., 1972) i.e. the red stars form a giant branch clump while the faint blue stars are the top of an evolved main-sequence with turn-off luminosity and colour $M_V = +1$, $B-V = .2$, as for NGC2477. Also the colour of the giant branch clump agrees approximately with that of NGC2477. Patenaude (1978) calculates the age of NGC2477 as 8×10^8 years, thus NGC152 and its surrounding field seems to consist of a homogeneous stellar population of age 8×10^8 years. The fact that the bright limit to the blue stars is so well defined indicates that the age of the population is well defined. Table 5.6 shows integrated photometry for NGC152 and K3 (from Alcaino, 1978) and for several galactic open clusters and individual stars from open clusters. Although no integrated photometry is available for a cluster of similar age to NGC2477, it is clear that the observed colours of NGC152 are consistent with the colours of individual objects in NGC2477, especially that in U-B, since the total U is dominated by main-sequence objects

TABLE 5.6

	$(B-V)_o$	$(U-B)_o$	Source
NGC152	.70	.18	Alcaino (1978)
K3	.69	.05	Alcaino (1978)
NGC7789 Incomplete	.71	.19	Arp (1964)
NGC7789 Complete	.62	.07	Arp (1964)
Typical T.O. Star in NGC2420	.4	-.03	McClure et al. (1974)
Typical T.O. Star in NGC2477	.2	.09	Hartwick et al. (1972)

and B nearly so, so that one expects the integrated U-B of a population 10^9 years old to be similar to that of a main-sequence turn-off star, which is what one observes in NGC152. Thus integrated photometry of NGC152 corroborates the interpretation that it is of age approximately 10^9 years.

The small number of blue objects brighter than B = 19.5 in Fig. 5.2c seems to be the main-sequence belonging to a younger population in the general field but at a much lower surface density than the NGC152 population.

An important point to note is the slight discrepancy in absolute magnitude of the important stellar groups in NGC152 compared to those in NGC2477. A difference of approximately $^m.3$ exists between the absolute magnitude of the giant clump in NGC152, assuming a distance modulus of 19.3, and that of NGC2477 derived by Hartwick et al. (1972). This may be due to the distance modulus of the SMC being too large, to NGC152 lying nearer to the Sun than the main body of the SMC, or to incorrect distance modulus for NGC2477. A difference in metallicity may also be the cause, this being consistent with the observed colours of the giant branch clump, B-V = .75 in the case of NGC152, cf. 0.9 in NGC2477. Hartwick et al. also report NGC2477 to be enhanced in heavy elements by a factor 1.5 compared to the Hyades. This latter is felt to be the most likely explanation of the discrepancy with the possible addition of an effect due to an incorrect distance modulus and reddening (for NGC2477, in view of the large absorption ($A_V \sim 1^m$) in front of that cluster).

5.3 Field Region A

This area is part of the general field south of NGC152, as can be seen in Fig. 5.1. It lies closer to the projecting tongue of HI to the south-west of the SMC, Fig. 5.3, and its C-M diagram may be seen in Fig. 5.4. This is similar to that of NGC152 so one is again detecting the 10^9 year old population to which NGC152 belongs but at a higher surface density, see Table 5.5. Also considerably higher in surface density is the $B \leq 19.5$ group. Thus it is clear that this region, approximately 1 Kpc from the optical centre of the SMC is dominated by a single stellar population of age approximately 10^9 years, supplemented by a younger group of age approximately 10^8 years, both of which are more dense in the areas of higher HI surface density, i.e. further south. It further appears that the surface density of the younger material has increased by a larger factor between the NGC152 vicinity and field region A than has the 10^9 year old population.

5.4 K3 and Field Region B

K3 is one of the richest clusters on the western side of the SMC and a sample of 649 stars was measured within the tidal radius of the cluster. For comparison, field region B, lying approximately 10 arcmin due south of K3 was measured. Figs. 5.5a,b show the C-M diagrams for the inner and outer annuli respectively. The inner annulus is badly affected by high background density and is useful only for indicating which groups belong to the cluster and which to the field, since it has a very high proportion of cluster members. It is immediately apparent that these diagrams differ from that for NGC152 and surroundings. Although the giant branch clump appears

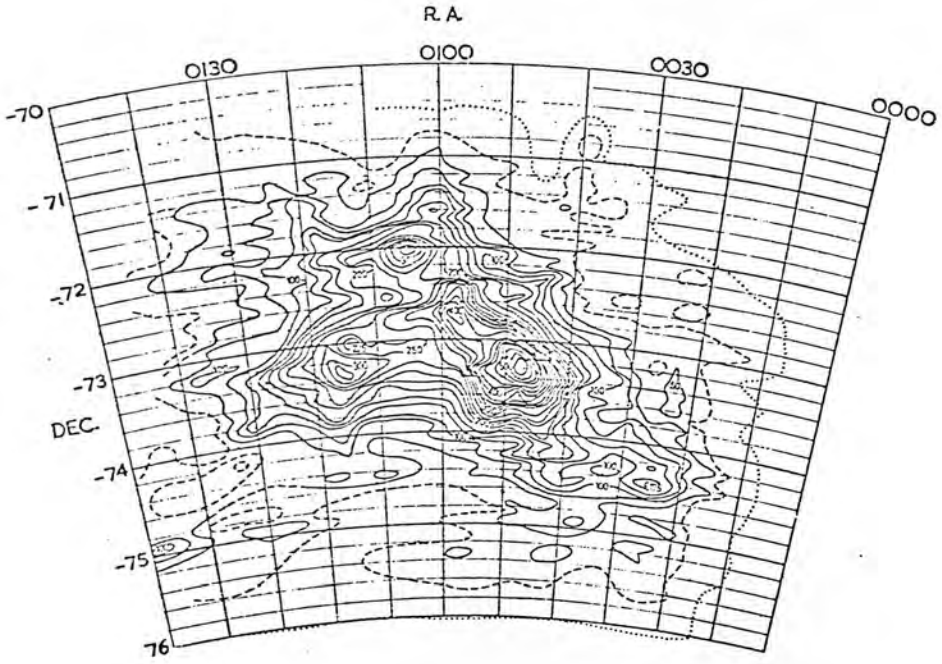

Fig. 5.3 Integrated HI surface density contours in SMC.

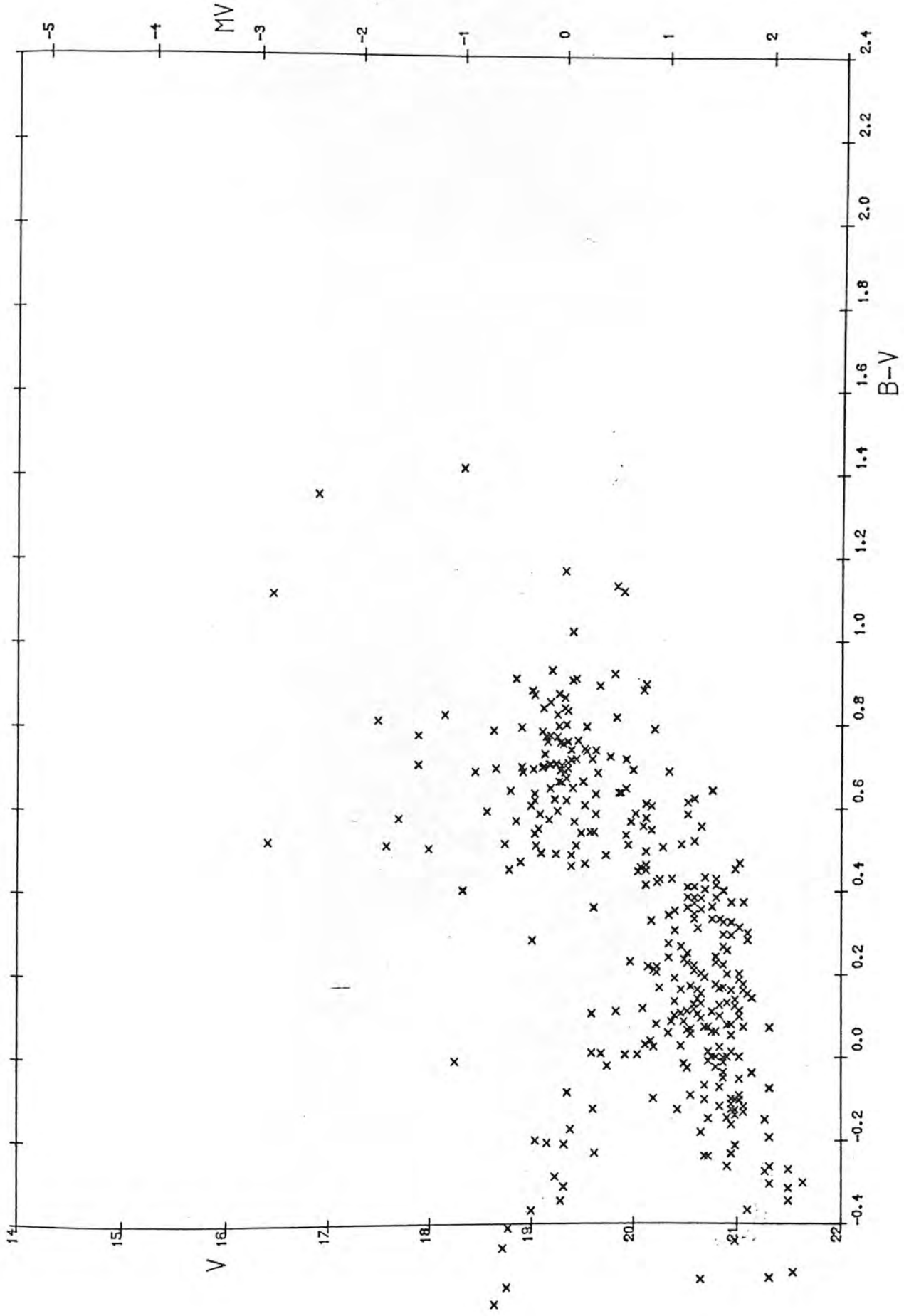
COLOUR-MAGNITUDE DIAGRAM FOR FLDA
MV
V
B-V
-5
-4
-3
-2
-1
0
1
2
14
15
16
17
18
19
20
21
22
-0.4
-0.2
0.0
0.2
0.4
0.6
0.8
1.0
1.2
1.4
1.6
1.8
2.0
2.2
2.4

Fig. 5.4

Fig. 5.5 a COLOUR-MAGNITUDE DIAGRAM FOR K3 Reg. 1

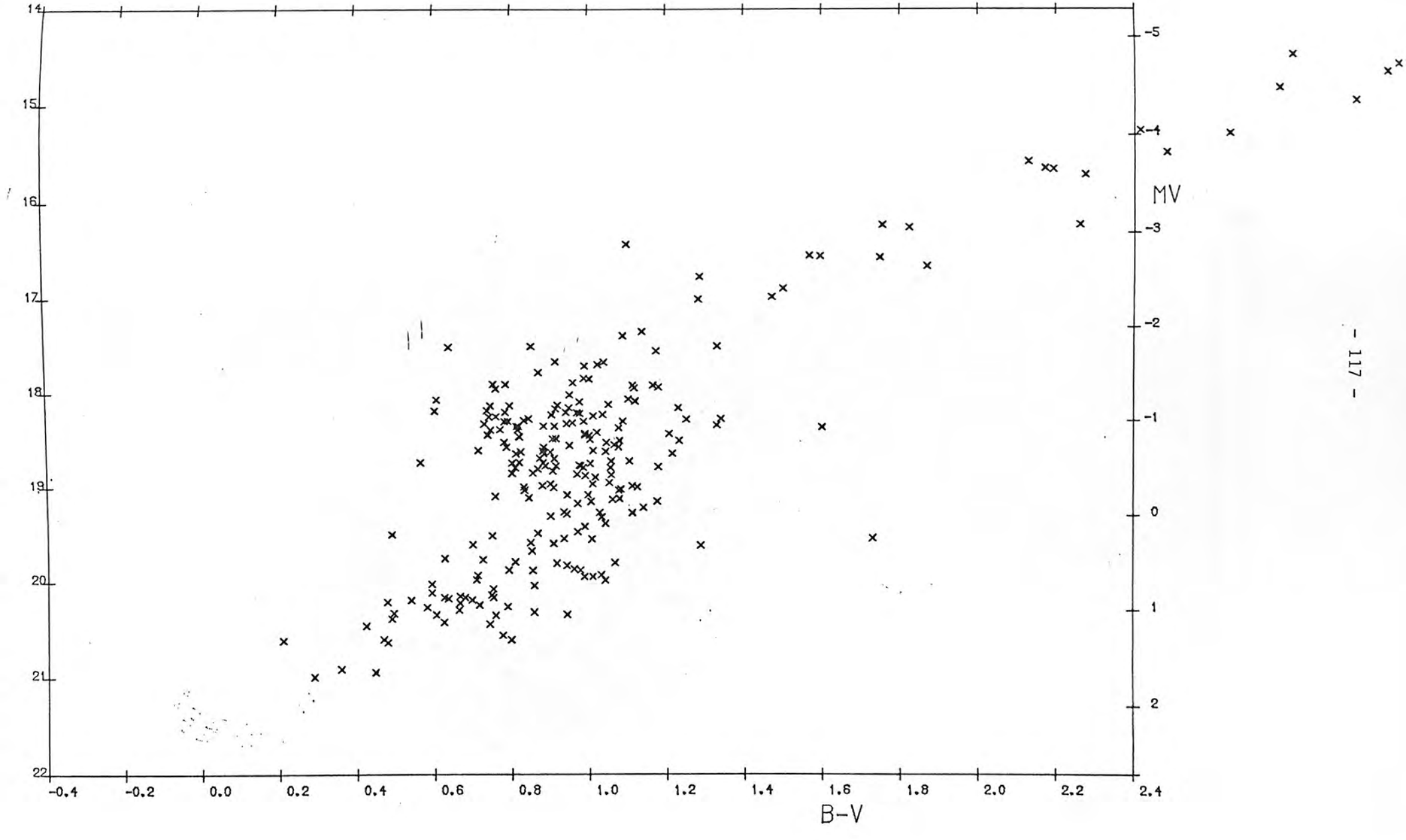

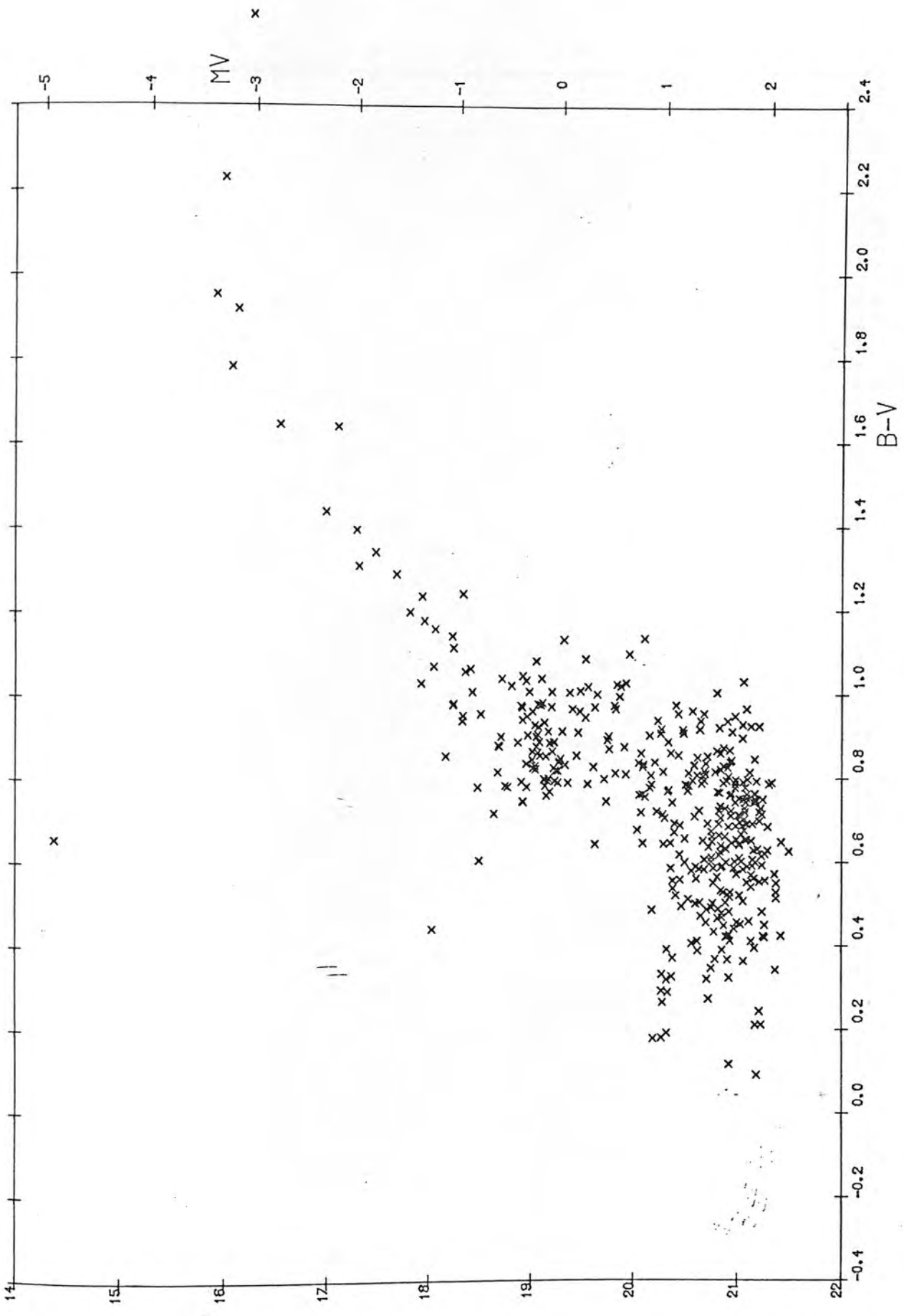
COLOUR-MAGNITUDE DIAGRAM FOR K3 Reg. 2
MV
V
B-V
-5
-4
-3
-2
-1
0
1
2
14
15
16
17
18
19
20
21
22
-0.4
-0.2
0.0
0.2
0.4
0.6
0.8
1.0
1.2
1.4
1.6
1.8
2.0
2.2
2.4

Fig. 5.5b

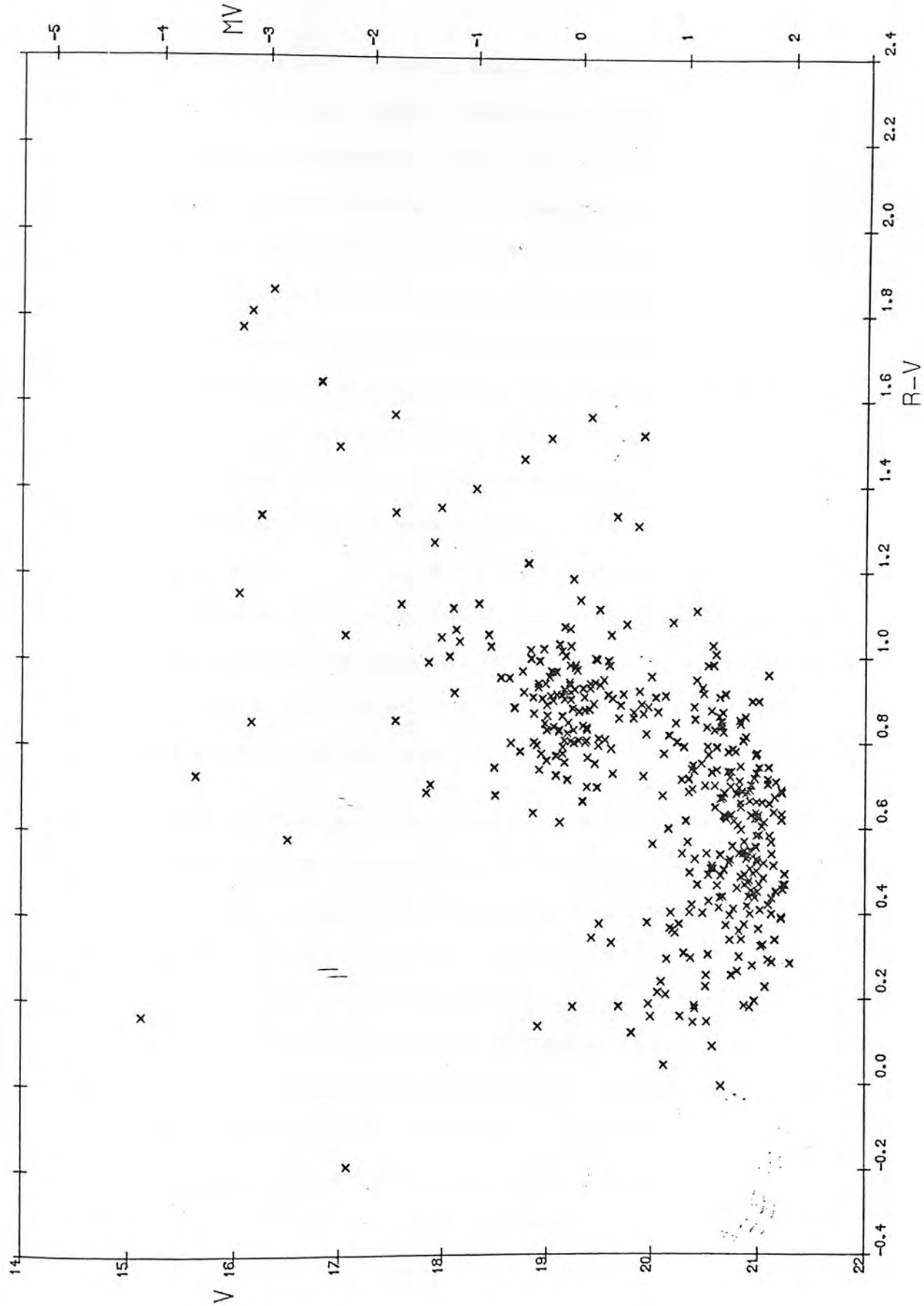
COLOUR-MAGNITUDE DIAGRAM FOR FLDB
MV
V
R-V
-5
-4
-3
-2
-1
0
1
2
14
15
16
17
18
19
20
21
22
-0.4
-0.2
0.0
0.2
0.4
0.6
0.8
1.0
1.2
1.4
1.6
1.8
2.0
2.2
2.4

Fig. 5.5 c

in K3, the faint blue stars appear in small numbers only in region 2 and not at all in the inner region. Instead, the dominant group of faint stars appears between B-V = .4 and .8 and fainter than V = 20.5. It seems clear that the faint blue stars belong to the field and not to the cluster, as the surface density is the same in the field as in the cluster, Table 5.7, but the giant branch clump and faint yellow stars are enhanced in the cluster by a factor 2 and 3 respectively. Thus Gascoigne's C-M diagram (Fig. 2.3) is misleading as it suggests a uniform population of objects to B-V = 0, whereas the cluster objects cease at B-V = .4. This is simply due to Gascoigne's B limit which just excludes the highly populated region of the CMD between B-V = .4 and .8. Correcting the field component for contamination by a NGC152 type population, one finds surface densities as on the lower two lines in Table 5.6, which shows an equal ratio of giant branch clump to faint yellow stars in field and cluster, which must be the case if the two are identical.

Thus again one finds a cluster embedded in a field of identical population type. However, the population is different from that of NGC152 and its surroundings. It is immediately clear that K3 is older than NGC152 since the faint blue stars are not found. Thus the main-sequence of K3 has burned down past B-V = .2. It is equally clear, from the existence of the faint yellow stars that K3 is not a classical globular cluster as such objects have a horizontal sequence much fainter, at M_V = +4, instead of the +2 of K3. It thus appears that K3 is of intermediate age with a turn-off colour of B-V = .4. The best studied cluster in the Galaxy with a turn-off colour of .4 is NGC2420 (McClure et al., 1974, see Fig. 1.5). NGC2158 (Arp, 1962) and

TABLE 5.7

Object	Faint Blue	GB	Faint Yellow
K3	2	7.5	16
Field B	2	4	5
K3 Corrected	0	5.5	16
Field B Corrected	0	2	5

TABLE 5.8

Object	Faint Blue	GB	Faint Yellow
Field C	1.5	5	6.5
Field C Corrected	0	3.5	6.5

NGC7789 (Arp, 1964) are further examples.

Comparing Fig. 5.5b with Fig. 1.5 shows K3 and NGC2420 to be very similar, bearing in mind that in K3 one has over 400 stars brighter than the turn-off, compared to approximately 30 in NGC2420. The absolute magnitude and colour of the horizontal sequence above the turn-off agree as do those of the giant branch clump.

An alternative approach to the problem of identifying K3 is through integrated photometry, as in NGC152. As can be seen in Table 5.6, the integrated B-V of K3 is the same as that of NGC152, but the integrated U-B is much bluer. Although apparently paradoxical at first, given the relative ages of the clusters, this result is easily understood in terms of the locus of main-sequence stars in the (B-V, U-B) plane, where the kink upward due to the Balmer Jump makes U-B at B-V = .4 considerably bluer than at B-V = .2. Table 5.6 shows individual photometry of a typical turn-off object in NGC2477 and in NGC2420, which shows this effect markedly.

Unfortunately no integrated photometry of a galactic open cluster of the age of NGC2420 is available, but Arp (1964) has constructed integrated colours from the known CMD of NGC7789. The results of this calculation are given in Table 5.6, the incomplete sample having only half the required number of turn-off stars, the complete result giving them full weight. The effect on the integrated cluster U-B of the main-sequence turn-off stars is quite marked and one arrives at colours similar to those of K3. Thus if one considers the known colours of turn-off stars in NGC2420 and the calculated integrated colours of NGC7789, it appears that the

integrated colours of K3 are similar to those of the former clusters, thus corroborating the identification of K3 as of intermediate age, similar to NGC2420.

Patenaude (op. cit.) calculates the age of NGC2420 as being 4×10^9 years, thus it would seem that this outer region of the SMC, approximately 2 Kpc from the optical centre is dominated by a homogeneous stellar population approximately 4×10^9 years old.

5.5 Field Region C

A third area of the SMC field adjacent to the new photoelectric standard sequence (Stewart-Cannon) was measured, partly to add another datum point concerning the population structure but also to check that no systematic errors arise from transferring standards across a plate, it being felt that if a given feature has the same magnitude and colour in widely separated areas of the plate then transfer errors are small. Field Region C is in the outlying area of the SMC, see Fig. 5.1, equidistant with Field Region B from the optical centre. It is not surprising, therefore that the colour-magnitude diagrams are very similar, Fig. 5.6 giving the CMD from Field Region C. Again one has the clump of giants and also the faint yellow stars and a small number of faint blue stars of the NGC152 main-sequence type. The surface densities of these groups are given in Table 5.8 and the results are very similar to those of Field Region B (Table 5.7). As in Field Region B, the amount of the young component with $B \leq 19.5$ which was detected in Field Region A and near NGC152 is very low and in fact has not been detected, the upper limit to its density thus being 0.1 objects per square arcmin,

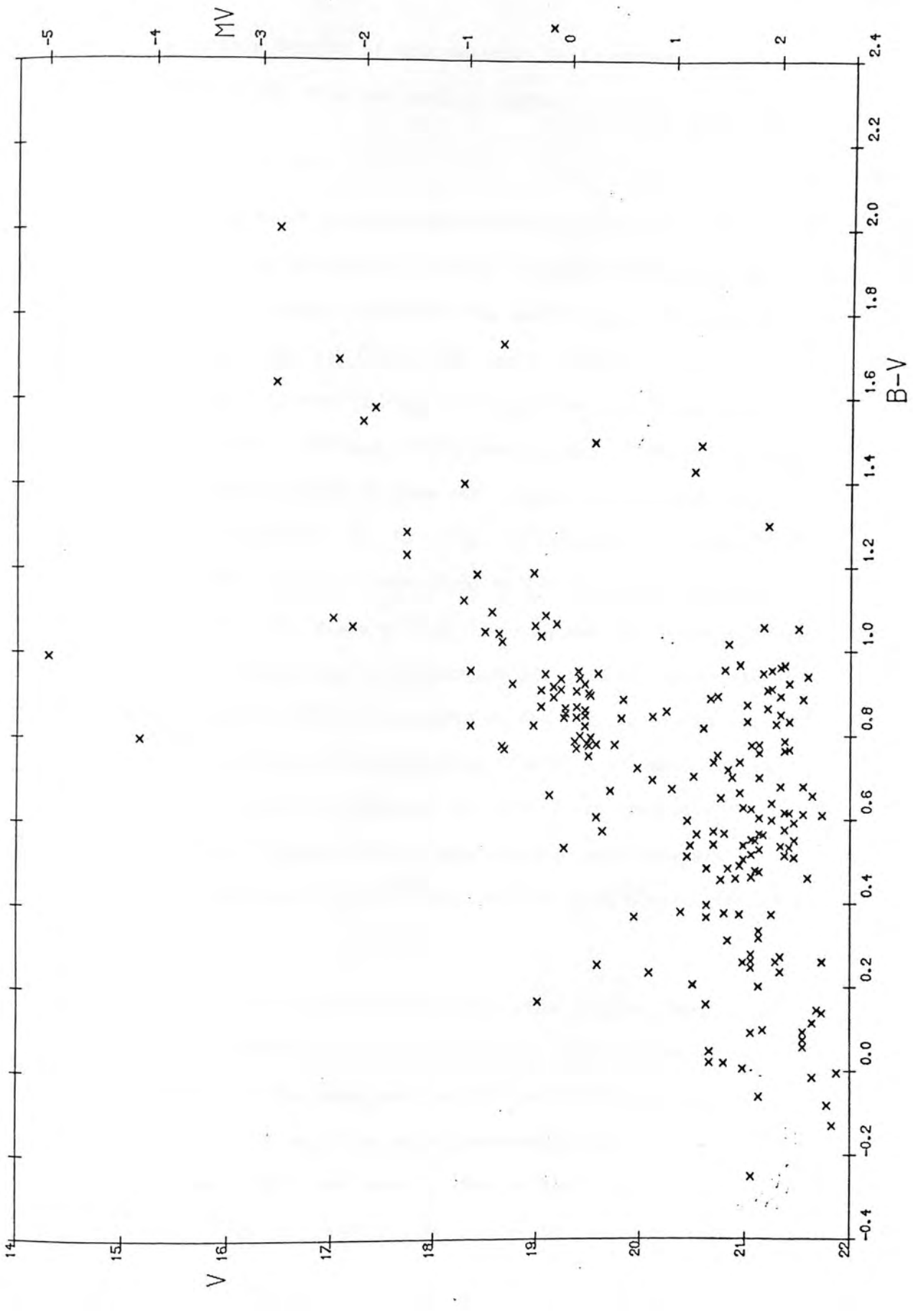
COLOUR-MAGNITUDE DIAGRAM FOR FLDC
MV
V
B-V
-5
-4
-3
-2
-1
0
1
2
14
15
16
17
18
19
20
21
22
-0.4
-0.2
0.0
0.2
0.4
0.6
0.8
1.0
1.2
1.4
1.6
1.8
2.0
2.2
2.4

Fig. 5.6

thus the surface density of this material falls off very rapidly between 1 and 2 Kpc from the optical centre.

5.6 L11, L12 and L13

These low mass clusters were measured on one plate in B and V but it proved very difficult to obtain a significant sample of cluster members, simply because of the small number of stars in these clusters. Table 5.1 gives the number of objects actually measured in each cluster and Fig. 5.7 shows the resulting colour-magnitude diagrams. Because of the small number of images in each case it is very difficult to make any reasonable interpretation of the CMD's. However that for L11 (Fig. 5.7a) seems to resemble the CMD for K3, with a giant branch clump at V = 19, B-V = .9, and a group of faint yellow stars between B-V = .5 and .9, although these are slightly brighter than the analogous group in K3, which may be due to the fact that L11 was measured on one pair of plates only. This interpretation is certainly consistent with a common origin for L11 and K3, which is suggested by their close proximity on the sky (separation 10 arcmin, 150 pc projected). Thus it appears that L11 belongs to the 4×10^9 years old population which includes K3.

L12 (Fig. 5.7b) seems to possess a giant branch clump, but also has some bluish stars at $V \approx 18.5$ whose origin is not clear. They may belong to the same group as is seen in Field Region A at $V \geq 18.5$, $B-V \approx -.1$, which is quite reasonable since L12 lies only 20 arcmin from Field A and seems to have a high surface density of field stars. They may, however, belong to the cluster as the number

is higher than one would expect given the surface density of such objects in Field A.

Unfortunately, the image of L13 is vignetted on plate 1571(B) because of the presence of the step-wedge calibration so reliable photometry is not possible, however a correction has been attempted based on the iris reading for the sky in the area of the sequence and near L13. Fig. 5.7c shows the resultant colour-magnitude diagram, which again has a group of red objects, which may be a giant branch clump, and some blue objects, which may be identical to the blue objects in Field A, the separation of Field A and L13 being 15 arcmin.

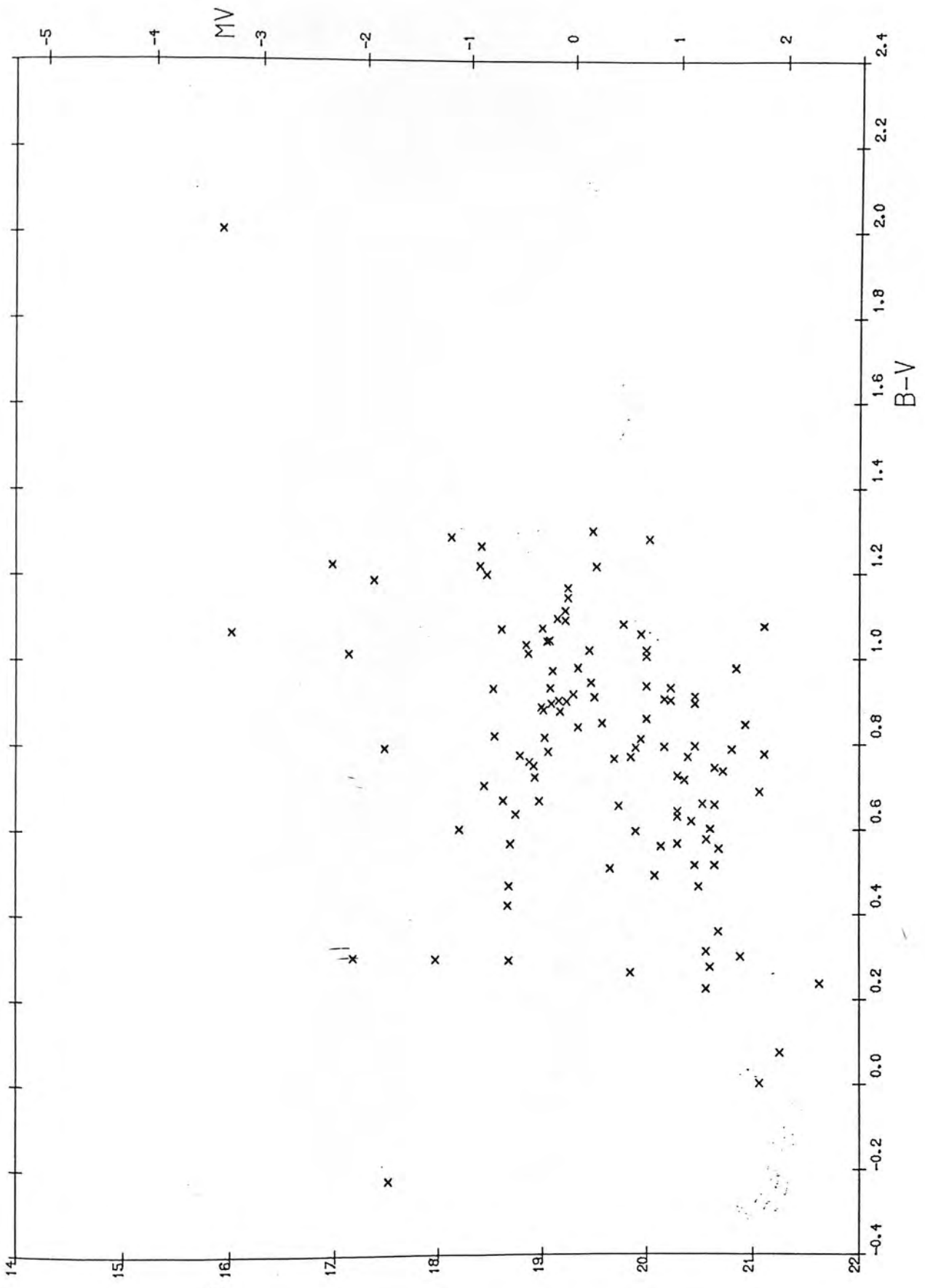

Fig. 5.7 a COLOUR-MAGNITUDE DIAGRAM FOR L11

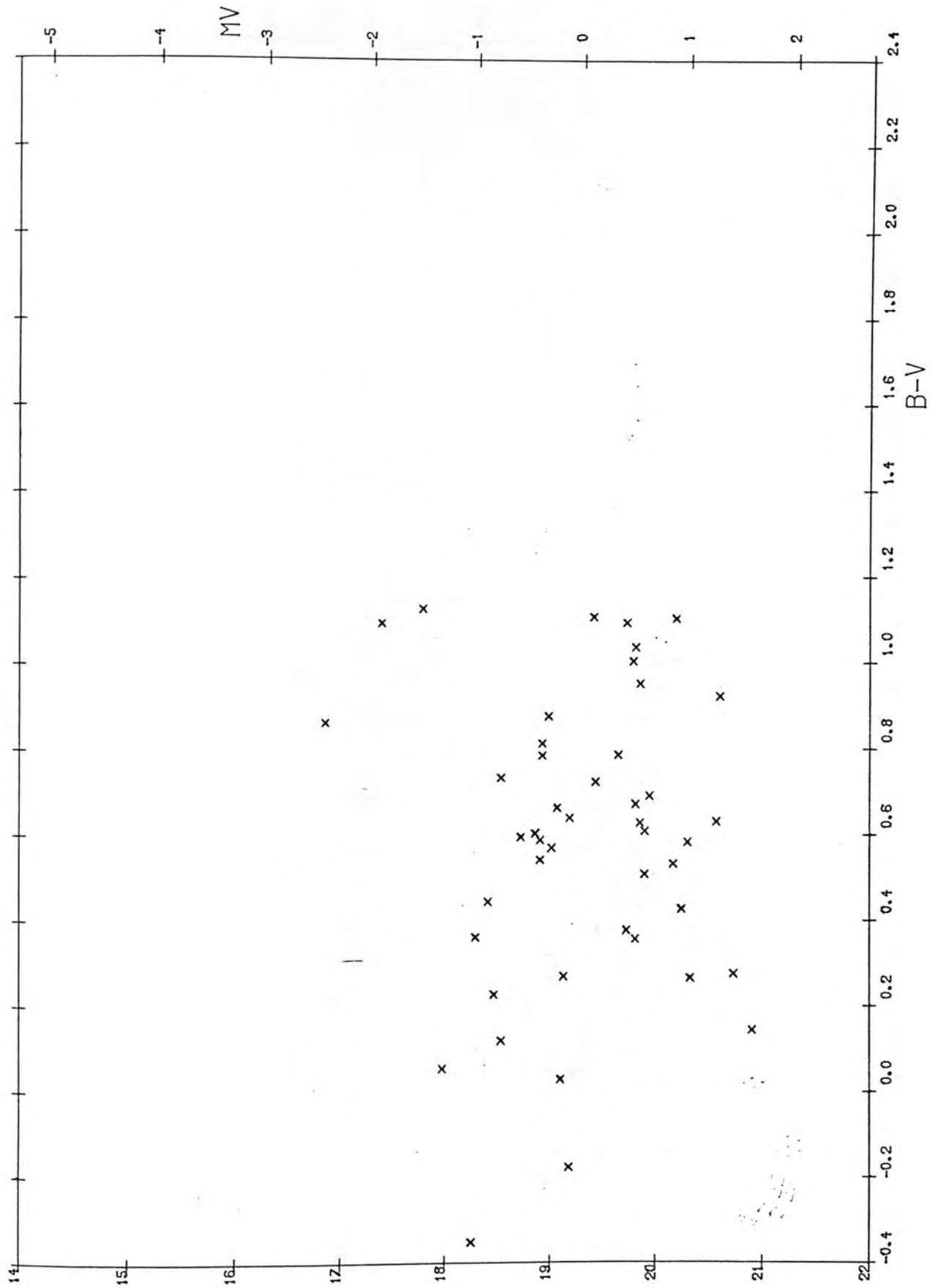
COLOUR-MAGNITUDE DIAGRAM FOR L12
V
MV
B-V
14
15
16
17
18
19
20
21
22
-5
-4
-3
-2
-1
0
1
2
-0.4
-0.2
0.0
0.2
0.4
0.6
0.8
1.0
1.2
1.4
1.6
1.8
2.0
2.2
2.4

Fig. 5.7 b

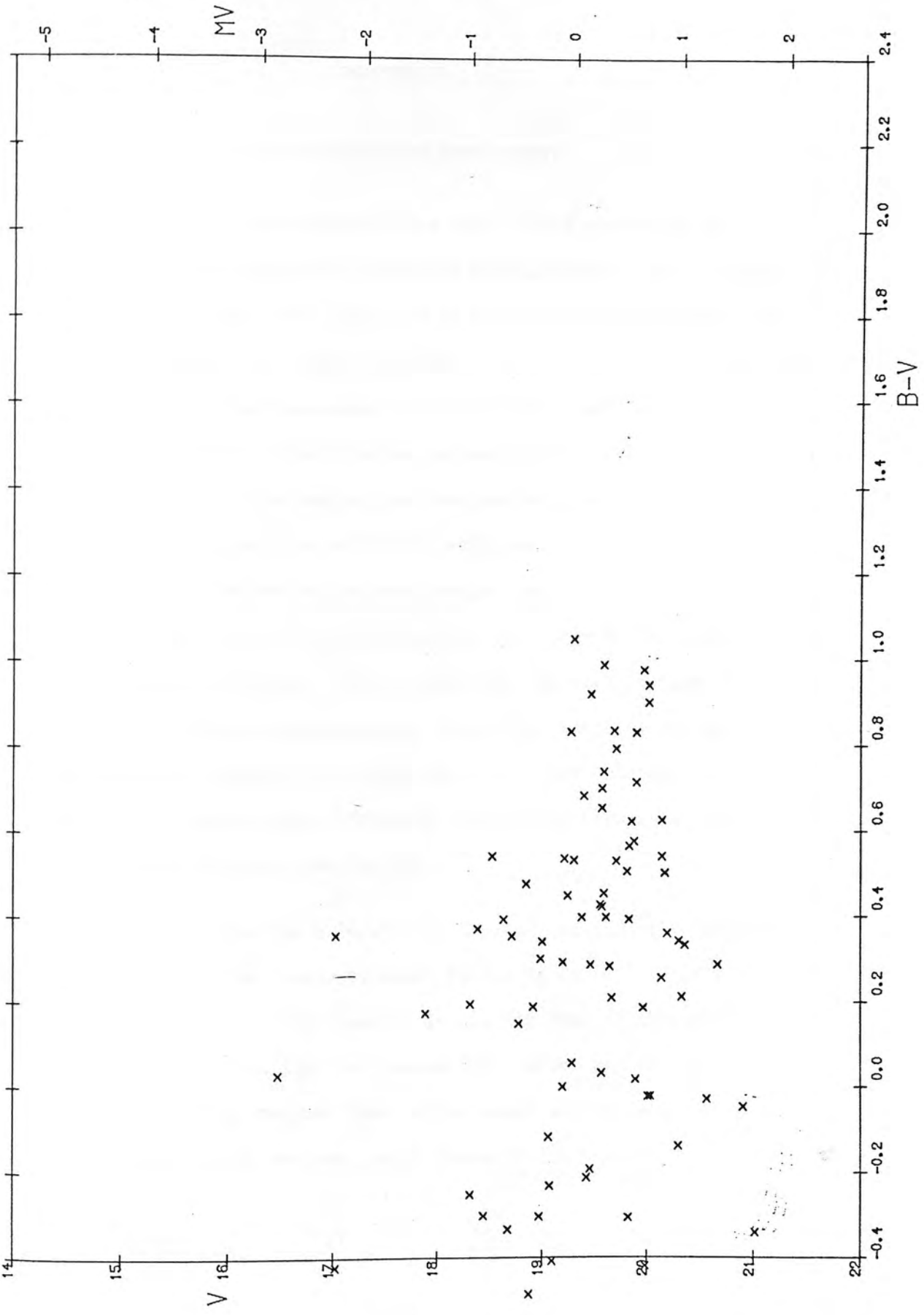
COLOUR-MAGNITUDE DIAGRAM FOR L13
MV
V
B-V
-5
-4
-3
-2
-1
0
1
2
14
15
16
17
18
19
20
21
22
-0.4
-0.2
0.0
0.2
0.4
0.6
0.8
1.0
1.2
1.4
1.6
1.8
2.0
2.2
2.4

Fig. 5.7 c

CHAPTER VI

RECAPITULATION AND DEVELOPMENT

The picture that emerges from the results presented in Chapter 5 of the population structure of the western outer regions of the SMC is that it is dominated by material of intermediate age. One has a widespread group of objects, including the clusters K3 and L11 which is of age approximately 4×10^9 years and is the dominant stellar population 2 Kpc from the optical centre of the SMC. Further in, at 1 Kpc from the centre, the dominant stellar population is of the same age as the cluster NGC152, which age is approximately 8×10^8 years. There also exists an even younger population of age less than 10^8 years which is confined strongly to the Bar and the areas of high HI surface density. It is clear that the scale height of the density is closely related to age, the oldest material having a large density scale height of the order of 1 Kpc, wide spatial extent whereas the young group is severely limited spatially, falling off rapidly with distance from the Bar.

The fact that the main stellar populations are of intermediate age may explain the observations of Blanco et al. (1978) of a greater ratio of carbon stars to M giants in the SMC than in the LMC which is in turn greater than that in the galactic centre region. Feast and Lloyd-Evans (1973) suggest that carbon stars are produced preferentially in intermediate-age systems, so if inequality 6.1 is true, one has an

$$\frac{M_{INTERM}}{M_{TOT}} \text{ (SMC)} > \frac{M_{INT}}{M_{TOT}} \text{ (LMC)} > \frac{M_{INT}}{M_{TOT}} \text{ (GAL.CEN)} \qquad 6.1$$

immediate explanation of the large numbers of C stars in the SMC. The spatial distribution of the objects found by Blanco et al. has not been published, so an important follow-up project would be to compare the density of C stars with that of intermediate-age material to check for detailed correlations.

It further seems clear from Chapter 5 that star formation in the SMC has occurred in discrete bursts, of which two have been detected, viz. a burst at about 4×10^9 years ago, another at 8×10^8 years ago. In addition there seems to have been sporadic star formation during the last 10^8 years. Although not detected in the present work, there may exist an earlier stellar population of even greater spatial extent and density scale height, viz. that represented by the RR Lyrae variables found by Graham and by the cluster NGC121. This last population has been classed as a conventional galactic halo, similar to that in our Galaxy in structure, origin and age, which is thought to be approximately 10^{10} years. Thus one finds that there seem to have been three main bursts of star formation in the SMC at intervals of 3 and 6×10^9 years. This result indicates immediately a profound difference between the evolutionary history of the SMC and of the Galaxy, the latter having experienced a widespread burst of star formation approximately 10^{10} years ago with an almost uniform star formation rate since then.

One can understand this difference in star formation history in terms of the kinematics of the SMC as compared with that of the Galaxy. In the Galaxy, HI unprocessed after the initial burst of star formation fell very rapidly, on a timescale of 3×10^8 years,

(Eggen, Lynden-Bell and Sandage, 1962) into a disc where star formation continued up to the present. The dynamical timescale for free-fall under gravity is given by Tayler (1970) as

$$t_d = \left(\frac{2R^3}{GM} \right)^{\frac{1}{2}} \qquad 6.2$$

thus for similar linear scales the dynamical timescale in the primordial SMC HI cloud is about ten times that in the Galaxy, or approximately 3×10^9 years. However the radius of the K3 population is approximately 3 Kpc, substituting which value into equation 6.2 gives $t_d \sim 2 \times 10^8$ years so that the remnant HI left over after the formation of the K3 population should have collapsed to very small dimensions long before the formation of the NGC152 population. Thus one is faced with the serious problem of explaining why the HI that went to produce the K3 population had not collapsed by the time, 3×10^9 years later, the NGC152 population was found. The most likely solution of this problem is that angular momentum in the primordial HI cloud leads to spin-up as the cloud contracts which stabilises the HI against further infall precisely as happened in the Galaxy. This may be expected to lead to flattening so one is probably dealing with a disc-shaped system, a configuration discussed by Westerlund (1972).

A further problem arising from such a picture of widespread star formation at well defined epochs is to find a mechanism that will produce star formation on such a scale. It is known that star formation occurred throughout the Galaxy 10^{10} years ago but since then it has been local, confined to spiral arms etc.

One possible mechanism to initiate star formation is shocking of HI by rapid perigalactic passage of the Magellanic Clouds in their orbit around the Galaxy as discussed in Matthewson et al. (1974). Such an orbit has been presented by Davies and Wright (1977) in explaining the origin of the Magellanic Stream as tidally-stripped HI drawn out of the LMC/SMC system (the so-called Magellanic Galaxy) by the Galaxy during the last perigalactic passage. The time since perigalactic passage which Davies and Wright found to best fit the HI radial velocity observations was 2-3 x 10^8 years. Matthewson et al. (1974) suggested a time of 5-10 x 10^8 years since the last perigalactic passage. These figures are in reasonable agreement with the 8 x 10^8 years age found for the NGC152 population in the SMC, suggesting the NGC152 group of stars may have been produced as a result of the last perigalactic passage.

One can carry this argument one step further and apply the same process to the K3 population and say that the 4 x 10^9 year old material also was produced by shocking of HI during perigalactic passage but on the previous cycle of the orbit. One must ensure that a period of 3-4 x 10^9 years is consistent with all available observations, which consist, inter alia, of Magellanic Cloud-Galaxy distance and radial velocity. Equation 6.3 (Kepler's Third Law) immediately gives one the semi-major axis, a for the orbit of the Magellanic Galaxy about the Galaxy.

$$P^2 = \frac{4\pi^2}{GM} a^3 \qquad 6.3$$

Assuming P = 3.5 ±.5 x 10^9 years one finds a = 63 ± 6 Kpc. This appears

to be a very reasonable semi-major axis, approximately equal to the present separation of the Galaxy and Magellanic Galaxy. Using the perigalactic distance of Davies et al., viz. 25 Kpc, equation 6.4 gives the eccentricity of the orbit, the value being .6 ± .04, which

$$Q = a(1 - e) \qquad 6.4$$

agrees extremely well with the best fit eccentricity of Davies et al. Equation 6.5 can now be used to calculate the maximum distance to the Magellanic Galaxy, viz. that at apogalacticon, the value being 101 Kpc.

$$R_{MAX} = a(1 + e) \qquad 6.5$$

Knowing the present distance to the Magellanic Galaxy, equations 6.6 and 6.7 (Van de Kamp, 1964, see Fig. 6.1 for definition of symbols) may be used to determine the present phase of the orbit, which can then be substituted into equation 6.8 to give the present radial velocity, which may be compared with observations.

$$r = a(1 - e \cos E) \qquad 6.6$$

$$\tan \frac{v}{2} = \sqrt{\frac{1 + e}{1 - e}} \tan \frac{E}{2} \qquad 6.7$$

$$V_r^2 = \frac{GM e^2 \sin^2 v}{a(1 - e^2)} \qquad 6.8$$

Using a present distance of 50 Kpc for the Magellanic Galaxy, v is 1.9 rads. (109^0) and V_r turns out to be 80 km sec^{-1}, having just passed through its maximum value of 89 km sec^{-1}. This figure agrees

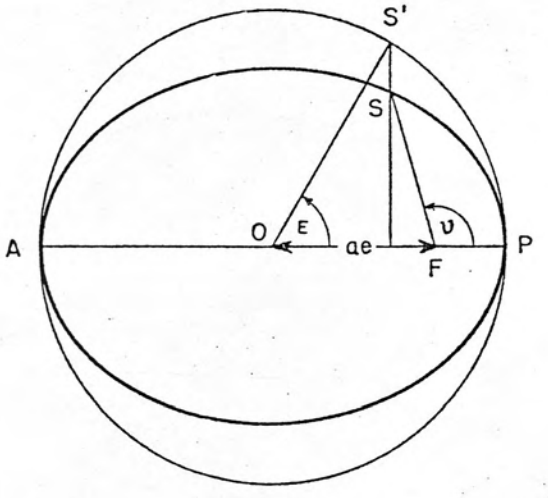

Fig. 6.1 Definition of symbols for elliptical orbit.

reasonably well with the observed radial velocity of the Magellanic Galaxy of approximately 50 km sec^{-1}.

One can further check for consistency among these data by calculating the phase from v, thus finding the time since perigalactic passage, t, which can then be compared with the value of approximately 5×10^8 years. Equation 6.9 gives $\phi = .66$ which implies $t = 4 \times 10^8$ years,

$$\phi = E - e \sin E = \frac{2\pi t}{P} \qquad 6.9$$

which agrees very well with the values of Davies et al., Matthewson and Cleary and with that derived from stellar ages in the SMC. From equation 6.10 one can calculate the total velocity of the Magellanic Clouds at perigalacticon, the value being 230 km sec^{-1}, while the total velocity at apogalacticon, given by 6.11 is only 56 km sec^{-1}.

$$V_P^2 = \frac{GM(1+e)^2}{a(1-e^2)} \qquad 6.10$$

$$V_A = V_P \frac{(1-e)}{(1+e)} \qquad 6.11$$

One thus arrives at a consistent orbit by imposing the constraint that the period be approximately 3.5×10^9 years, with the further properties that the time since perigalactic passage is approximately 5×10^8 years, present distance 50 Kpc and furthest separation 100 Kpc, which will be reached in about 10^9 years.

Hence it appears feasible that successive perigalactic passages could give rise to widespread star formation in the Magellanic Clouds leading to the observed discrete populations with older objects being more widespread and tenuous.

To test these ideas it will be necessary to determine how widespread these star formation bursts have been. One should observe these populations wherever in the Magellanic Clouds the HI density was high enough to condense into stars, which should mean that the K3 population, for instance is a circular disc, elliptical on the sky with diameter approximately 5 Kpc centred approximately on the Bar. Hardy (1979) finds a good deal of intermediate-age material in the region of the cluster NGC419 which is of the same age as NGC2158, i.e. about 4×10^9 years. Hardy (1977) may also have found considerable quantities of intermediate-age stellar material in the Bar of the LMC. Further follow-up projects would clearly be to map the intermediate-age population in both Clouds and correlate the surface density with that of HI. If it was found that both Large and Small Clouds had stellar populations with similar formation times, it would be very difficult to explain in ways other than gravitational interaction with the Galaxy. A search might also be made for stars in the Magellanic Stream, although even if star formation was initiated at the last perigalactic passage, it is not obvious that stars would be found in the tidally stripped material, since if braking of the gas by an intergalactic medium or internal dissipation occur the gas and stars will decouple kinematically and separate, as suggested by Oort (1974). If, on the other hand, gas and stars move together, as

a pure gravitational interaction would require, one would expect stars present in the Magellanic Stream which were actually older than the Stream, viz. objects which belonged to the SMC which were tidally stripped along with the HI, which could have any age whatever.

In summary, it appears that the history of star formation in the SMC has consisted of three discrete bursts, the last two of which were initiated by perigalactic passage of the Magellanic Clouds about the Galaxy. Between bursts the unused HI has fallen, in the form of a disc, slowly in toward the centre of mass, being supported by rotation, so that the spatial extent of the stellar populations is smaller the more recently they were formed.

BIBLIOGRAPHY

Ahmed, F., Lawrence, L.C. & Reddish, V.C. (1965), R.O.E. Publications Vol. 3, No. 7.

Alcaino, G. (1975), A. & A. Supp., 21, 279.

Alcaino, G. (1978), A. & A. Supp., 34, 431.

Allen, C.W. (1973), Astrophysical Quantities, Athlone Press, London.

Ardeberg, A. & Maurice, E. (1977), A. & A. Supp., 30, 261.

Argue, A.N. (1960), Vistas in Astronomy, 3, 184.

Arp, H.C. (1955), A.J., 60, 317.

Arp, H.C. (1956), A.J., 63, 58.

Arp, H.C. (1958a), A.J., 63, 118.

Arp, H.C. (1958b), A.J., 63, 273.

Arp, H.C. (1958c), A.J., 63, 487.

Arp, H.C. (1959a), A.J., 64, 175.

Arp, H.C. (1959b), A.J., 64, 254.

Arp, H.C. (1962), Ap. J., 136, 66.

Arp, H.C. (1964), IAU/URSI Symposium No. 20 (Aust. Acad. Sci., Canberra, 1964).

Arp, H.C. & Cuffey, J. (1962), Ap. J., 136, 51.

Arp, H.C., Baum, W.A. & Sandage, A.R. (1952), A.J., 57, 4.

Arp, H.C., Baum, W.A. & Sandage, A.R. (1953), A.J., 58, 4.

Azzopardi, M. & Vigneau, J. (1977), A. & A., 56, 151.

Baade, W. (1944), Ap. J., 100, 137.

Baade, W. & Swope, H. (1961), Ap. J., 66, 300.

Baum, W.A. (1952), A.J., 57, 222.

Baum, W.A. (1954), A.J., 59, 422.

Becker, W. & Biber, C. (1956), Zs. f. Ap., 41, 52.

Blanco, B.M., Blanco, V.M. & McCarthy, M.F. (1978), Nature, 271, 638.

Brück, M.T. (1975), M.N.R.A.S., 173, 327.

Brück, M.T. (1978), A. & A., 68, 181.

Brück, M.T. & Marsoglu, A. (1978), A. & A., 68, 193.

Butler, C.J. (1976), A. & A. Supp., 24, 299.

Cannon, R.D. (1974), M.N.R.A.S., 167, 551.

Cannon, R.D. & Stobie, R.S. (1973), M.N.R.A.S., 162, 207.

Christy, R. (1966), Ap. J., 144, 108.

Chun, M.S. (1978), A. J., 83, 1062.

Davies, R.J. & Wright, A. (1977), M.N.R.A.S., 180, 71.

Dufour, R.J. & Harlow, W.V. (1977), Ap. J., 216, 207.

Dufour, R.J. & Killen, R.M. (1977), Ap. J., 211, 68.

Eggen, O.J. & Sandage, A.R. (1959), M.N.R.A.S., 119, 255.

Eggen, O.J. & Sandage, A.R. (1969), Ap. J., 158, 667.

Eggen, O.J., Lynden-Bell, D. & Sandage, A.R. (1962), M.N.R.A.S., 136, 748.

Faulkner, J. (1966), Ap. J., 144, 978.

Feast, M. (1964), IAU/URSI Symposium No. 20, 330 (Aust. Acad. Sci., Canberra, 1964).

Feast, M. & Lloyd-Evans, T. (1973), M.N.R.A.S., 164, 15P.

Freeman, K.C. & Gascoigne, S.C.B. (1977), Proc. Ast. Soc. Aust., 3, 136.

Gascoigne, S.C.B. (1966), M.N.R.A.S., 134, 59.

Gascoigne, S.C.B. (1971),"The Magellanic Clouds"; Ed. Muller, Reidel, Amsterdam.

Gascoigne, S.C.B. (1978), Private Communication.

Gascoigne, S.C.B. & Kron, G. (1952), P.A.S.P., 64, 196.

Gascoigne, S.C.B., Norris, J., Bessell, M.S., Hyland, A.R. & Visvanathan, N. (1976), Ap. J. Letts., 209, L25.

Gustaffson, B., Bell, R.A. & Hejlesen, P.M. (1977), Ap. J., 216, L7.

Graham, J. (1973), I.A.J., 12, 138.

Graham, J. (1975), P.A.S.P., 87, 641.

Greenstein, J. (1939), Ap. J., 90, 387.

Grindlay, J.E. (1978), Ap. J. Letts., 224, L107.

Hardy, E. (1977), Ap. J., 211, 718.

Hardy, E. (1979), IAU Symposium on Magellanic Clouds, Montreal.

Harris, G. & Deupree, R.G. (1976), Ap. J., 209, 402.

Hartwick, F.D.A. (1968), Ap. J., 154, 75.

Hartwick, F.D.A. & Hesser, J. (1974), Ap. J. Letts., 194, L129.

Hartwick, F.D.A., Hesser, J. & McClure, R.D. (1972), Ap. J., 174, 557.

Hartwick, F.D.A. & McClure, R.D. (1972), Ap. J. Letts., 176, L57.

Hartwick, F.D.A. & Van den Bergh, S. (1973), P.A.S.P., 85, 355.

Hawkins, M.R.S. (1977), Ph.D. Thesis, Cambridge University.

Hawkins, M.R.S. (1979), M.N.R.A.S., 188, 691.

Helfer, H.L., Wallerstein, G. & Greenstein, J. (1959), Ap. J., 129, 700.

Hertzsprung, E. (1929), M.N.R.A.S., 89, 660.

Hindman, J.V. (1967), Aust. J. Phys., 78, 147.

Hindman, J.V., Kerr, F.J. & McGee, R.X. (1963), Aust. J. Phys. Supp., 16, 570.

Hodge, P. (1960), Ap. J., 131, 351.

Hodge, P.W. & Wright, F.W. (1974), A. J., 79, 858.

Hogg, H. (1963), Publs. David Dunlap Obs., 2, No. 12.

Hoyle, F. & Hazelgrove, C.B. (1959), M.N.R.A.S., 119, 112.

Iben, I. (1967), Ann. Rev. Astr. & Ap., 5, 57.

Iben, I. (1968), Nature, 220, 143.

Iben, I. (1969), Nature, 224, 1006.

Iben, I. & Rood, R.T. (1970), Ap. J., 159, 603.

Janes, K.A. & Carney, B.W. (1977), B.A.A.S., 9, 295.

Johnson, H.L. & Morgan, W.N. (1953), Ap. J., 117, 313.

Johnson, H.L. & Sandage, A.R. (1955), Ap. J., 121, 616.

Johnson, H.L. & Sandage, A.R. (1956), Ap. J., 124, 379.

Kelly, B.D. (1977), Ph.D. Thesis, St. Andrews University.

Kinman, T. (1959), M.N.R.A.S., 119, 538.

Kontizas, M. (1976), Ph.D. Thesis, University of Edinburgh.

Kron, G. (1956), P.A.S.P., 68, 125.

Kuiper, G.P. (1939), Ap. J., 89, 548.

Lindsay, E. (1958), M.N.R.A.S., 118, 172.

Lloyd-Evans, T. (1978a), M.N.R.A.S., 183, 305.

Lloyd-Evans, T. (1978b), M.N.R.A.S., 183, 319.

Matthewson, D.S., Cleary, M.N. & Murray, J.D. (1974), IAU Symposium No. 58, 367.

McClure, R.D., Forrester, W.T. & Gibson, J. (1974), Ap. J., 189, 409.

McClure, R.D. & Van den Bergh, S. (1968), A. J., 73, 313.

McMullan, D., Powell, J.P. & Curtis, W.A. (1972), Adv. El. E. P., 33A, 37.

McMullan, D. & Powell, J.P. (1976), IAU Coll. No. 40.

Melbourne, W.G. (1960), Ap. J., 132, 101.

Menzies, J. (1967), Nature, 214, 689.

Morgan, D. & Nandy, K. (1978), A. & A., 70, 785.

Oort, J. (1957), Rome Conference on Stellar Populations, North Holland, Amsterdam.

Oort, J. (1974), IAU Symposium No. 58.

Osmer, P. (1973a), Ap. J., 181, 327.

Osmer, P. (1973b), Ap. J., 184, L127.

Pagel, B.E.J., Edmunds, M.G., Fosbury, R.A.E. & Webster, B.L. (1978), M.N.R.A.S., 184, 569.

Patenaude, M. (1978), A. & A., 66, 225.

Peimbert, M. (1975), Ann. Rev. Astr. & Ap., 13, 113.

Peimbert, M. & Torres-Peimbert, S. (1974), Ap. J., 193, 327.

Peimbert, M. & Torres-Peimbert, S. (1976), Ap. J., 203, 581.

Penny, A.J. (1975), M.N.R.A.S., 172, 65P.

Penny, A.J. (1976), Ph.D. Thesis, Sussex University.

Penston, M.V. & Cannon, R.D. (1970), R.G.O. Bull. No. 159.

Popper, D.M. (1947), Ap. J., 105, 204.

Pratt, N.M. (1977), Vistas in Astronomy, 21, 1.

Przybylski, A. (1976), "The Galaxy and the Local Group", R.G.O. Bull. No. 182.

Robertson, J. (1973), Ap. J., 180, 425.

Samson, W.B. (1971), Ph.D. Thesis, University of Edinburgh.

Sandage, A.R. (1953), A. J., 58, 61.

Sandage, A.R. (1964), Observatory, 84, 254.

Sandage, A.R. (1969), Ap. J., 157, 515.

Sandage, A.R. (1970), Ap. J., 162, 841.

Sandage, A.R. & Eggen, O.J. (1969), 158, 685.

Sandage, A.R. & Schwarzschild, M. (1952), Ap. J., 116, 463.

Sandage, A.R. & Walker, M.F. (1955), A. J., 60, 230.

Sandage, A.R. & Wildey, R.L. (1967), Ap. J., 150, 469.

Sanduleak, N. (1969), A. J., 74, 47.

Schilt, J., Epstein, I. & Hill, S.J. (1955), A. J., 60, 341.

Schlesinger, B.M. (1969), Ap. J., 157, 533.

Schwarzschild, M., Spitzer, L. & Wildt, R. (1951), Ap. J., 114, 398.

Shapley, H. (1920), Ap. J., 51, 140.

Shapley, H. (1930), "Star Clusters", McGraw-Hill, London.

Shapley, H. & Lindsay, E. (1963), I.A.J., 6, 74.

Simoda, H. & Iben, I. (1968), Ap. J., 152, 509.

Stromberg, G. (1933), M.N.R.A.S., 94, 68.

Stromberg, G. (1936), Ap. J., 84, 412.

Tayler, R.J. (1970), "The Stars: Their Structure and Evolution", Wykeham Press, London.

Thackeray, A.D. (1958), M.N.R.A.S., 118, 117.

Tifft, W.G. (1963a), M.N.R.A.S., 125, 199.

Tifft, W.G. (1963b), M.N.R.A.S., 126, 209.

Trumpler, R.J. (1925), P.A.S.P., 37, 307.

Van de Kamp, P. (1964), "Elements of Astromechanics", W.H. Freeman, San Francisco.

Van den Bergh, S. (1967), A. J., 72, 70.

Van den Bergh, S. (1975), "Stars and Stellar Systems", Vol. 9, Univ. of Chicago Press.

Vaucouleurs, G. de & Vaucouleurs, A. de (1964), "Ref. Catalogue of Bright Galaxies", Univ. of Texas.

Vaucouleurs, G. de & Freeman, K.C. (1973), Vistas in Astronomy, 14 163.

Walker, M.F. (1970), Ap. J., 161, 363.

Walker, M.F. (1971), Ap. J., 167, 1.

Walker, M.F. (1972a), M.N.R.A.S., 156, 459.

Walker, M.F. (1972b), M.N.R.A.S., 159, 379.

Walker, M.F. (1974), M.N.R.A.S., 169, 199.

Walker, M.F. (1979a), M.N.R.A.S., 186, 767.

Walker, M.F. (1979b), M.N.R.A.S., 188, 735.

Walker, M.F. & Kron, G. (1967), P.A.S.P., 79, 551.

Wallerstein, G. & Helfer, H.L. (1966), P.A.S.P., 79, 551.

Weaver, H. (1962), Encyclopaedia of Physics, Vol. LIV, 130.

Westerlund, B.A. (1964), IAU Symposium No. 20, Canberra.

Westerlund, B.A. (1972), Vistas in Astronomy, 12, 335.

Westerlund, B.A. & Glaspey, J. (1971), A. & A., 10, 1.

Wildey, R.L., Burbidge, E.M., Sandage, A.R. & Burbidge, G.R. (1962), Ap. J., 135, 94.

APPENDIX 1

COORDINATES OF PHOTOMETRIC STANDARD SEQUENCE

1	00 26 18,21	-72 59 54,80	5844	6131
2	00 26 38,18	-72 56 11,30	6393	5663
3	00 27 19,12	-73 01 06,53	5452	4720
4	00 26 41,39	-72 59 17,27	6041	5591
5	00 26 33,71	-72 59 58,19	5824	5771
6	00 27 27,46	-73 00 03,70	5785	4523
7	00 27 58,43	-72 59 52,13	5839	3803
8	00 27 51,10	-72 58 02,16	6427	3966
9	00 27 14,81	-72 58 15,00	6367	4811
10	00 27 08,81	-72 56 46,91	6627	4951
11	00 27 13,44	-72 56 39,53	6676	4838
13	00 26 11,42	-72 57 47,02	6502	3492
14	00 27 54,48	-73 02 11,01	5100	3904
15	00 27 26,39	-72 57 29,50	6607	4539
16	00 27 52,97	-72 56 41,93	6654	3917
17	00 27 30,57	-72 58 44,57	6206	4446
18	00 27 37,96	-72 59 30,22	5961	4277
19	00 27 50,54	-72 58 45,35	6189	3982
20	00 27 50,53	-72 59 31,32	5952	3985
21	00 27 00,64	-72 59 25,37	5992	5144
22	00 27 33,56	-73 01 24,51	5353	4386
23	00 27 05,75	-72 58 13,26	6378	5021
24	00 26 45,42	-72 58 19,55	6348	5495
25	00 26 58,82	-72 57 21,31	6657	5297
26	00 25 51,10	-72 58 40,75	6241	6759
27	00 27 08,25	-72 57 16,56	6678	4960
28	00 27 07,48	-72 57 45,80	6524	4980
29	00 26 57,83	-72 57 50,94	6605	5204
30	00 27 20,27	-72 58 34,49	6262	4685
32	00 27 27,88	-72 59 05,33	6080	4510
33	00 26 52,77	-72 59 49,77	5866	5328
34	00 26 45,87	-72 59 46,04	5887	5488
35	00 26 47,97	-72 59 36,97	5935	5439
36	00 27 42,05	-72 58 21,73	6325	4179
37	00 27 46,27	-72 59 31,71	5951	4084
38	00 27 26,15	-72 58 29,26	6287	4548
39	00 27 31,76	-72 58 02,67	6429	4416
40	00 27 36,41	-72 57 36,20	6575	4958
41	00 27 20,13	-72 57 32,38	6593	4685
42	00 27 35,67	-72 57 46,35	6514	4324
43	00 27 41,05	-72 57 49,69	6496	4199
44	00 27 16,23	-72 59 33,00	5951	4781
45	00 27 41,97	-72 59 48,99	5860	4185
46	00 27 39,46	-72 59 44,50	5884	4243
47	00 27 13,39	-73 00 07,45	5768	4850
48	00 27 19,92	-73 00 39,85	5594	4700
49	00 27 23,74	-73 01 44,06	5251	4615
50	00 27 09,93	-73 01 42,72	5261	4935
51	00 27 34,57	-72 57 52,79	6481	4350
42	00 27 35,67	-72 57 45,36	6515	4323
52	00 27 04,17	-72 57 04,45	6745	5055
53	00 26 56,25	-72 58 11,27	6390	5196
54	00 26 58,06	-72 58 19,34	6347	5201
55	00 26 53,86	-72 58 29,30	6292	5299
56	00 26 49,14	-72 58 12,31	6386	5408
57	00 26 45,10	-72 58 09,05	6404	5502
58	00 26 44,12	-72 59 03,31	6115	5527
59	00 27 32,75	-72 58 16,14	6357	4393
60	00 27 20,89	-72 59 53,09	5843	4675
61	00 27 20,63	-72 59 15,57	6043	4679
62	00 27 25,22	-72 58 51,93	6168	4571
63	00 27 11,60	-72 59 39,96	5917	4888
64	00 27 37,68	-72 58 49,51	6178	4281
65	00 27 36,11	-72 59 02,82	6107	4272
66	00 27 31,98	-72 59 30,67	5960	4416
67	00 27 38,11	-72 59 02,82	6107	4272
68	00 26 53,18	-72 59 40,75	5914	5318
69	00 27 02,38	-72 56 08,46	7043	5094

APPENDIX 2: MAGNITUDES AND COLOURS

NGC152 REG.1

152	2 271							
1A1	19.391	0.623	1A2	19.379	0.050	1A3	18.578	0.912
1A4	19.149	0.748	1A5	20.473	0.480	1A6	19.355	0.932
1A7	19.935	0.856	1A9	18.925	0.430	1A10	18.861	0.596
1A11	20.532	0.408	1A12	19.057	0.750	1A13	19.629	0.846
1A15	19.495	0.653	1A16	20.438	0.340	1A18	20.788	0.273
1A19	19.639	0.610	1A20	19.914	0.426	1A21	19.925	0.275
1A23	17.753	0.960	1A22	18.025	0.796	1A24	18.981	0.838
1A25	20.617	0.272	1A26	15.541	2.565	1A27	17.321	1.031
1A28	19.837	0.745	1A29	18.839	0.827	1A30	19.172	0.532
1A31	19.591	1.132	1A32	17.891	0.430	1A33	18.808	0.407
1A34	19.057	0.942	1A35	19.581	0.133	1A37	18.976	0.599
1A38	20.167	0.253	1A39	19.613	0.191	1A39	19.563	0.363
1A40	20.052	0.286	1A41	19.637	0.782	1A42	19.582	0.008
1A43	19.229	0.800	1A44	19.875	0.456	1A45	18.923	0.645
1A46	19.626	0.530	1A47	19.514	0.714	1A48	18.890	0.640
1A51	19.014	0.647	1A53	17.368	0.177	1A55	16.012	1.614
1A56	15.422	1.411	1A57	17.775	0.707	1A58	18.205	0.684
1A59	19.021	0.564	1A60	18.845	0.779	1A61	18.705	0.745
1A62	19.337	0.496	1A63	16.950	0.197	1D1	17.980	0.753
1D2	19.606	0.921	1D7	19.658	1.103	1D6	20.354	0.249
1D8	20.617	0.341	1D8	20.393	0.160	1D10	19.266	0.713
1D11	18.943	0.543	1D12	18.978	0.732	1D13	19.299	0.668
1D14	19.238	0.672	1D15	19.446	0.324	1D16	20.208	0.462
1D17	20.747	-0.088	1D18	20.176	0.284	1D19	20.747	0.364
1D20	19.926	-0.024	1D21	19.758	0.457	1D22	18.349	0.421
1D23	18.424	0.778	1D24	19.563	0.076	1D25	18.531	0.662
1D26	19.596	0.696	1D27	19.215	0.630	1D28	20.041	0.188
1D29	19.414	0.509	1D30	16.772	0.785	1D31	17.590	0.883
1D32	17.650	0.875	1D33	19.238	0.809	1D34	19.176	0.550
1D35	19.880	0.339	1D37	19.177	0.770	1D38	20.121	0.496
1D39	20.052	0.512	1D40	19.026	0.518	1D41	18.945	0.786
1D42	18.545	0.868	1D43	18.899	0.677	1D44	19.570	0.357
1D45	18.844	0.536	1D46	19.302	-0.078	1D47	18.320	0.413
1D48	19.477	0.580	1D49	19.974	0.333	1D50	19.678	0.220
1D51	19.246	0.678	1D52	20.032	0.049	1D53	20.140	0.404
1D54	18.270	0.302	1D55	17.845	0.770	1D56	16.740	-0.151
1D57	19.552	0.649	1D58	14.737	2.173	1D59	16.636	1.210
1D60	16.572	1.244	1D61	16.106	0.389	1D62	16.088	1.002
1D63	14.445	2.560	1D64	17.476	0.003	1C1	17.678	0.540
1C2	18.649	0.893	1C3	18.645	0.656	1C4	20.357	0.217
1C5	19.432	0.598	1C6	19.092	0.648	1C7	19.115	0.467
1C8	19.010	0.732	1C9	19.166	0.767	1C10	19.840	0.664
1C11	20.658	0.293	1C13	19.826	0.684	1C14	20.447	0.322
1C15	19.102	0.953	1C16	19.150	0.639	1C17	18.911	0.645
1C18	19.961	0.826	1C19	20.040	0.145	1C20	18.886	0.286
1C21	20.506	0.215	1C22	19.302	0.718	1C24	18.173	0.540
1C25	17.917	0.774	1C26	16.040	0.980	1C27	14.230	1.963
1C28	19.054	0.124	1C29	18.247	0.734	1C31	18.946	0.613
1C32	19.759	0.043	1C33	19.789	1.029	1C34	17.675	0.357
1C35	20.228	0.350	1C36	17.365	0.839	1C37	19.053	0.483
1C43	19.940	0.615	1C42	20.151	0.384	1C41	20.561	0.123
1C44	20.256	0.285	1C45	20.703	0.423	1C46	20.585	0.118
1C47	19.210	0.717	1C48	19.152	0.586	1C49	19.203	0.768
1C50	19.729	0.278	1C51	19.854	0.197	1C52	19.634	-0.125
1C53	20.086	0.482	1C54	19.195	0.644	1C55	19.354	0.692
1C56	17.748	0.985	1C57	20.379	0.269	1C58	18.642	0.666
1C61	19.139	1.173	1C62	17.435	0.221	1C67	17.779	0.599
1C68	19.535	0.278	1C70	19.041	0.550	1C71	19.142	0.671
1C72	19.619	0.512	1B1	20.317	0.311	1B3	20.457	0.364
1B4	19.038	0.572	1B5	19.589	0.384	1B7	17.952	0.786
1B9	19.040	0.285	1B10	19.859	0.660	1B11	18.864	0.830
1B12	20.366	0.000	1B14	19.083	0.876	1B15	16.929	1.203

1827	19.062	-0.165	1829	13.819	2.240	1830	16.475	-0.041
1833	19.661	0.120	1834	19.109	0.526	1835	19.829	0.167
1836	19.829	0.627	1837	19.480	0.515	1838	17.768	0.336
1839	19.037	0.704	1840	16.161	1.449	1841	17.822	0.753
1843	17.999	0.673	1844	18.812	0.664	1845	19.779	0.136
1847	17.166	0.718	1848	19.058	0.843	1849	19.993	0.381
1850	19.761	0.376	1851	19.616	0.479	1852	18.458	0.805
1856	19.173	0.646	1857	19.102	0.449	1859	19.758	0.517
1860	19.588	-0.016	1861	19.078	0.433	1862	20.475	0.269
1863	19.448	0.357	1864	19.924	0.204	1865	18.333	0.494
1866	19.778	0.009	1868	19.044	-0.182	1870	18.667	0.957
1871	19.883	0.017	1872	17.946	0.778	1873	19.030	0.356
1874	17.455	1.014	1C74	19.754	0.232	1C75	19.895	0.011
1A8	20.029	0.351	1A14	20.490	0.516	1A17	20.269	0.621
1A40	19.799	0.008	1A50	19.562	0.157	182	20.295	0.298
184	20.490	0.781	188	20.490	0.371	1813	20.548	0.446
1816	20.433	0.353	1825	19.973	0.373	1828	18.831	0.708
1831	20.191	0.117	1832	19.696	0.192	1842	19.777	0.140
1846	20.191	0.165	1853	20.116	0.212	1855	20.091	0.550
1854	20.322	0.518	1858	20.116	0.553	1867	19.862	0.202
103	19.883	0.418	194	20.116	0.217	105	20.461	0.513
1036	20.020	0.660	1C12	20.030	0.626	1C23	19.996	0.486
1C30	19.798	0.229	1C38	20.548	0.404	1C39	20.519	0.514
1C40	20.377	0.730	1C58	20.043	0.764	1C59	19.716	0.491
1C69	20.116	0.021	1C76	19.928	0.399	1C77	20.322	0.269
1C78	20.322	0.269						

21
21
21
21
21
21
21
21
21

NGC152 REG.2

152	2.224							
2A1	19.819	0.640	2A2	20.430	0.398	2A3	19.657	0.950
2A4	20.132	0.319	2A5	20.279	0.329	2A6	16.110	1.777
2A7	19.439	0.735	2A8	19.978	0.779	2A9	20.055	0.304
2A12	19.719	0.239	2A13	17.972	1.096	2A14	18.313	0.761
2A14	20.342	0.310	2A15	20.272	0.357	2A16	19.630	0.561
2A17	20.431	0.463	2A18	20.553	0.310	2A19	20.551	0.270
2A20	20.291	0.507	2A21	19.855	0.713	2A22	20.012	0.131
2A23	19.665	0.735	2A24	18.423	1.030	2A25	20.278	0.266
2A26	19.319	1.038	2A27	17.920	0.815	2A28	18.786	1.110
2A29	20.267	0.606	2A30	20.336	0.166	2A31	20.245	0.313
2A32	20.645	0.303	2A33	20.545	0.433	2A36	19.117	0.739
2A35	20.414	0.343	2A34	20.438	0.334	2A37	20.534	0.230
2A38	20.039	0.304	2A39	20.653	0.372	2A40	20.514	0.399
2A41	20.598	0.188	2A42	20.033	0.161	2A43	19.383	0.677
2A45	20.682	0.148	2A46	19.989	0.769	2A47	19.186	0.812
2A48	19.963	0.795	2A49	20.207	0.397	2A50	20.100	0.267
2B1	19.918	1.339	2B1	17.295	1.082	2B2	19.447	0.799
2B3	19.700	0.656	2B4	19.673	0.772	2B5	18.953	0.764
2B6	19.916	0.835	2B7	20.074	0.556	2B8	19.448	0.532
2B9	19.120	0.717	2B10	19.819	0.689	2B11	19.357	0.760
2B12	20.222	0.156	2B13	18.871	0.925	2B14	20.385	0.291
2B15	19.186	0.744	2B16	18.829	0.782	2B17	18.262	0.798
2B18	19.158	0.882	2B20	20.484	0.300	2B19	20.620	0.635
2B21	19.243	0.867	2B22	19.084	0.763	2B23	20.112	0.326
2B25	19.496	0.654	2B26	19.321	0.780	2B27	19.397	0.872
2B28	19.832	0.459	2B29	19.070	0.511	2B30	20.996	0.085
2B31	19.201	0.582	2B32	20.236	0.394	2B33	17.919	1.395
2B34	20.280	0.497	2B36	19.920	0.669	2B37	20.636	0.465
2B38	20.686	0.448	2B39	19.295	-0.046	2B40	18.829	0.857
2B41	20.301	0.304	2B42	20.515	0.152	2B43	19.987	0.141
2B45	18.282	1.051	2B46	19.118	0.748	2B44	20.647	0.542
2B47	20.641	0.527	2B48	19.070	0.903	2B50	18.081	0.842
2B51	20.423	-0.092	2B54	19.350	0.798	2B55	20.267	0.262
2B52	20.169	0.342	2B53	20.447	0.390	2B56	20.555	0.481
2B58	19.712	1.183	2B59	19.787	0.775	2B60	19.072	0.721
2B61	20.662	0.269	2C1	19.418	0.572	2C2	19.629	0.760
2C3	20.354	0.290	2C4	20.430	0.607	2C5	19.584	-0.003
2C6	20.091	0.005	2C7	20.590	0.341	2C8	19.303	0.631
2C9	18.679	0.787	2C10	19.419	0.681	2C11	19.492	0.716
2C12	19.624	0.688	2C13	18.640	0.325	2C14	18.583	0.910
2C15	20.648	0.261	2C16	20.436	0.372	2C17	20.371	0.469
2C18	20.169	0.293	2C19	19.261	0.685	2C22	19.532	0.654
2C21	19.398	1.477	2C23	19.618	0.953	2C24	17.076	1.256
2C25	17.472	0.940	2C26	20.236	0.415	2C29	20.834	0.278
2C27	20.196	0.225	2C28	19.834	1.021	2C31	19.078	0.780
2C32	20.544	0.556	2C33	19.189	0.959	2C30	20.636	0.475
2C34	19.611	0.743	2C35	18.535	0.924	2C36	20.332	0.382
2C37	20.529	0.431	2C38	19.891	0.017	2C39	18.667	0.689
2C40	19.171	0.755	2C41	17.769	0.737	2C42	18.135	0.535
2C43	19.655	0.789	2C44	19.371	0.435	2C46	18.405	0.937
2C47	19.939	0.818	2C48	18.501	0.985	2C49	18.688	0.693
2C50	17.388	0.795	2C51	19.860	0.742	2C52	19.973	0.194
2C53	20.193	0.374	2C55	20.680	0.350	2C56	20.533	-0.356
2C57	20.609	0.440	2D1	18.797	0.796	2D2	20.530	0.376
2D3	20.646	0.300	2D4	20.520	0.436	2D5	17.507	0.542
2D6	19.231	0.043	2D7	18.586	0.955	2D10	20.122	0.195
2D9	19.858	0.461	2D11	19.124	0.697	2D12	19.022	0.765
2D13	19.352	0.301	2D14	19.559	0.674	2D15	19.414	0.604
2D16	19.179	0.320	2D17	18.438	0.918	2D8	20.462	0.540
2D18	20.604	0.372	2D20	20.104	0.175	2D21	20.857	0.410
2D22	20.210	0.311	2D23	19.294	1.203	2D24	18.355	0.213

2028	20.677	0.127	2029	20.626	0.311	2030	20.541	0.363
2031	19.134	0.679	2032	18.870	0.797	2033	19.589	0.749
2034	19.399	0.799	2035	19.017	0.679	2036	20.351	0.322
2037	20.479	0.243	2038	20.481	0.527	2039	20.208	0.402
2040	19.827	0.860	2041	19.327	0.894	2042	20.451	0.266
2043	19.319	0.661	2044	18.823	0.949	2045	19.021	0.635
2046	20.678	0.417	2047	20.615	0.021	2048	19.339	0.745
2048	20.363	0.437	2050	20.630	0.197	2051	19.375	0.801
2052	20.059	0.177	2053	19.515	0.201	2054	18.239	0.826
2055	17.674	0.256	2057	18.685	0.876	2056	18.742	0.911
2A53	16.252	0.991	2A11	19.056	0.414	2A52	17.536	1.128
2A54	15.631	1.420	2C53	15.983	0.935	2C29	17.371	0.478
2C54	20.830	0.423	2B49	20.242	0.710			

NGC 152 REGS. 3+4

N152	[illegible]							
4A1	17.109	0.971	4A2	19.229	0.737	4A3	19.311	0.767
4A4	19.214	0.303	4A5	19.012	0.589	4A6	20.538	0.363
4A7	20.417	0.635	4A8	20.527	-0.055	4A9	20.430	0.247
4A10	19.737	0.053	4A11	17.856	0.794	4A12	19.001	0.792
4A13	20.444	0.436	4A14	19.206	0.787	4A15	20.574	0.103
4A16	19.388	0.603	4A17	19.684	0.820	4A18	20.374	0.064
4A19	19.328	0.706	4A20	17.651	0.766	4A21	19.171	0.429
4A22	14.922	1.449	4A23	19.527	0.316	4A24	20.471	0.180
4A25	19.619	0.846	4A26	20.271	0.066	4A27	19.851	-0.070
4A28	20.035	0.202	4A29	19.589	0.938	4A30	19.338	0.688
4A31	19.535	0.911	4A32	20.516	0.261	4A33	19.134	0.855
4A34	19.344	0.301	4A35	17.103	1.139	4A37	19.049	0.658
4A36	20.286	0.122	4A38	20.508	0.043	4A39	20.390	0.373
4A40	19.239	0.662	4A41	19.384	0.886	4A42	18.897	0.651
4A43	19.756	0.795	4A44	19.358	0.920	4A45	20.521	-0.030
4A46	19.816	0.708	4A47	19.154	0.777	4A48	19.209	0.767
4A49	19.176	0.554	4A51	19.181	0.650	4A52	17.302	1.050
4A53	19.853	0.105	4A54	19.957	0.703	4A55	19.262	0.719
4A56	19.388	0.826	4A57	18.145	0.894	4A58	17.005	1.124
4A59	20.224	0.509	4A60	19.360	0.742	4A61	19.021	-0.051
4A62	19.546	0.738	4A63	19.669	0.624	4A64	18.510	0.658
4A65	19.158	0.716	4A66	19.998	0.357	4A67	18.936	0.426
4A68	20.102	0.123	4A69	19.197	0.844	4A70	19.097	0.580
4A71	19.742	0.097	4A72	19.508	-0.196	4A73	19.333	0.699
4A74	19.925	0.437	4A75	20.017	0.117	4A76	19.316	0.648
4A77	19.892	0.097	4A78	20.325	0.232	4A80	18.981	0.677
4A81	17.772	0.935	3A1	19.939	1.012	3A2	18.432	0.889
3A3	19.218	0.980	3A4	19.247	0.685	3A6	20.794	0.516
3A7	20.252	0.146	3A8	20.064	0.367	3A9	20.565	0.273
3A11	20.309	0.134	3A10	20.555	0.127	3A12	18.973	0.833
3A13	19.197	0.650	3A14	20.426	0.175	3A15	20.407	0.151
3A16	20.286	0.095	3A17	20.460	0.327	3A18	20.351	0.469
3A19	19.178	0.724	3A20	20.598	0.139	3A22	20.500	0.284
3A21	20.430	0.115	3A23	19.673	0.395	3A24	20.113	0.274
3A25	19.259	0.781	3A27	20.377	0.255	3A28	15.658	2.408
3A29	19.427	0.929	3A30	19.988	-0.064	3A31	19.644	-0.025
3A33	19.754	0.261	3A32	20.007	0.598	3A34	14.463	0.618
3A36	19.288	0.741	3A37	20.257	0.424	3A38	19.465	0.718
3A39	19.266	0.774	3A40	20.210	0.265	3A41	19.254	0.607
3A42	20.235	0.189	3A43	17.536	1.061	3A44	18.548	0.988
3A45	19.352	0.759	3A46	20.363	0.063	3A47	18.178	0.469
3A48	19.732	0.398	3A49	19.757	0.615	3A50	20.238	0.523
3A51	19.566	0.814	3A52	20.073	0.104	3A53	19.094	0.733
3A55	20.571	0.177	3A56	20.491	0.048	3A57	18.428	0.617
3A58	19.720	0.646	3A59	20.133	-0.051	3A60	19.512	0.581
3A61	19.178	0.764	3A62	19.022	0.559	3A63	17.389	0.653
3A64	20.161	0.130	3A65	18.861	0.926	3A66	19.103	-0.214
3A68	17.559	1.041	3A67	18.687	0.705	3A69	20.442	0.143
3A70	20.312	0.312	3A71	19.714	0.663	3A72	19.759	0.456
3A73	20.352	0.164	3B1	18.678	0.670	3B2	20.431	0.185
3B3	19.350	0.913	3B4	19.163	0.747	3B5	20.500	0.310
3B6	19.778	0.887	3B7	20.292	0.296	3B8	20.510	0.184
3B9	19.810	0.564	3B10	19.492	0.741	3B11	19.104	-0.773
3B12	19.622	0.656	3B13	20.357	0.303	3B14	18.780	0.914
3B15	20.315	0.193	3B16	19.172	0.068	3B17	17.902	0.564
3B18	19.263	1.563	3B19	18.071	0.567	3B20	18.903	0.884
3B21	20.040	0.225	3B22	20.480	0.332	3B23	20.227	0.086
3B24	19.276	0.847	3B25	20.323	0.262	3B26	20.011	0.214
3B27	19.279	0.874	3B28	19.052	0.782	3B29	19.252	0.722
3B31	20.736	0.327	3B32	20.048	0.001	3B33	20.232	0.183
3B35	19.254	0.982	3B36	19.431	0.598	3B37	17.839	0.922

3841	19.569	0.736	3842	19.002	0.716	3844	19.385	0.747
3843	19.060	1.100	3845	18.917	0.794	3846	20.129	0.209
3847	20.188	0.934	3848	18.971	0.917	3849	20.464	0.560
3851	19.353	0.913	3852	20.085	0.361	3853	19.897	0.486
3854	20.426	0.306	3855	19.221	0.894	3856	20.440	0.294
3857	20.795	0.208	3858	20.368	0.422	3859	20.048	0.494
3860	20.694	0.271	3861	19.855	0.633	3862	19.735	0.556
3863	19.229	0.755	3864	20.301	0.251	481	20.437	0.197
482	20.387	0.088	483	19.218	0.831	484	19.964	0.195
485	20.188	0.474	487	19.861	0.487	488	20.457	0.307
489	20.621	0.128	4810	19.687	0.900	4814	19.177	0.876
4811	20.144	0.163	4812	20.017	0.093	4813	20.330	0.279
4815	19.145	0.613	4816	20.227	0.199	4817	19.159	0.639
4818	19.078	0.844	4819	18.964	1.001	4820	18.531	0.926
4822	19.268	0.774	4823	19.984	0.701	4825	20.020	0.589
4826	20.319	0.492	4827	19.234	0.762	4828	18.504	0.751
4829	19.279	0.964	4830	20.133	0.736	4831	18.057	0.977
4832	17.708	-0.174	4833	19.008	0.692	4835	17.512	1.010
4836	19.939	0.481	4837	19.049	0.652	4838	19.101	0.908
4839	19.475	-0.154	4840	20.165	0.259	4841	18.94[illegible]	0.709
4842	19.140	0.712	4843	20.158	-0.047	4844	15.912	2.117
4845	20.070	0.899	4846	20.388	0.136	4847	20.176	0.462
4862	19.957	0.748	4848	19.042	0.811	4849	19.198	0.877
4850	18.339	0.014	4851	20.404	0.224	4853	18.855	0.784
4854	19.877	0.597	4855	18.930	0.857	4856	20.359	0.141
4857	19.998	0.709	4858	19.058	0.998	4860	19.400	0.798
4859	19.371	0.863	4861	20.240	0.624	3A26	17.784	0.811
3A35	18.860	0.557	486	20.563	0.353	4834	18.735	0.876
4852	19.722	1.073	3866	20.487	0.327	3330	20.785	0.612
3850	20.225	0.566	4A50	19.177	0.797			

REC. I

NGC 152

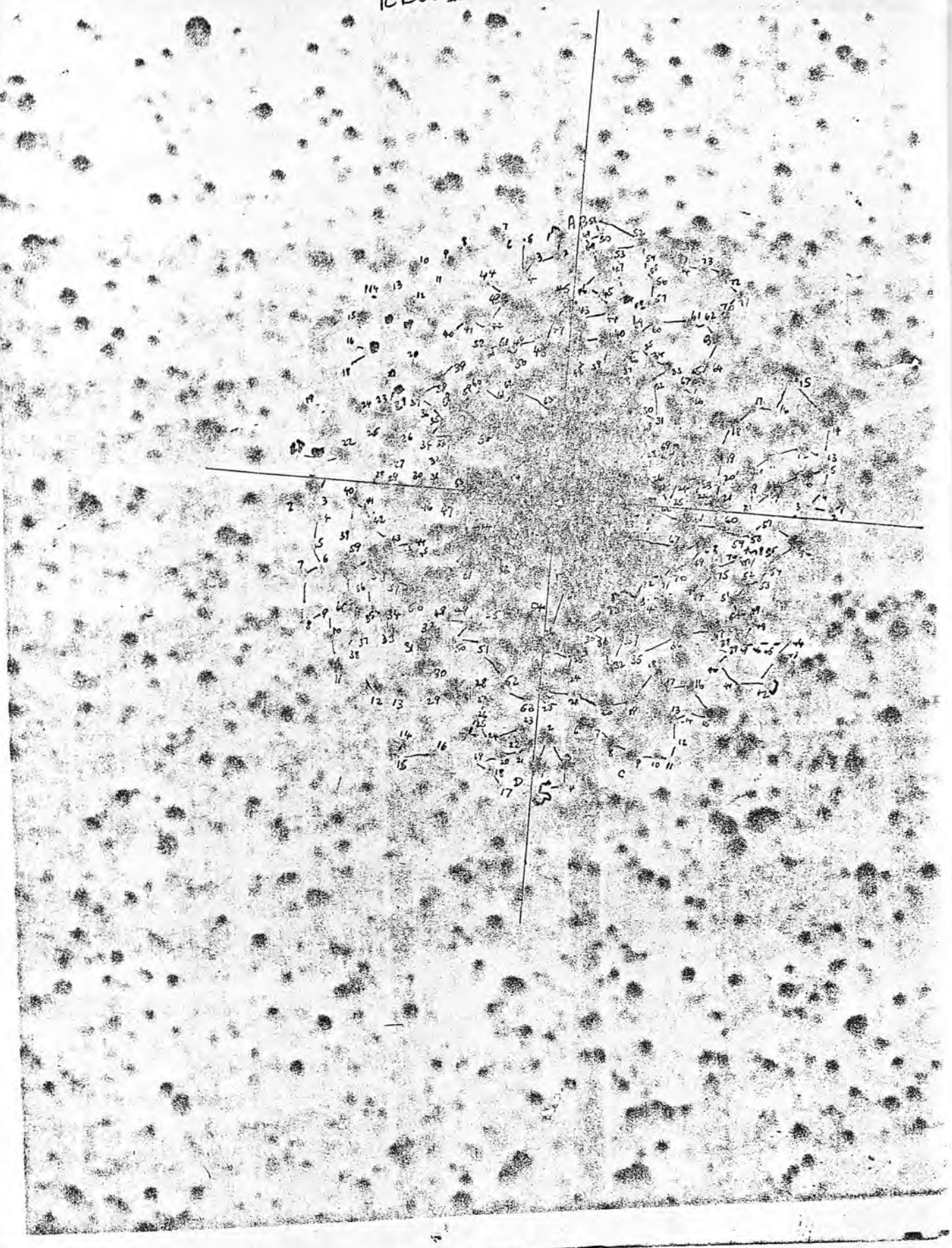

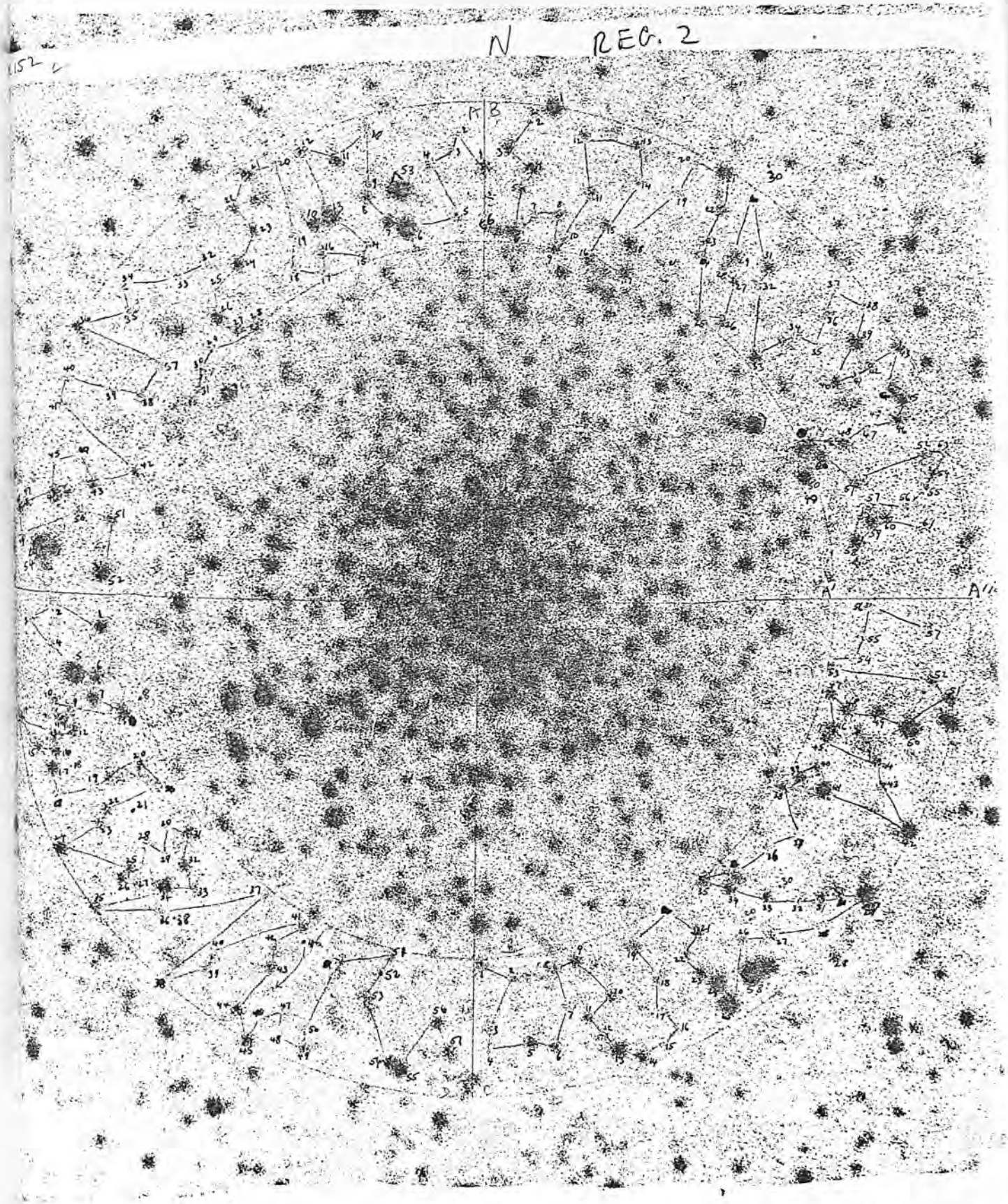
N REG. 2
A
B
C
A'

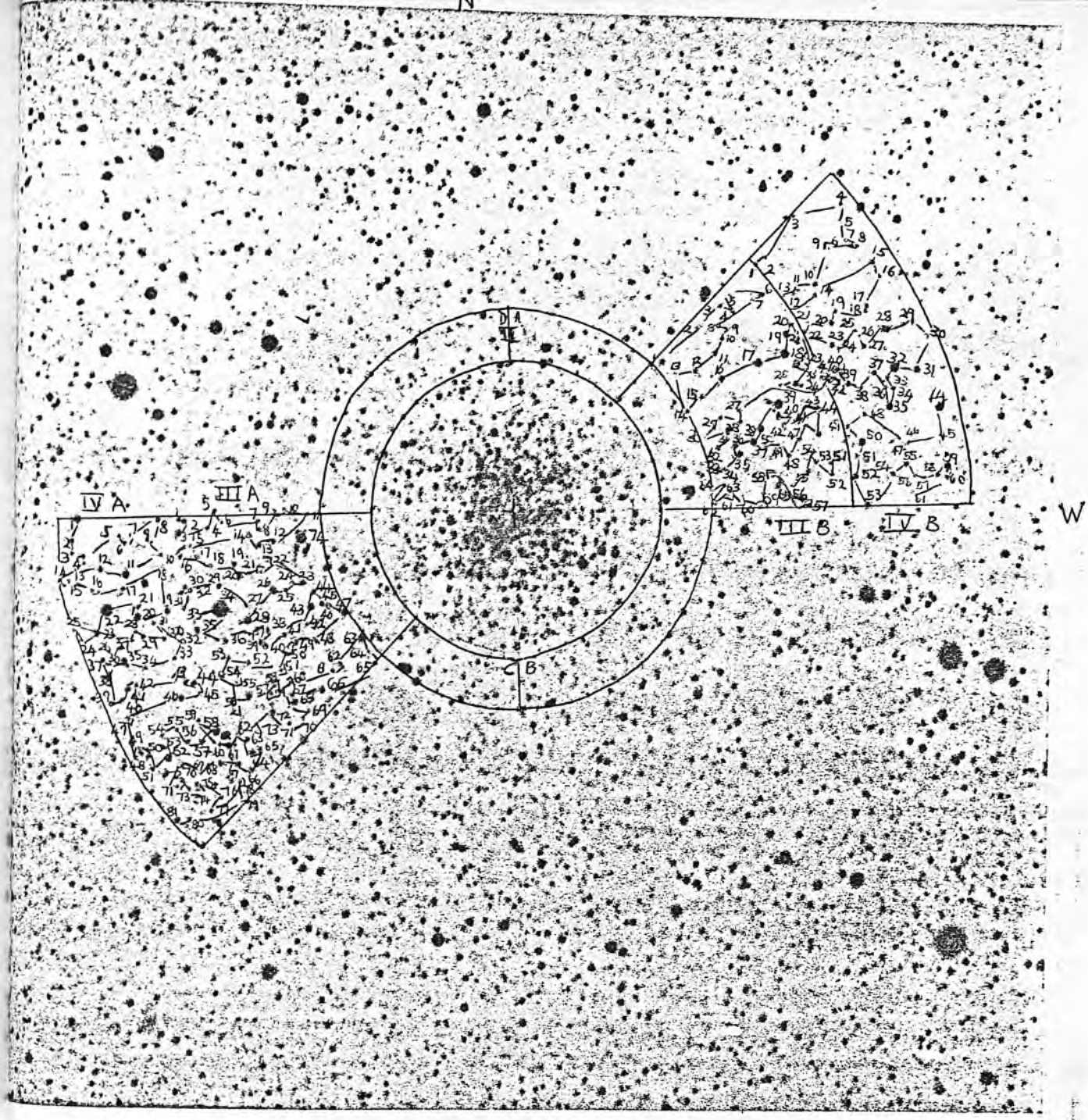

NGC 152 RECS. 3 & 4

FIELD REC. A

FLDA	4 353							
Y1	19.239	0.119	Y2	20.829	0.233	Y3	19.579	0.777
Y4	21.109	-0.307	Y5	20.942	0.079	Y7	19.343	0.896
Y8	19.092	0.055	Y9	19.312	1.227	Y10	19.616	0.798
Y11	20.163	0.667	Y12	20.685	-0.089	Y13	20.199	0.085
Y14	20.218	0.421	Y15	20.583	0.594	Y16	20.246	0.225
Y17	20.617	0.378	Y18	21.029	0.264	Y19	19.579	0.091
Y20	19.422	0.969	Y21	20.792	0.293	Y22	20.084	0.951
Y23	17.559	0.644	Y25	19.144	-0.101	Y26	19.616	0.694
Y27	20.199	0.269	Y28	20.392	0.192	Y29	20.792	0.062
Y30	19.616	0.647	Y31	19.374	0.780	Y32	19.374	0.780
Y33	20.651	-0.124	Y34	19.616	-0.142	Y35	20.486	0.295
Y36	19.374	0.531	Y37	19.715	0.548	Y38	20.720	-0.181
Y40	19.171	0.776	Y41	20.942	-0.063	Y42	18.994	-0.252
Y43	16.435	1.266	Y44	20.583	0.398	Y45	20.792	0.125
Y46	20.756	0.173	Y47	18.637	0.785	Y48	20.685	0.132
Y49	19.018	0.698	Y50	18.983	0.687	Y51	19.312	-0.110
Y52	20.454	0.222	Y53	20.980	-0.038	Y54	19.096	0.770
Y55	20.362	0.143	Y56	19.406	0.634	Y57	20.583	0.452
Y58	20.980	0.197	Y59	19.598	0.605	Y60	20.685	0.507
Y6	20.163	0.387	Y348	19.912	0.775	Y61	21.491	-0.269
Y62	20.332	0.298	Y63	19.525	0.797	Y64	20.518	0.312
Y65	19.821	0.179	Y66	18.435	0.786	Y67	21.020	0.015
Y68	18.779	0.729	Y69	20.583	0.175	Y70	20.332	0.116
Y71	19.888	1.188	Y72	17.396	-1.728	Y73	18.725	0.608
Y74	20.685	0.257	Y75	20.110	0.636	Y76	19.327	0.686
Y77	19.757	0.782	Y78	19.268	0.823	Y79	20.720	0.073
Y349	19.983	0.751	Y80	20.720	0.049	Y81	21.538	-0.448
Y82	19.959	0.625	Y84	19.561	0.605	Y85	19.507	0.533
Y86	21.633	-0.216	Y87	21.491	-0.191	Y88	18.834	0.657
Y89	19.171	0.720	Y90	20.792	0.038	Y91	19.525	0.854
Y92	16.389	0.688	Y93	19.655	0.952	Y94	19.171	0.776
Y95	20.518	0.287	Y96	20.903	-0.204	Y97	16.659	-1.928
Y98	20.110	0.966	Y99	20.110	0.520	Y100	19.067	0.664
Y101	20.980	0.212	Y102	20.550	-0.034	Y103	21.020	-0.039
Y104	21.100	0.370	Y105	20.651	0.215	Y106	20.110	0.508
Y107	20.218	0.275	Y108	19.018	0.620	Y350	20.392	0.153
Y109	21.020	0.172	Y110	20.084	0.615	Y111	20.792	0.492
Y112	20.583	0.438	Y113	19.343	0.773	Y114	19.422	0.781
Y115	19.312	0.927	Y116	20.033	0.071	Y117	20.518	0.477
Y118	19.030	-0.091	Y119	20.866	0.063	Y120	20.866	0.402
Y121	21.141	0.225	Y122	18.763	-0.285	Y123	20.980	-0.150
Y124	20.903	0.274	Y125	20.866	0.051	Y126	20.583	0.271
Y127	20.756	0.406	Y128	20.942	0.120	Y129	19.092	0.771
Y130	18.714	-0.330	Y131	19.343	0.823	Y132	20.903	0.065
Y133	20.163	0.606	Y134	18.994	0.375	Y135	20.903	0.334
Y136	19.055	0.630	Y137	20.829	0.408	Y138	19.240	0.889
Y139	20.792	0.461	Y140	21.060	-0.065	Y141	21.100	0.388
Y142	21.100	0.233	Y143	19.675	0.086	Y144	20.829	-0.060
Y145	20.423	-0.067	Y146	19.579	0.182	Y147	20.980	-0.063
Y148	21.020	0.397	Y149	20.866	0.025	Y150	20.866	0.025
Y151	21.060	-0.052	Y152	20.651	-0.473	Y153	20.980	-0.384
Y154	19.225	-0.182	Y155	19.374	0.559	Y156	21.311	-0.235
Y157	21.311	0.005	Y158	19.736	0.055	Y159	21.141	0.036
Y160	21.311	-0.119	Y161	19.912	0.593	Y162	19.422	0.578
Y163	20.942	-0.100	Y164	20.685	0.132	Y165	19.268	0.759
Y166	19.890	0.371	Y167	20.008	0.645	Y168	20.366	0.371
Y169	19.254	0.733	Y170	20.392	0.413	Y171	19.225	0.775
Y172	14.348	-1.164	Y173	21.060	0.147	Y174	19.327	0.739
Y175	20.685	-0.044	Y176	19.283	0.770	Y177	19.374	0.804
Y178	20.720	-0.090	Y179	20.651	0.633	Y180	19.312	0.903
Y181	20.518	0.450	Y182	20.110	0.093	Y183	19.343	0.908
Y184	20.829	0.233	Y186	20.550	0.126	Y187	20.583	0.412
Y188	17.469	0.940	Y190	19.489	0.726	Y192	19.595	0.429
Y193	20.332	0.758	Y194	20.518	0.424	Y195	19.507	0.603

Y199	20.942	-0.038	Y200	20.486	0.041	Y201	20.756	0.436
Y202	21.491	-0.238	Y203	21.311	-0.469	Y204	20.058	0.515
Y205	21.268	-0.206	Y206	19.472	0.606	Y207	19.240	0.665
Y208	20.190	-0.036	Y209	20.084	0.179	Y210	20.218	0.138
Y351	20.942	0.148	Y211	19.821	1.200	Y212	19.225	0.566
Y213	19.090	0.780	Y214	20.392	0.366	Y215	20.550	0.231
Y216	20.583	0.283	Y217	20.136	0.278	Y218	21.020	0.070
Y219	19.637	-0.460	Y220	19.598	-0.040	Y221	19.507	0.671
Y222	19.131	0.843	Y223	20.756	0.436	Y224	21.060	0.240
Y225	20.651	0.154	Y226	20.513	0.123	Y227	20.942	0.374
Y228	19.157	0.649	Y229	19.283	0.730	Y230	20.392	0.249
Y231	20.513	0.659	Y232	19.439	0.824	Y233	18.768	0.546
Y234	19.374	-0.078	Y235	21.311	0.159	Y236	20.942	0.148
Y237	21.060	0.464	Y238	20.332	0.402	Y239	19.327	0.864
Y240	21.020	0.561	Y241	20.559	0.114	Y242	20.583	0.479
Y243	20.651	0.266	Y244	20.617	0.164	Y245	20.518	0.032
Y246	20.720	0.273	Y247	20.792	0.125	Y248	20.454	0.085
Y249	21.311	-0.192	Y250	20.332	0.116	Y251	19.312	-0.208
Y252	19.283	-0.240	Y253	20.942	-0.173	Y254	20.829	-0.012
Y255	19.105	0.772	Y256	19.912	0.075	Y257	18.879	0.560
Y258	21.020	0.187	Y259	19.866	0.695	Y260	20.617	0.200
Y261	21.268	-0.076	Y262	20.866	0.341	Y263	20.454	0.164
Y264	20.685	0.132	Y265	19.636	0.743	Y266	19.821	0.878
Y267	19.118	0.801	Y268	20.903	-0.086	Y269	20.792	0.508
Y270	20.454	0.581	Y271	20.454	0.327	Y272	19.184	0.994
Y273	20.829	0.088	Y274	20.685	0.477	Y275	18.902	0.768
Y276	20.866	0.013	Y277	20.583	0.186	Y278	20.518	0.169
Y279	20.866	0.238	Y280	20.651	0.191	Y281	17.679	0.755
Y282	20.651	0.453	Y283	20.720	0.134	Y284	19.390	0.966
Y285	19.254	0.937	Y286	16.876	1.482	Y287	18.315	1.491
Y288	19.080	0.574	Y289	19.390	1.081	Y290	20.362	0.492
Y291	17.073	0.823	Y292	17.979	0.624	Y293	19.171	0.920
Y294	20.246	0.488	Y295	19.912	0.706	Y296	21.060	0.256
Y297	20.583	0.701	Y298	20.486	0.144	Y299	20.829	0.192
Y300	19.312	0.754	Y301	20.651	0.425	Y302	20.942	0.407
Y303	21.020	0.280	Y304	20.903	0.201	Y305	19.030	0.592
Y306	18.757	-0.424	Y307	18.616	0.875	Y352	20.930	0.544
Y308	19.144	0.830	Y309	19.959	0.292	Y353	20.617	0.225
Y310	20.190	0.859	Y311	19.105	0.908	Y312	19.171	0.842
Y313	19.254	0.862	Y354	20.942	0.458	Y314	20.332	0.332
Y315	19.843	0.696	Y316	19.799	0.982	Y317	19.343	0.761
Y318	19.157	0.776	Y319	20.756	0.123	Y355	20.942	0.235
Y356	20.866	0.483	Y357	20.756	0.732	Y320	20.274	0.568
Y321	21.020	-0.025	Y322	20.110	0.671	Y323	18.834	0.986
Y324	18.549	0.691	Y325	19.225	0.775	Y326	18.134	0.929
Y327	19.240	0.838	Y328	19.390	0.714	Y329	20.218	0.264
Y330	18.994	0.953	Y331	20.110	0.474	Y332	20.792	0.312
Y333	18.315	0.516	Y334	19.212	0.693	Y335	20.942	-0.051
Y336	20.829	0.166	Y337	20.685	-0.180	Y338	20.792	0.243
Y339	20.903	0.146	Y340	19.935	0.570	Y341	20.756	0.061
Y342	20.866	0.306	Y343	20.980	-0.076	Y358	21.020	0.070
Y344	19.297	0.819	Y359	20.518	0.689	Y345	20.110	0.554
Y346	19.018	0.942	Y347	20.163	0.100			

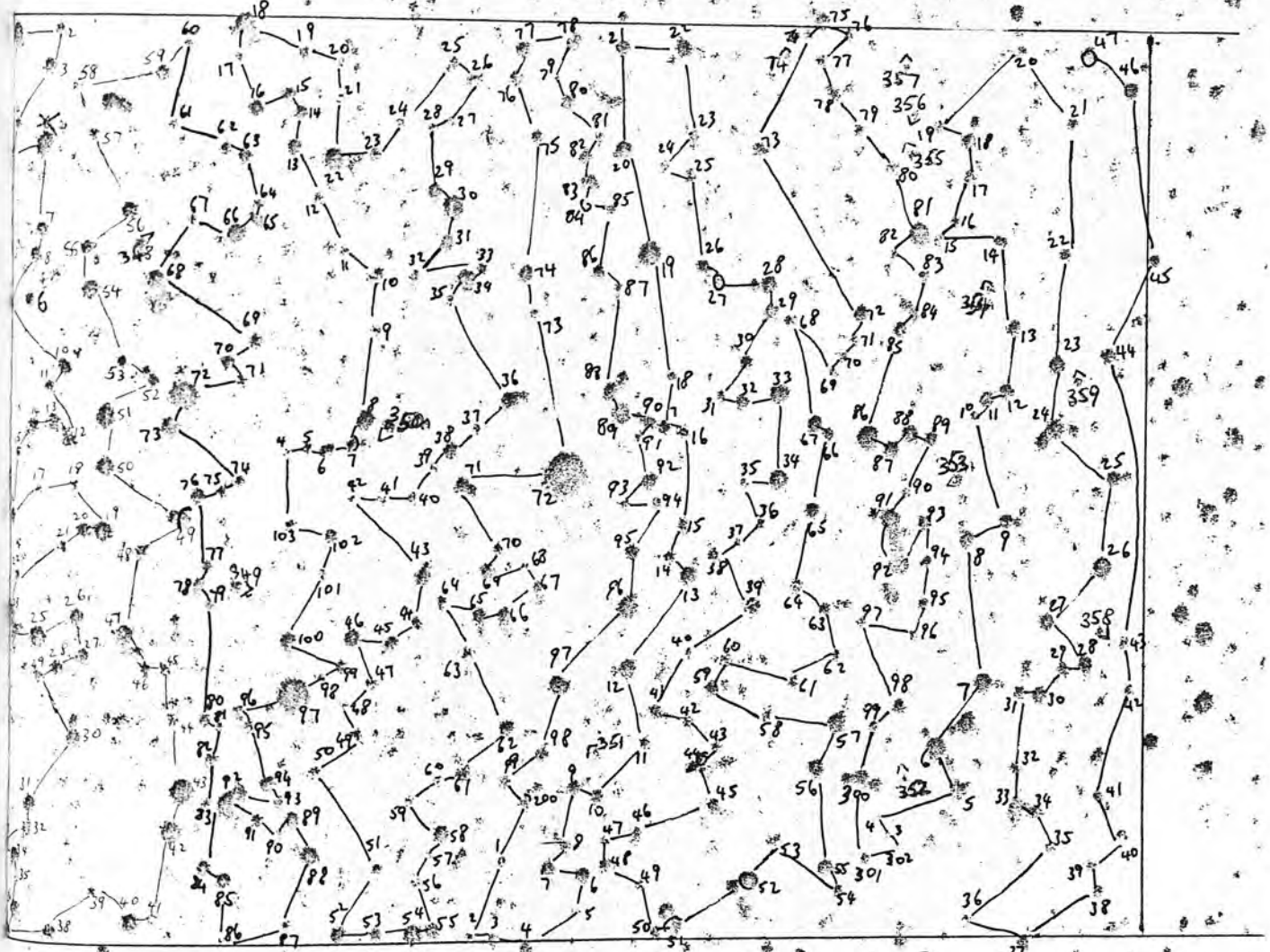
N
FIELD REC. 17

K3 REG. 1

K3	11.272							
1A4	19.407	1.334	1A1	20.990	0.208	1A2	20.552	0.777
1A4	19.640	0.710	1A5	19.855	0.962	1A7	14.575	3.079
1A8	19.303	0.774	1A10	19.320	0.960	1A11	19.579	0.350
1A12	20.215	0.504	1A13	20.157	0.600	1A14	19.561	0.952
1A15	19.005	1.113	1A17	20.107	0.594	1A18	17.907	0.756
1A19	19.510	1.061	1A20	19.305	0.785	1A21	17.502	0.855
1A22	18.213	0.972	1A24	17.719	0.992	1A25	19.396	0.818
1A26	19.541	1.571	1A28	20.183	0.540	1A29	16.559	1.752
1A32	19.398	1.002	1A33	19.256	0.745	1A34	18.445	0.741
1A35	19.546	1.509	1A36	17.849	1.004	1A38	17.696	1.026
1A39	19.137	0.749	1A40	19.157	1.232	1A41	18.221	0.979
1A42	19.073	0.610	1A43	16.972	1.475	1A45	18.847	0.803
1A46	19.664	0.917	1A48	19.530	1.047	1A48	19.465	0.971
1A50	19.981	0.981	1A51	20.382	0.490	1A52	20.215	0.666
1A53	20.157	0.826	1A54	19.962	1.011	1A55	19.019	1.084
1A56	19.806	0.870	1A57	19.772	0.916	1A58	19.278	0.944
1A59	19.507	1.059	1A60	19.354	0.913	1A61	18.206	0.787
1A62	19.575	0.790	1A63	19.625	0.826	1A64	19.167	0.972
1A66	19.244	1.026	1A67	19.028	0.835	1A68	20.263	0.581
1A71	19.772	0.939	1A69	20.418	0.625	1A70	20.170	0.637
1B5	19.103	0.946	1B6	18.020	0.953	1B4	20.632	0.479
1B3	20.434	0.743	1B2	19.757	0.727	1B1	19.922	0.713
1B7	19.552	1.067	1B8	19.542	1.008	1B9	18.996	0.834
1B10	19.078	0.909	1B11	19.301	0.902	1B12	18.525	0.784
1B13	20.320	0.495	1B14	20.143	0.667	1B15	17.956	0.763
1B16	18.987	3.282	1B20	18.469	0.823	1B21	18.331	0.945
1B22	19.329	0.733	1B23	18.356	0.885	1B24	18.294	0.835
1B25	19.423	1.023	1B26	19.148	1.006	1B27	19.746	0.628
1B28	19.870	0.855	1B29	18.455	1.003	1B30	20.613	0.208
1B31	19.359	0.816	1B32	18.234	0.906	1B33	18.742	0.804
1B34	19.734	0.567	1B35	20.066	0.753	1B37	19.791	1.067
1B38	15.478	2.401	1B39	19.509	0.701	1B40	19.589	0.909
1B41	19.617	0.883	1B42	16.220	1.758	1B44	18.207	0.943
1B45	19.193	0.605	1B46	15.636	2.172	1B47	16.651	1.871
1B49	17.918	1.168	1B50	18.132	0.922	1B51	18.365	1.601
1B52	19.036	0.988	1B53	18.951	1.054	1B54	18.434	1.208
1B55	19.747	1.005	1B56	20.183	0.698	1B57	20.290	0.664
1B58	19.211	1.141	1B59	18.343	1.331	1B62	18.229	1.038
1C2	19.692	0.875	1C3	18.645	0.885	1C4	18.491	0.908
1C5	19.703	1.180	1C6	16.885	1.504	1C7	18.066	1.105
1C9	15.253	2.415	1C10	18.495	1.005	1C11	14.654	3.049
1C13	18.790	0.987	1C14	19.001	0.910	1C15	19.258	0.937
1C16	19.611	0.717	1C17	18.275	0.847	1C19	17.934	1.182
1C20	19.123	1.053	1C21	19.079	0.945	1C22	18.772	0.980
1C23	19.026	0.988	1C24	18.791	0.812	1C25	18.739	0.883
1C26	19.734	0.822	1C27	20.253	0.790	1C28	19.918	1.032
1C29	19.875	0.992	1C30	18.613	1.013	1C31	18.645	0.814
1C32	19.358	0.920	1C33	17.891	0.962	1C34	16.762	1.290
1C35	19.568	2.130	1C37	18.630	0.992	1C38	19.160	0.951
1C39	19.609	0.912	1C40	20.457	0.423	1C41	18.846	0.857
1C43	19.701	0.910	1C44	17.513	0.643	1C45	15.699	2.275
1C46	19.521	0.985	1C47	17.550	1.177	1C48	18.790	1.057
1C49	19.252	0.763	1C50	19.377	1.043	1D2	15.646	2.193
1D3	19.588	1.122	1D5	14.484	2.800	1D6	17.843	0.990
1D7	19.119	1.080	1D8	19.030	1.078	1D9	18.246	1.014
1D10	19.044	1.120	1D12	14.946	2.963	1D14	18.449	0.992
1D15	20.230	0.859	1D16	19.609	1.288	1D17	17.918	1.116
1D19	20.309	0.958	1D20	19.534	1.731	1D21	19.538	0.936
1D22	19.145	1.177	1D23	19.135	0.799	1D25	18.623	1.045
1D27	19.245	1.113	1D28	19.410	0.990	1D29	19.302	1.090
1D30	19.693	1.042	1D31	18.963	0.982	1D33	18.723	1.106
1D32	19.493	0.492	1D34	19.311	1.034	1D35	18.487	0.917
1D36	19.138	0.740	1D37	18.508	1.234	1D38	18.432	0.992
1D39	19.642	0.822	1D40	19.048	0.976	1D43	18.859	0.971
1D44	20.230	0.243	1D45	19.094	1.126	1D46	14.592	3.313

1D50	16.215	2.261	1D51	19.263	1.029	1D52	18.576	1.073
1D53	17.239	1.253	1D54	19.125	1.062	1D55	19.865	0.794
1D56	18.722	1.059	1D58	17.345	1.141	1D59	18.764	0.977
1D60	19.535	0.751	1D61	20.339	0.605	1D63	17.095	0.979
1D64	17.598	6.408	1A3	20.208	0.479	1A9	18.394	0.749
1A16	20.918	0.358	1A23	17.907	0.769	1A37	19.089	0.760
1A47	20.342	0.759	1A65	18.373	1.079	1C1	20.600	0.799
1C8	18.642	1.216	1C12	19.795	0.917	1C36	19.480	0.869
1C42	20.156	0.753	1B16	18.303	0.989	1B17	18.179	0.916
1B18	18.303	0.794	1B36	20.943	0.447	1B60	14.820	2.767
1B61	15.282	2.641	1B63	16.999	1.286	1D1	17.670	1.042
1D4	16.424	1.103	1D13	18.274	1.342	1D17	19.934	1.010
1D24	19.664	0.353	1D41	20.235	0.717	1D42	20.600	0.469
1D47	18.893	1.018	1D49	17.781	0.873	1D57	20.131	0.749
1D62	19.817	0.043						

K3 REG.2

K3	19.411							
2A2	19.616	0.644	2A3	20.050	0.762	2A7	20.255	0.908
2A0	20.380	0.422	2A5	21.324	0.790	2A4	21.162	0.764
2A3	21.156	0.561	2A2	20.839	0.533	2A1	21.233	0.593
2A10	21.391	0.787	2A11	20.676	0.955	2A12	21.207	0.553
2A13	21.360	0.528	2A15	21.362	0.342	2A16	20.374	0.371
2A17	17.393	1.309	2A19	20.374	0.538	2A18	21.168	0.764
2A20	20.011	0.423	2A21	20.965	0.586	2A22	19.326	0.834
2A24	20.620	0.724	2A23	20.472	0.917	2A25	15.914	2.881
2A26	17.026	1.329	2A27	20.607	0.809	2A29	20.389	0.631
2A30	20.320	0.665	2A31	19.755	0.872	2A32	21.062	0.676
2A33	19.254	0.920	2A34	20.720	0.273	2A36	17.809	1.199
2A35	21.014	0.641	2A37	16.119	1.919	2A38	20.169	0.486
2A39	20.404	0.975	2A40	20.336	0.773	2A41	19.009	0.961
2A42	19.918	0.747	2A43	19.819	0.967	2A44	20.720	0.637
2A45	20.260	0.332	2A46	19.314	1.132	2A49	19.479	0.961
2A50	19.972	1.009	2A47	21.009	0.713	2A48	20.866	0.874
2A53	19.224	0.705	2A52	21.034	0.602	2A51	20.753	0.650
2A54	16.353	2.611	2A55	19.355	1.056	2A56	19.525	1.086
2A59	20.231	0.317	2A60	20.197	0.840	2A61	20.282	0.644
2A63	19.649	0.781	2A64	20.316	0.319	2A65	20.752	0.661
2A71	20.903	0.797	2A70	21.038	0.654	2A69	21.208	0.925
2A74	19.545	0.788	2A73	21.021	0.645	2A72	20.745	0.602
2A77	19.332	1.242	2A78	19.373	1.006	2A76	20.582	0.834
2A75	21.029	0.452	2A79	20.676	0.796	2A80	19.223	0.869
2A81	20.525	0.512	2A82	19.858	0.997	2A84	18.901	0.794
2A83	20.676	0.583	2A85	19.123	0.799	2A86	17.097	1.640
2A87	18.239	1.113	2A88	20.263	0.919	2A89	20.642	0.938
2A90	18.030	1.439	2A91	20.878	0.661	2A92	19.233	0.820
2A93	19.917	0.811	2A94	20.989	0.572	2A95	20.937	0.723
2A98	20.561	0.406	2A97	14.376	0.656	2A96	21.069	0.720
2A99	20.227	0.939	A102	20.653	0.789	A104	19.046	1.081
A103	20.350	0.646	A104	17.953	1.178	A105	19.453	0.911
205	18.404	1.063	204	18.422	1.008	202	20.331	0.888
201	21.093	0.590	208	21.203	0.699	209	20.865	0.830
2010	20.506	0.710	2011	20.772	0.434	2012	20.894	0.795
2013	18.764	0.781	2014	20.264	0.292	2016	20.556	0.580
2015	20.309	0.693	2017	20.860	0.529	2018	20.579	0.831
2019	20.841	0.588	2020	19.202	0.866	2021	19.046	0.901
2022	20.924	0.517	2023	20.935	0.711	2024	20.501	0.786
2025	19.177	0.806	2026	18.806	1.023	2027	20.949	0.912
2028	21.207	0.685	2029	21.060	1.031	2047	20.150	0.779
2030	21.221	0.729	2032	20.709	0.693	2031	21.153	0.629
2035	20.603	0.561	2034	21.189	0.631	2033	20.862	0.790
2036	20.087	0.835	2037	20.166	0.787	2039	18.045	1.069
2040	19.940	1.003	2041	20.480	0.909	2042	20.664	0.806
2043	20.835	0.734	2044	21.015	0.610	2045	20.078	0.764
2046	20.446	0.559	2048	20.566	0.962	2049	19.919	1.029
2050	21.053	0.583	2051	21.129	0.925	2054	20.631	0.585
2055	20.566	0.796	2057	20.870	0.449	2058	18.632	0.717
2059	19.076	0.889	2060	18.671	0.816	2061	19.902	0.877
2062	20.821	0.723	2063	18.916	0.745	2065	19.214	0.826
2064	20.889	0.685	2066	20.922	0.426	2067	18.712	1.040
2069	19.282	0.849	2068	21.181	0.794	2070	19.008	0.866
2071	19.475	1.010	2074	18.243	0.980	2073	19.032	0.831
2075	20.264	0.189	2076	20.886	0.503	2079	19.163	0.801
2078	21.080	0.744	2077	21.015	0.752	2080	19.218	0.888
2081	17.290	1.395	2082	20.364	0.326	2083	19.098	1.040
2084	19.232	0.929	2085	20.602	0.837	2086	20.613	0.851
2087	21.032	0.708	2090	20.065	0.862	2089	20.389	0.672
2088	21.024	0.708	2091	19.196	0.972	2092	18.947	0.837
2093	21.150	0.808	2094	20.930	0.840	2095	18.029	0.441
2096	20.421	0.657	2097	20.079	0.729	2098	20.635	0.913
2099	21.233	0.715	B103	18.327	0.939	B102	20.930	0.412
B101	21.170	0.211	B104	19.139	0.355	B105	15.911	1.953
B107	19.832	0.823	B106	20.835	0.321	B108	20.837	0.649
B109	21.090	0.552	B110	21.145	0.606	285	18.164	0.855
284	21.021	0.496	283	21.363	0.514	281	21.362	0.553

2812	21.906	0.937	2813	20.371	0.743	2814	20.837	0.706
2818	19.255	0.792	2817	20.764	0.586	2816	20.316	0.392
2820	21.053	0.750	2819	21.091	0.763	2821	18.488	0.605
2822	19.209	0.542	2823	20.103	0.757	2824	20.832	0.625
2825	21.129	0.541	2826	19.119	0.800	2827	20.820	0.617
2828	2 .217	0.727	2829	21.040	0.897	2830	20.029	0.678
2831	20.785	0.551	2832	19.290	0.914	2833	19.153	0.795
2834	21.258	0.420	2835	20.942	0.646	2836	20.924	0.868
2836	20.011	0.466	2844	20.083	0.646	2847	20.147	0.904
2842	2 .750	0.502	2841	21.091	0.691	2845	21.246	0.423
2846	21.983	0.687	2847	19.176	0.770	2848	21.053	0.792
2849	2 .078	0.743	2851	21.207	0.244	2852	20.904	0.367
2853	21.227	0.615	2854	20.817	0.692	2855	20.930	0.528
2856	21.170	0.600	2858	19.126	0.935	2857	21.163	0.847
2859	19.143	0.760	2860	20.814	0.438	2861	20.906	0.827
2862	19.528	1.646	2863	19.199	1.008	2864	20.596	0.501
2865	2 .736	0.308	2866	20.530	0.783	2867	19.400	0.967
2869	20.615	0.359	2868	20.835	0.861	2870	20.995	0.456
2871	19.011	0.275	2872	20.186	0.178	2873	18.475	0.760
2874	21.129	0.570	2875	20.097	1.135	2876	20.919	0.116
2877	20.942	0.844	2878	20.645	0.472	2879	18.913	0.942
2880	20.324	0.770	2881	20.931	0.760	2882	20.520	0.772
2883	21.441	0.619	2884	19.059	0.864	5102	19.081	0.856
2885	19.675	0.880	2886	19.601	0.829	2888	19.009	0.826
2887	19.954	0.950	2889	20.800	1.005	2890	21.129	0.651
2891	19.685	0.878	2892	19.705	0.800	2894	19.224	0.796
2893	20.634	0.504	2895	20.528	0.814	2896	20.706	0.320
2897	19.057	0.907	2898	19.130	0.784	2899	19.091	0.977
5100	18.960	1.158	5102	19.353	0.791	5103	18.907	0.971
5104	18.742	0.784	5105	20.274	0.715	5106	19.871	1.021
5107	19.947	1.035	5108	19.832	1.025	201	18.962	0.905
202	19.002	0.947	203	17.676	1.289	204	20.490	0.600
5101	19.504	0.955	205	19.262	0.840	206	20.696	0.456
207	20.710	0.854	208	21.168	0.750	2010	20.630	0.818
209	21.141	0.592	2022	17.929	1.236	2012	21.044	0.687
2011	20.050	0.468	2013	20.967	0.441	2014	15.991	2.229
2015	19.637	1.002	2016	18.230	1.141	2017	20.677	0.607
2018	19.738	0.803	2019	20.826	0.767	2020	21.118	0.815
2021	21.021	0.712	2023	20.748	0.346	2024	21.239	0.750
2025	20.807	0.769	2026	20.906	0.523	2033	19.437	0.856
2032	21.972	0.602	2031	21.087	0.966	2030	21.226	0.212
2029	21.259	0.450	2034	20.431	0.857	2035	20.374	0.556
2036	21.792	0.816	2037	21.063	0.729	2038	20.883	0.634
2039	19.064	0.878	2040	20.295	0.706	2041	20.460	0.495
2042	19.332	0.951	2043	19.106	0.981	2044	19.068	0.925
2050	21.318	0.191	2049	20.848	0.478	2048	21.071	0.654
2047	21.055	0.507	2046	21.143	0.692	2057	19.524	0.947
2037	20.043	0.764	2056	20.800	0.867	2051	21.263	0.556
2052	21.978	0.949	2053	20.978	0.778	2054	21.207	0.720
2055	21.091	0.753	2058	18.868	0.888	2059	19.616	0.971
2061	19.014	1.046	2062	20.356	0.586	2063	20.596	0.590
2064	18.662	1.783	2065	21.064	0.704	2066	18.235	0.977
2068	19.726	0.746	2069	19.162	0.914	2070	20.043	0.839
2071	19.015	0.814	2072	21.075	0.779	2073	20.978	0.787
2074	21.277	0.265	2075	20.747	0.612	2076	20.082	0.829
2077	19.044	0.878	2078	20.689	0.811	2079	20.747	0.492
2080	21.026	0.921	2081	21.021	0.521	2084	20.066	0.720
2083	20.813	0.411	2089	18.901	0.975	2088	21.162	0.395
2090	19.250	0.982	2091	21.109	0.459	2092	17.464	1.341
2093	20.320	0.289	2094	21.176	0.745	2095	20.889	0.600
2096	21.080	0.454	2097	21.037	0.667	2098	20.803	0.565
2A14	21.418	0.643	2A57	19.703	0.901	2A62	20.744	0.674
2A67	21.153	0.743	2A66	21.234	0.482	2A63	21.183	0.991
4103	2 .792	0.487	206	21.060	0.363	2038	20.920	0.482
2072	21.133	0.411	2027	21.418	0.424	2023	21.084	0.692
2063	19.540	1.020	2067	20.356	0.862	2082	20.423	0.955
2085	20.952	0.591	2086	20.922	0.323	2087	20.852	0.390

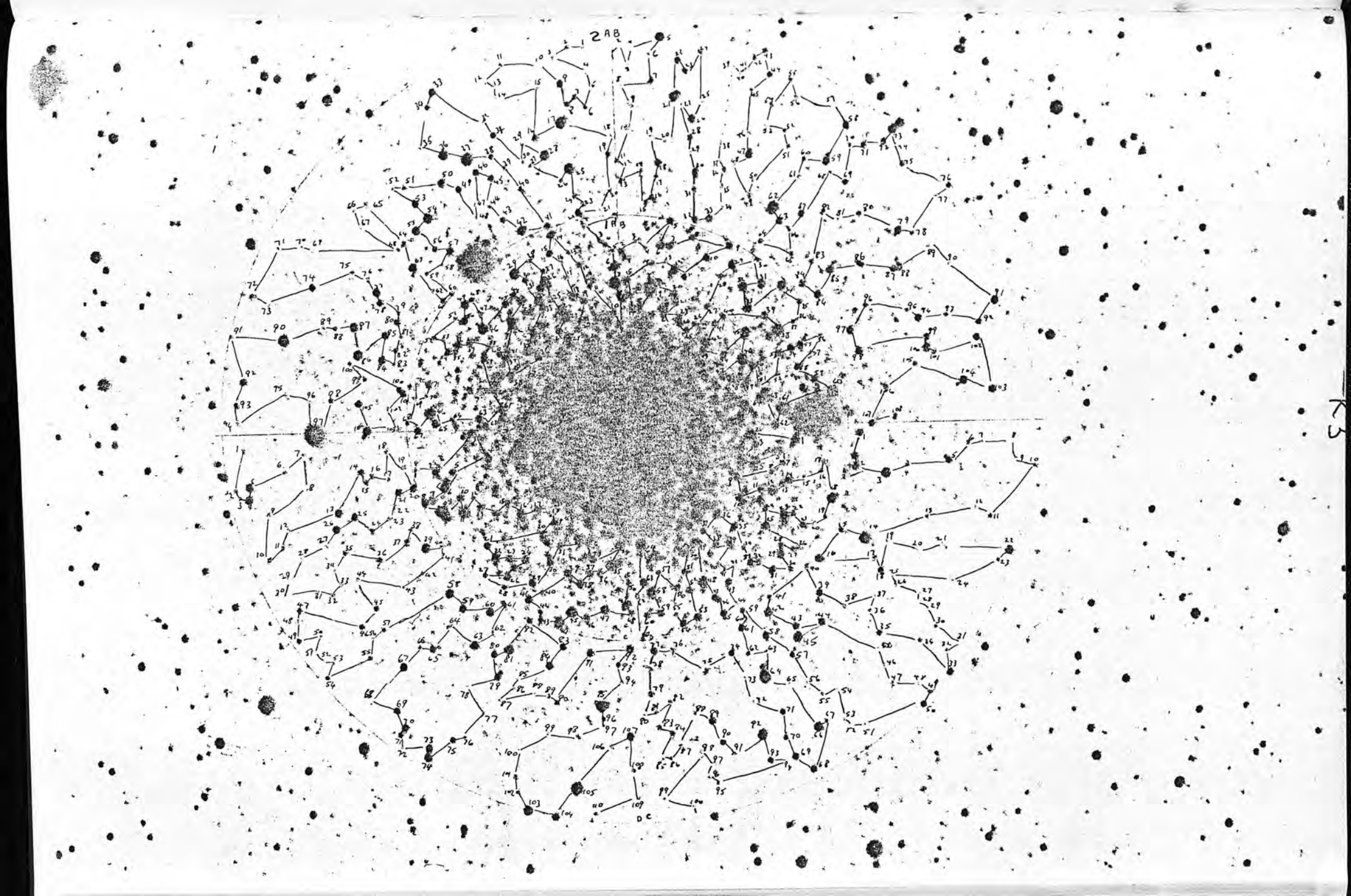
2AB
1AB
DC

FIELD REG. B

[illegible]	12.404							
X5	19.373	0.832	X6	20.734	0.339	X4	20.276	0.715
X5	19.991	0.000	X2	20.282	0.527	X1	21.248	0.493
X8	18.995	1.403	X7	21.009	0.743	X3	20.787	0.781
X11	21.600	0.434	X10	21.164	0.452	X12	20.757	0.559
X13	20.925	0.400	X14	20.740	0.699	X16	18.498	0.673
X15	21.035	0.605	X17	20.393	0.145	X18	17.854	0.990
X19	19.219	0.902	X20	19.260	0.977	X21	21.004	0.993
X22	20.645	0.400	X23	20.591	0.701	X24	20.575	0.507
X25	21.827	0.360	X26	20.701	0.624	X27	19.131	0.913
X28	20.972	0.624	X29	20.949	0.278	X30	19.303	1.135
X31	19.156	0.997	X32	20.540	0.598	X33	19.497	0.936
X34	21.052	0.519	X35	18.452	1.027	X36	18.092	1.116
X37	19.134	0.964	X38	20.872	0.184	X39	17.838	0.685
X40	21.665	0.441	X41	20.576	0.088	X42	20.615	0.467
X43	21.196	0.658	X44	21.055	0.615	X45	18.334	1.127
X46	20.838	0.650	X47	20.646	0.671	X48	20.953	0.495
X49	19.543	0.809	X50	20.479	0.402	X51	20.532	0.492
X52	20.115	0.944	X53	19.600	0.788	X55	18.857	0.637
X54	21.918	0.441	X56	20.978	0.557	X57	19.214	0.805
X58	19.082	0.915	X59	18.976	0.940	X60	19.022	1.514
X61	21.029	0.324	X62	19.913	0.723	X65	20.575	0.983
X64	20.861	0.306	X63	20.934	0.631	X66	16.144	0.852
X67	17.586	1.126	X68	19.052	0.839	X69	17.076	-0.191
X70	20.082	0.555	X71	21.104	0.583	X72	20.570	1.029
X73	19.113	0.615	X74	20.925	0.690	X75	20.897	0.419
X76	20.672	0.491	X78	18.961	1.021	X77	20.987	0.776
X79	19.136	1.016	X80	19.618	0.729	X81	21.231	0.457
X82	21.218	0.633	X84	16.026	1.152	X83	21.146	0.638
X85	20.736	0.721	X86	19.032	0.969	X87	17.903	1.279
X89	19.450	0.941	X88	21.223	0.684	X90	21.155	0.674
X91	21.714	0.734	X92	21.217	0.389	X93	20.996	0.521
X94	19.434	0.892	X95	21.091	0.715	X97	18.487	0.743
X96	20.744	0.734	X98	20.838	0.487	X100	18.908	0.932
X99	20.725	0.520	X101	20.825	0.711	X102	20.963	0.449
X105	20.153	0.600	X103	21.132	0.286	X104	21.301	0.284
X107	19.160	1.073	X106	20.907	0.473	X108	20.984	0.663
X109	18.551	0.954	X110	18.811	1.221	X111	20.515	0.255
X112	19.682	0.883	X113	19.574	0.913	X114	19.247	0.801
X115	18.909	0.136	X116	20.795	0.682	X117	19.157	0.756
X118	21.146	0.513	X119	20.823	0.542	X120	18.857	0.908
X121	18.771	0.920	X122	18.987	0.760	X123	20.946	0.898
X124	20.964	0.718	X125	20.561	0.876	X127	19.157	0.926
X126	20.927	0.548	X128	19.611	0.332	X129	20.971	0.195
X130	21.070	0.228	X131	21.020	0.409	X132	20.665	0.872
X133	19.293	0.874	X135	18.969	0.847	X134	20.820	0.697
X136	19.677	0.725	X137	17.977	1.048	X133	19.749	1.079
X139	19.306	0.879	X140	19.423	0.344	X141	19.876	0.922
X142	20.292	0.792	X143	20.902	0.536	X144	20.979	0.637
X145	20.936	0.500	X146	19.404	1.564	X147	21.216	0.600
X148	21.214	0.392	X149	20.335	0.569	X150	20.054	0.215
X151	19.913	0.869	X152	20.522	0.146	X154	16.047	1.771
X153	20.515	0.338	X155	20.533	0.773	X156	19.492	1.113
X157	20.996	0.452	X158	20.920	0.665	X159	20.825	0.854
X160	18.153	1.039	X161	21.123	0.568	X162	21.233	0.469
X165	19.213	0.993	X164	20.876	0.469	X163	20.514	0.542
X166	20.810	0.609	X167	17.875	0.704	X168	19.587	0.982
X169	21.048	0.688	X170	21.098	0.960	X171	20.985	0.730
X172	19.733	0.841	X176	20.902	0.564	X174	20.465	0.754
X173	21.340	0.633	X172	21.164	0.709	X177	20.527	0.982
X178	20.520	0.529	X180	21.011	0.585	X181	21.220	0.620
X182	21.049	0.873	X183	20.377	0.422	X184	21.128	0.400
X186	19.677	0.359	X185	21.005	0.632	X188	18.106	0.919
X187	19.998	1.520	X189	20.602	0.374	X190	20.588	0.831
X191	20.630	0.988	X193	19.034	0.776	X192	20.898	0.667
X194	20.415	1.119	X195	21.129	0.437	X19-	20.523	0.793

X203	20.079	0.772	X202	20.717	0.780	X201	20.857	0.542
X206	20.300	0.693	X207	21.098	0.421	X208	21.128	0.540
X209	19.355	0.877	X210	20.699	0.915	X211	20.872	0.375
X212	19.236	1.234	X213	18.994	0.865	X214	21.098	0.292
X217	19.764	1.465	X216	20.845	0.340	X218	20.825	0.299
X219	21.038	0.661	X220	20.836	0.660	X222	20.429	0.469
X221	20.031	0.861	X224	19.292	0.807	X223	20.671	0.673
X225	19.448	0.753	X226	19.633	0.953	X227	20.196	0.362
X228	20.376	0.740	X229	20.139	0.294	X230	21.098	0.744
X231	20.656	0.850	X232	20.484	0.917	X233	20.199	1.084
X234	19.870	0.071	X235	20.566	0.732	X236	19.026	0.911
X237	19.632	1.019	X238	21.009	0.470	X239	20.349	0.686
X240	19.719	0.915	X241	20.032	0.845	X243	20.283	0.541
X244	19.242	0.931	X245	19.211	1.069	X246	19.652	1.331
X247	19.693	0.796	X248	20.608	0.738	X249	19.106	0.832
X250	20.524	0.650	X251	21.047	0.327	X252	18.914	0.739
X253	21.072	0.439	X254	19.139	0.776	X255	20.029	0.907
X256	19.304	1.396	X257	20.406	0.529	X258	19.990	0.158
X259	19.810	0.120	X260	19.351	0.908	X261	19.817	0.859
X262	19.694	0.089	X264	20.257	0.376	X263	21.051	0.484
X265	20.597	1.009	X266	20.669	0.826	X267	20.317	0.619
X268	20.870	0.548	X269	16.498	0.576	X270	17.044	1.054
X403	19.685	0.102	X271	20.087	0.240	X272	19.894	0.891
X273	19.208	0.037	X274	20.302	0.307	X275	19.369	0.837
X276	18.945	0.985	X277	19.603	1.054	X278	15.620	0.725
X279	19.971	0.188	X280	19.217	1.023	X281	20.760	0.786
X282	20.342	0.715	X283	20.633	0.863	X284	20.217	0.848
X285	21.511	0.229	X286	19.377	0.767	X287	19.941	0.822
X288	20.405	0.184	X289	19.045	0.967	X290	19.220	0.919
X291	20.347	0.718	X292	19.373	0.698	X293	19.485	0.811
X294	20.410	0.177	X296	17.517	1.568	X295	19.492	0.377
X297	19.532	0.248	X298	19.618	0.905	X409	18.864	0.803
X299	19.189	1.032	X300	17.536	0.854	X301	19.470	0.697
X302	20.679	0.503	X415	20.642	0.439	X414	20.771	0.412
X303	19.368	0.807	X304	19.405	0.939	X305	17.972	1.351
X306	19.013	0.956	X307	16.137	1.309	X309	16.808	1.644
X308	20.355	0.497	X310	18.736	0.781	X311	20.133	0.210
X312	20.219	0.356	X313	18.908	0.940	X314	16.341	1.859
X315	17.530	1.340	X316	18.058	1.004	X317	19.336	0.928
X318	20.156	0.819	X319	20.870	0.569	X321	19.081	0.967
X320	20.676	0.631	X322	20.356	0.404	X323	20.120	0.911
X324	19.574	0.993	X325	20.096	0.678	X327	19.954	0.380
X326	20.500	0.701	X328	19.186	0.715	X329	19.333	0.664
X330	19.404	0.929	X331	20.735	0.527	X332	20.174	0.403
X333	20.306	0.736	X334	20.688	0.628	X335	19.162	0.917
X336	19.050	0.900	X337	19.919	0.993	X338	20.808	0.265
X339	19.235	0.881	X340	19.191	0.915	X341	18.120	1.066
X343	19.255	0.926	X342	20.632	0.415	X344	19.192	0.849
X345	20.189	0.367	X346	19.241	1.185	X348	18.990	0.831
X347	20.646	0.538	X349	20.472	0.930	X352	19.159	0.903
X353	19.355	0.882	X354	20.363	0.296	X351	20.833	0.682
X355	21.555	0.506	X356	19.469	0.996	X357	20.654	-0.005
X358	19.453	0.998	X359	20.985	0.583	X361	20.772	0.619
X360	20.833	0.815	X362	20.395	0.385	X363	19.169	1.005
X364	19.819	0.872	X365	19.104	0.828	X366	19.204	0.943
X367	19.436	0.795	X368	20.935	0.455	X370	19.262	0.963
X369	20.991	0.479	X371	19.953	0.885	X372	21.160	0.339
X373	19.140	0.702	X374	20.609	0.791	X375	20.229	0.803
X376	20.496	0.856	X377	20.924	0.506	X378	19.186	0.824
X379	21.002	0.704	X380	20.334	0.749	X381	20.752	0.255
X382	20.196	0.776	X387	19.242	0.102	X383	19.757	0.969
X389	19.539	0.999	X390	20.267	0.159	X386	20.537	0.430
X385	20.934	0.702	X384	20.802	0.461	X382	21.002	0.624
X392	19.888	0.956	X391	20.952	0.534	X393	20.648	0.838
X394	20.826	0.180	X395	20.658	0.842	X396	20.567	0.514
X397	20.734	0.307	X398	20.413	0.948	X399	19.857	1.309
X401	19.629	1.254	X242	19.445	0.801	X350	20.732	0.630

FIELD REC. B

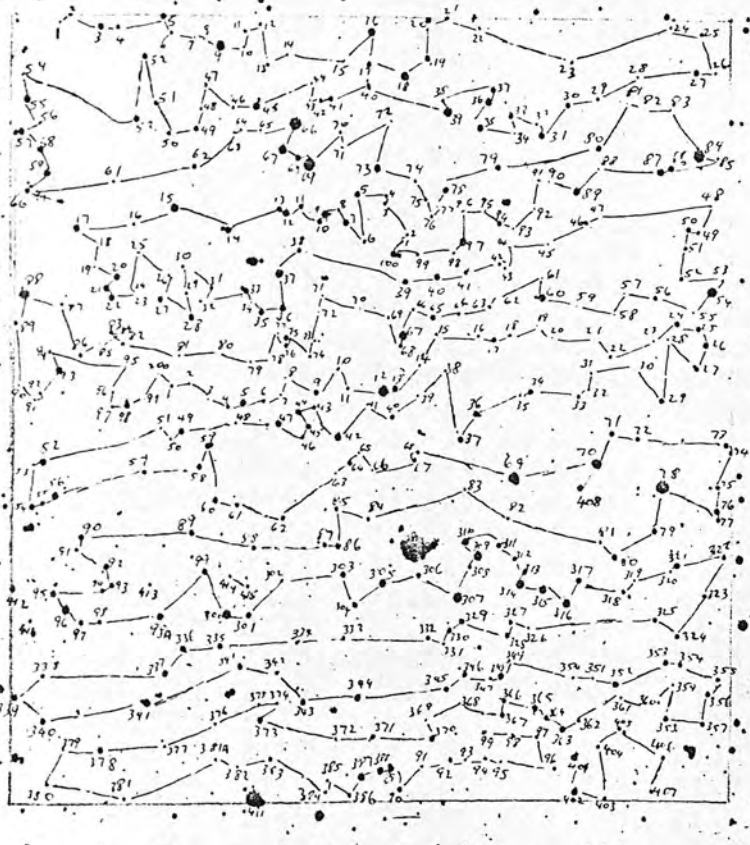

[illegible]	[illegible]	[illegible]	Z2	19.220	[illegible]	Z3	21.054	0.777
Z4	18.275	1.398	Z5	20.978	0.259	Z7	19.070	1.085
Z6	21.640	0.114	Z8	20.696	0.541	Z9	21.376	0.786
Z10	21.732	0.138	Z11	21.827	-0.130	Z12	21.292	0.260
Z13	20.798	0.956	Z14	21.550	0.678	Z15	21.251	0.955
Z16	21.334	0.950	Z17	20.108	0.846	Z18	21.334	0.962
Z19	19.177	1.065	Z20	21.334	0.678	Z21	21.376	0.966
Z22	21.211	0.908	Z23	21.131	0.566	Z24	21.016	0.834
Z25	19.456	0.823	Z26	21.292	0.827	Z28	21.418	0.766
Z27	21.594	0.940	Z29	18.551	1.094	Z30	21.092	0.550
Z31	21.505	1.053	Z32	21.640	0.656	Z33	21.334	0.272
Z34	21.251	0.639	Z35	21.131	0.790	Z39	19.619	0.573
Z36	19.936	0.368	Z37	21.054	0.262	Z38	21.418	0.833
Z40	20.078	0.905	Z41	20.942	0.664	Z42	21.251	0.911
Z43	20.942	0.490	Z44	21.054	-0.251	Z45	21.334	0.536
Z46	19.373	0.770	Z47	21.376	0.575	Z48	21.550	0.612
Z49	21.462	0.550	Z50	21.054	0.625	Z51	19.373	0.906
Z52	19.456	0.861	Z201	16.444	1.639	Z52	19.456	0.848
Z54	21.418	0.615	Z55	21.875	-0.005	Z56	21.131	0.317
Z57	21.418	0.924	Z58	21.054	0.552	Z59	21.550	0.887
Z60	21.550	0.074	Z62	21.376	0.764	Z61	21.732	0.610
Z63	21.171	1.057	Z64	19.031	0.870	Z65	21.131	0.475
Z66	21.732	0.260	Z67	21.211	0.865	Z68	18.347	0.955
Z69	21.686	0.145	Z70	19.581	0.254	Z71	21.334	0.894
Z72	20.978	0.505	Z73	19.508	0.796	Z74	20.534	0.565
Z75	19.738	0.779	Z76	21.131	0.604	Z85	19.405	0.800
Z84	21.054	0.516	Z83	21.131	0.334	Z82	21.171	0.564
Z81	21.376	0.616	Z80	20.798	0.567	Z79	20.382	0.380
Z78	21.462	0.592	Z86	20.978	0.628	Z87	21.251	0.373
Z88	21.376	0.514	Z89	20.663	0.020	Z90	21.171	0.097
Z91	20.905	0.460	Z92	21.016	0.374	Z93	20.240	0.859
Z94	21.054	0.090	Z95	21.418	0.533	Z96	21.334	0.236
Z97	19.490	0.752	Z98	19.581	0.948	Z99	17.288	1.547
Z100	20.942	0.737	Z101	20.663	0.889	Z102	21.171	0.948
Z103	20.630	0.159	Z104	20.696	0.572	Z106	21.251	0.599
Z107	20.942	0.968	Z108	21.462	0.509	Z109	19.389	0.953
Z110	21.594	0.460	Z111	21.131	0.759	Z112	21.131	0.529
Z113	21.054	0.463	Z114	20.833	0.719	Z115	19.802	0.842
Z117	20.833	0.311	Z118	21.640	-0.016	Z116	21.211	1.298
Z119	20.565	1.489	Z120	19.960	0.723	Z121	19.356	0.787
Z122	20.730	0.753	Z123	19.070	0.947	Z124	17.403	1.579
Z125	19.373	0.369	Z126	20.869	0.701	Z131	17.045	1.693
Z132	18.275	1.121	Z127	20.833	1.017	Z128	21.092	0.478
Z129	21.550	0.056	Z130	21.131	0.779	Z133	19.490	0.777
Z134	18.650	1.023	Z135	19.109	2.479	Z136	20.503	1.427
Z137	19.249	0.533	Z136	20.503	0.206	Z137	19.249	0.843
Z135	19.109	0.659	Z138	20.798	0.377	Z139	20.442	0.598
Z140	17.189	1.060	Z141	19.264	0.854	Z142	20.730	0.894
Z143	19.150	0.917	Z144	17.002	1.081	Z145	20.503	0.703
Z146	21.550	0.092	Z147	19.006	0.166	Z148	20.108	0.695
Z149	19.544	1.496	Z150	19.697	0.669	Z151	19.823	0.886
Z152	20.764	0.457	Z153	19.562	0.780	Z154	20.472	0.539
Z155	19.456	0.823	Z156	18.957	1.186	Z157	18.969	1.060
Z158	19.672	0.769	Z159	18.617	1.042	Z160	20.296	0.673
Z161	18.650	0.776	Z162	19.150	0.892	Z161	18.650	1.729
Z163	21.131	0.201	Z164	20.798	0.018	Z165	20.833	0.483
Z166	20.630	0.367	Z167	20.663	0.046	Z168	20.630	0.484
Z169	18.405	1.183	Z170	19.405	0.937	Z171	20.764	0.651
Z172	20.942	0.374	Z173	19.508	0.896	Z174	16.469	2.003
Z175	19.220	0.935	Z176	20.978	0.539	Z177	20.630	0.396
Z178	19.473	0.782	Z179	17.716	1.284	Z180	19.031	0.909
Z181	20.442	0.512	Z182	21.779	-0.082	Z183	21.054	0.278
Z184	20.597	0.313	Z185	15.157	0.797	Z186	20.082	0.235
Z187	19.031	1.036	Z188	18.749	0.924	Z189	21.131	-0.061
Z190	18.347	0.825	Z191	19.562	0.606	Z192	21.054	0.246
Z193	18.484	1.046	Z194	20.696	0.736	Z195	19.264	0.866
Z196	18.957	0.825	Z197	19.373	0.344	Z198	17.716	1.230
Z200	14.200	0.221						

FIELD REC. C

L11

L11	6 115							
A1	21.624	0.237	A2	21.107	1.076	A3	20.595	0.602
A4	20.880	0.301	A5	18.601	1.070	A6	18.732	0.637
A7	20.673	0.360	A8	19.834	0.264	A9	20.795	0.789
A10	18.917	0.724	A11	19.000	0.382	A12	19.637	0.509
A14	19.933	0.313	A17	19.935	0.938	A13	20.837	0.979
A19	19.764	1.082	A20	19.560	0.851	A21	19.207	1.091
A22	19.157	0.879	A23	20.634	0.745	A24	19.133	1.095
A25	19.834	0.771	A26	20.484	0.466	A27	19.233	1.167
A28	19.220	0.902	A29	20.345	0.717	B1	18.117	1.286
B2	18.089	1.072	B4	17.472	0.792	B3	18.520	0.932
B5	18.906	0.750	B6	17.124	1.013	B8	17.513	-0.226
B10	18.979	0.889	B11	16.002	1.065	B12	20.279	0.631
B13	20.125	0.561	B14	19.329	0.980	B15	20.345	0.717
B16	20.379	0.771	B17	16.965	1.223	B18	19.032	1.041
B19	19.919	0.817	B20	19.505	1.217	B21	19.286	0.919
B22	20.673	0.555	B23	20.558	0.225	B24	20.713	0.737
B25	20.448	0.516	B26	18.393	1.218	B27	20.155	0.795
B28	19.233	1.144	B29	21.060	0.689	C1	19.087	0.974
C2	15.918	2.007	C3	19.935	1.006	C4	20.216	0.934
C5	18.835	1.033	C6	18.855	1.013	C7	20.067	0.492
C8	19.065	0.934	C9	19.454	0.946	C10	19.678	0.767
C11	19.076	0.897	C12	20.279	0.567	C13	19.471	1.300
C14	21.060	0.002	C15	20.634	0.659	C16	20.558	0.577
C17	21.107	0.777	C18	20.012	1.281	C19	19.882	0.793
C20	20.279	0.644	C21	19.043	0.784	C22	19.437	1.020
C23	17.968	0.296	C24	18.613	0.669	C25	18.657	0.422
C26	17.169	0.300	C27	15.561	3.875	C28	18.532	0.820
C29	19.488	0.912	C30	18.679	0.567	D1	20.520	0.661
D2	19.207	1.114	D3	19.145	0.904	D4	20.216	0.904
D5	18.432	0.704	D6	20.155	0.907	D7	21.253	0.074
D8	19.933	1.058	D9	20.448	0.796	D10	17.366	1.186
D11	20.448	0.896	D12	20.279	0.726	D13	19.882	0.597
D14	18.406	1.265	D15	18.668	0.293	D16	18.774	0.775
D17	18.866	0.760	D18	18.195	0.601	D19	18.668	0.468
D20	18.958	0.668	D21	20.413	0.620	D22	19.720	0.657
D23	19.054	1.044	D24	19.935	0.861	D25	19.329	0.841
D26	20.634	0.516	D27	20.924	0.847	D28	19.935	1.020
D29	20.558	0.313	D30	20.595	0.276	D31	20.448	0.913
D33	18.458	1.198						

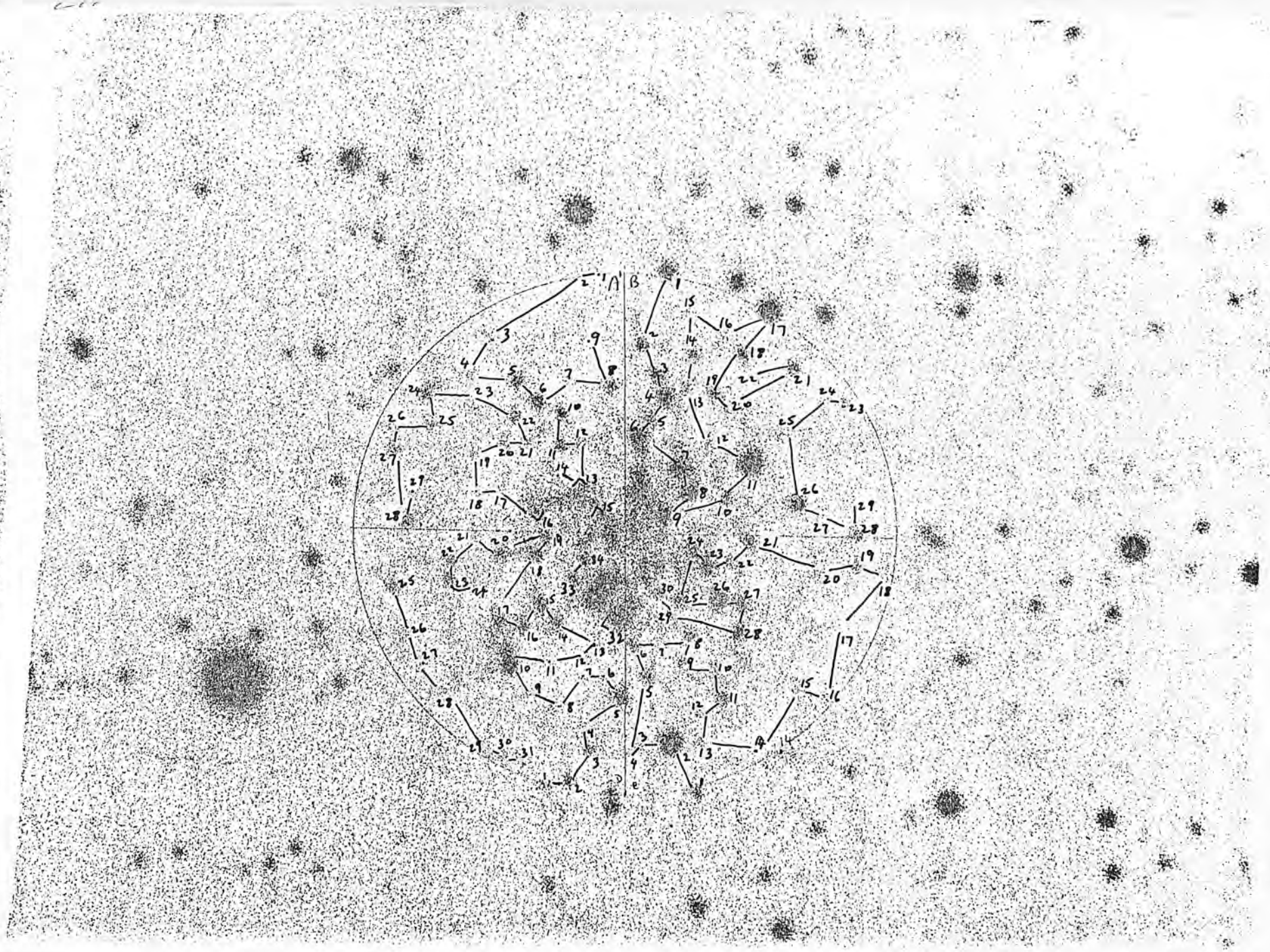
A
B
C
D

L12

L12	7	47						
A1	19.177	0.640	A2	19.845	0.953	A3	18.897	0.588
A4	19.202	0.672	A5	20.240	0.426	A10	18.529	0.733
A9	19.780	1.004	A6	20.186	1.103	A11	18.251	-0.352
A12	18.529	0.119	A13	18.201	-0.689	B1	19.177	-0.177
B2	19.845	0.629	B3	18.897	0.542	B4	18.851	0.603
B5	20.296	0.583	B7	18.981	0.877	B8	18.921	0.813
B9	18.405	0.444	B12	19.802	0.357	B13	19.890	0.508
B14	20.565	0.631	B15	20.597	0.923	C4	19.718	0.377
C5	20.730	0.275	C6	20.905	0.143	C7	20.324	0.265
C8	20.160	0.532	C9	19.123	0.269	C10	19.096	0.029
C11	16.848	0.863	C12	19.890	0.609	C13	17.384	1.093
C14	17.974	0.054	C16	19.006	0.570	D2	18.462	0.227
D3	18.716	0.595	D4	18.921	0.785	D5	19.638	0.786
D6	19.422	0.724	D8	19.936	0.691	D7	19.405	1.107
D9	17.779	1.127	D10	19.057	0.663	D11	18.287	0.361
D12	19.802	1.036	D13	19.718	1.093			

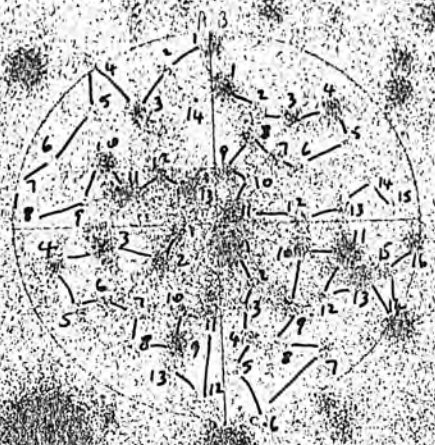

L13

L13	8	38						
A1	19.456	0.971	A2	19.868	0.577	A3	19.960	0.977
A4	19.090	0.715	A5	19.658	0.210	A6	19.279	0.056
A7	19.600	0.399	A8	18.311	0.195	A9	18.311	-0.252
A10	19.070	-0.356	A12	18.263	-1.525	A13	19.192	0.293
A14	18.672	-0.334	A15	18.287	-0.908	A16	12.528	-2.079
A17	17.023	0.356	A18	18.981	0.301	A19	19.562	0.655
A20	19.845	0.623	A21	19.294	1.049	A22	19.581	0.989
A23	19.294	0.533	A24	19.677	0.836	A25	19.562	0.701
B1	18.451	-0.982	B2	19.638	0.283	B3	19.697	0.794
B4	20.133	0.626	B5	20.160	0.503	B6	20.133	0.542
B7	20.296	0.343	B8	20.324	0.212	B9	18.628	0.393
B10	18.518	0.542	B11	19.823	0.566	B12	19.562	0.033
B13	18.469	0.029	B14	18.772	0.149	B15	18.909	0.189
B16	19.802	0.507	B17	20.008	-0.022	B18	19.373	0.399
B19	20.353	0.333	B20	19.544	0.429	B21	16.734	-3.968
B22	19.235	0.450	B23	20.186	0.361	B24	20.296	-0.138
C1	19.070	-0.232	C2	18.874	-0.487	C3	19.823	-0.306
C9	18.439	-0.302	C4	19.890	0.013	C7	19.823	0.394
C8	17.950	-0.641	C10	18.382	0.371	C11	19.960	0.186
C12	19.456	0.287	C13	20.663	0.287	C14	20.905	-0.047
C15	21.016	-0.341	C16	19.562	0.424	C17	19.984	-0.420
C18	18.374	-0.789	C19	20.032	-0.021	D1	17.023	-0.421
D2	19.296	0.537	D3	20.565	-0.029	D4	19.581	0.740
D5	19.192	0.000	D6	20.133	0.256	D7	19.456	-0.192
D8	19.422	-0.212	D9	19.096	-0.409	D10	18.705	0.355
D13	19.057	-0.116	D14	18.969	-0.304	D15	19.581	0.455
D16	19.890	0.332	D17	19.389	0.684	D18	18.994	0.341
D19	20.008	0.942	D21	20.008	0.902	D22	19.697	0.531
D23	19.264	0.334	D24	18.840	0.477	D25	18.562	-0.917
D26	17.886	0.173						

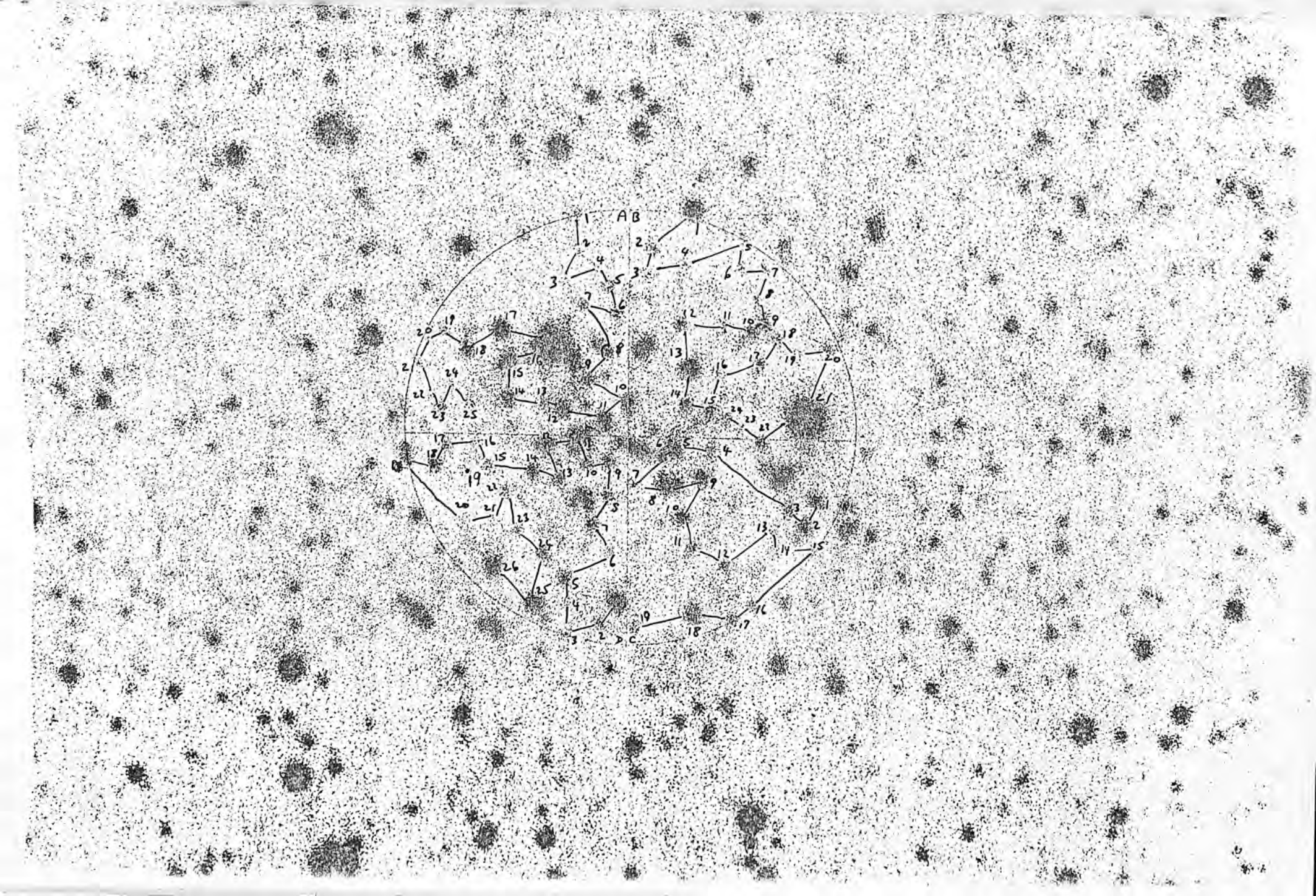
A
B
C

GASCOIGNE - KS SEQUENCE
12
11
25
14
10
W88
16
17
18
29
28
19
20
22
8
7
4
5
6

WALKER K3 SEQUENCE

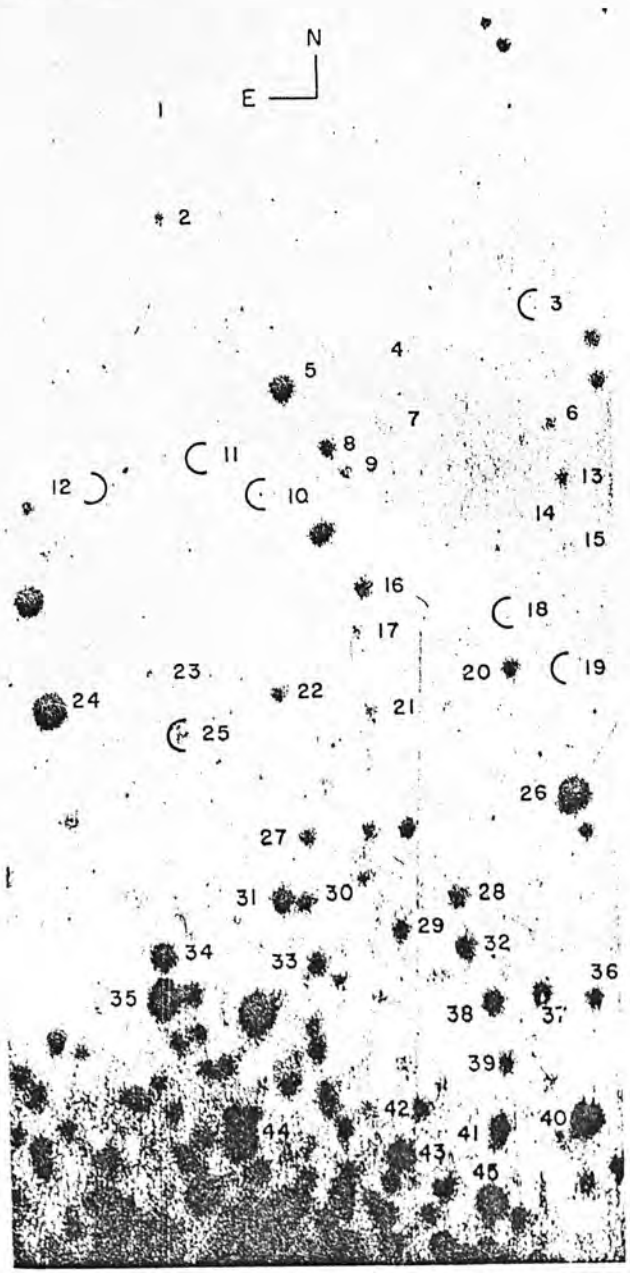

Fig. 2.—Electrograph of the north end of Kron 3, in yellow light. Exposure, 3h00m. Measured stars are

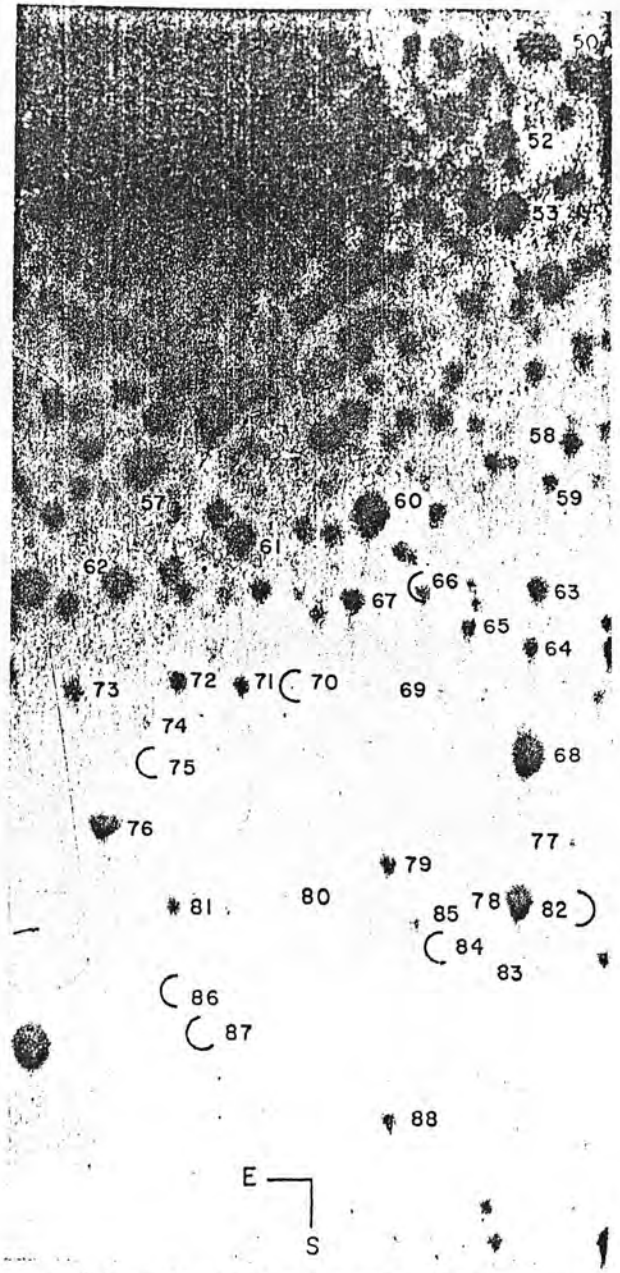

Fig. 3.—Electrograph of the south end of Kron 3, in yellow light. Expos , 3h00m. Measured stars